THE PREDICTION OF CHATTER STABILITY IN HARD TURNING

A Dissertation
Presented to
The Academic Faculty

By

Jong-Suh Park

In Partial Fulfillment
Of the Requirements for the Degree
Doctor of Philosophy in Mechanical Engineering

George W. Woodruff School of Mechanical Engineering
Georgia Institute of Technology
April 2004

THE PREDICTION OF CHATTER STABILITY IN HARD TURNING

Approved:

Dr. Ye-Hwa Chen, Chairman

Dr. Dewey H. Hodges

Dr. Thomas R. Kurfess

Dr. Steven Y. Liang

Dr. Chen Zhou

April 1, 2004

DEDICATION

To my mother, for everything.

ACKNOWLEDGEMENT

First of all, I would like to express my deepest gratitude to my advisor, Dr. Ye-Hwa Chen. I am most grateful for his guidance, inspiration and limitless patience. Without him, this dissertation would be nearly impossible.

I also would like to express great appreciation to Dr. Thomas R. Kurfess , Dr. Steven Y. Liang and Dr. Shreyes N. Melkote , members of the ATP Hard Turning Group meeting. They provided me with consistent support and valuable advise on my research. My gratitude is extended to Dr. Dewey H. Hodges and Dr. Chen Zhou, who served on my dissertation committee. Their stimulating discussions and judicious suggestions greatly helped the completion of this thesis.

I am also thankful to Sangil Han, Ty G. Dawson, Yong Huang and Steven Sheffield of the Precision Machining Research Consortium (PMCR) for their inspiring discussion and enormous help.

I owe great appreciation to my mother, Jungja Cho for her endless encouragement and sacrifice. Words are not enough to express my thanks to my wife, Mina, and my daughter Ashley for love and joy they constantly give me.

TABLE OF CONTENTS

LIST OF TABLES

LIST OF FIGURES

LIST OF SYMBOLS

ζ Damping ratio

δ Dirac delta function

θ Local time $\in [-h,\, 0]$

υ Cutting speed [m/sec]

σ Load distribution

ω Chatter frequency

α Positive constant in load distribution

Ω Cutting speed [rev/sec]

$\Delta\delta$ Displacement variation for two consecutive turns

β_1 Coefficient for the square term of the structural stiffness

η_1 Constant in the linear relation between k_c/k_m and β_1

λ_1 Slope of the linear relation between k_c/k_m and β_1

β_2 Coefficient for the cubic term of the structural stiffness

η_2 Constant in the linear relation between k_c/k_m and β_2

λ_2 Slope of the linear relation between k_c/k_m and β_2

ΔF_x Amount of the variation in F_x

ω_n Natural frequency

σ_p Standard deviation of the sample

Δs Variation of the feed rate with respect to a nominal feed rate

Δx Radial displacement

a	Real part of a complex number
a_0	Bias term in Fourier series
A_0	Offset input
A_1	Amplitude of sinusoidal input
a_1	First harmonic term in Fourier series
b	Imaginary part of a complex number
b_1	First harmonic term in Fourier series
c	Damping coefficient
c_1	Coefficient for the square term of the cutting stiffness
c_2	Coefficient for the cubic term of the cutting stiffness
C_s	Side cutting edge angle
doc	Depth of cut
doc_{new}	Depth of cut in an empirical model
F_x	Radial cutting force
G	Linear element
h	Time to pass the contact region between the tool and the workpiece, l/υ
k_c	Cutting stiffness
k_m	Structural stiffness
l	Flank wear length
m	Mass of the tool
M	Mean value
n	Branch identifier in the root locus, integer ≥ 0
N_0	Describing function for a biased term

N_1	Describing function for the first harmonic terms
n_p	Sample size
n_s	Exponent in non-uniform load distribution function
s	Complex number $= a + jb$
t	Time
t_α	Constant in the formula of the confidence interval
T_p	Period of the workpiece, $1/\Omega$
u_0	Offset input
u_1	Sinusoidal input
u_{1T}	Delayed sinusoidal input
VB	Flank wear length
$W(t)$	Nonlinear output
woc	Width of cut
woc_{new}	Width of cut in an empirical model
$x(t)$	Displacement in the radial direction at the current turn
x_T	Displacement in the radial direction at the previous turn
$y(t)$	Output
z	Location on the workpiece in the axial direction
z_l	Local coordinate at the tool tip $\in [-l, 0]$

SUMMARY

The development of more wear-resistant tool materials such as Polycrystalline Cubic Boron Nitride (PCBN) and ceramics have made hard turning a potential alternative to grinding operations in the finishing of hard materials. However, hard turning is more sensitive to chatter than conventional mild turning. The reasons include both a high precision requirement in finishing and the relatively brittle property of PCBN cutting inserts. Therefore, the ability to predict chatter-free cutting conditions is very important for hard turning in order to be an economically viable manufacturing process. Despite a large demand from industry, a realistic chatter modeling for hard turning has not been available due to the complexity of the problem, which is mainly caused by flank wear and nonlinearity in hard turning.

This thesis attempts to develop a chatter model for predicting chatter stability conditions in hard turning. First, a linear model is developed by introducing non-uniform load distribution on a tool tip to account for the flank wear effect. Then a nonlinear model is developed by further incorporating nonlinearity in the structure and cutting force. Stability analysis based on the root locus method and the harmonic balance method is conducted to determine a critical stability parameter. To validate the models, a series of experiment is carried out to determine the stability limits as well as certain characteristic parameters for facing and straight turning. Chatter in hard turning has the feature that the critical stability limits increase very rapidly when the cutting speed is higher than 13 rev/sec for all feed directions. From these, it is shown that the nonlinear model provides more accurate predictions than the linear model, especially in the high-speed range.

Furthermore, the stabilizing effect due to flank wear is confirmed through a series of experiments. To fully account for the validity of linear and nonlinear models, finally, an empirical model is proposed to fit in with the experimental stability limits in the full range of cutting speed.

The main contributions of the thesis are threefold. First, chatter-free cutting conditions are predicted and can be used as a guideline for designing tools and machines. Second, the characteristics of chatter in hard turning, which is observed for the first time, helps to broaden our physical understanding of the interactions between the tool and the workpiece in hard turning. Third, experimental stability limits for different flank wear can contribute to lead more reasonable ways to consider the flank wear effect in chatter models of hard turning. Based on these contributions, the proposed linear and nonlinear chatter models will support to improve the productivity in many manufacturing processes. In addition, the chatter experimental data will be useful to develop other chatter models in hard turning.

CHAPTER 1

INTRODUCTION

<u>1.1. Background</u>

Turning is one of the most commonly used cutting processes in industry. In the

turning operation, a workpiece rotates with a certain value of cutting speed and a tool

which is set at a certain value of the depth of cut or the width of cut removes a layer of

material. The feed rate is the distance that a tool travels per unit revolution of a

workpiece. As shown in Figure 1-1, the tool moves along the axial or the radial direction

of the workpiece in turning operations. Turning with the axial feed direction is called

"straight turning" and turning with the radial direction is called "facing". Cutting

parameters such as cutting speed, the feed rate and the depth of cut determine the material

removal rate of turning. However, there is a certain limit of the material removal rate and

chatter is one of factors causes such a restriction.

Chatter is a self-excited mechanical vibration during machining processes. The self-

excited vibration is caused by the interaction of the material removal process and the

structure of the machine tool. If there is energy, which is not dissipated by either the

damping of the structure or the friction of the cutting process, the relative motion

between the tool and the workpiece grows beyond the acceptable range at one of system's

natural frequencies. In contrast to forced vibration, which is caused by periodic applied

force from motors and pumps, chatter typically begins with a disturbance in the cutting
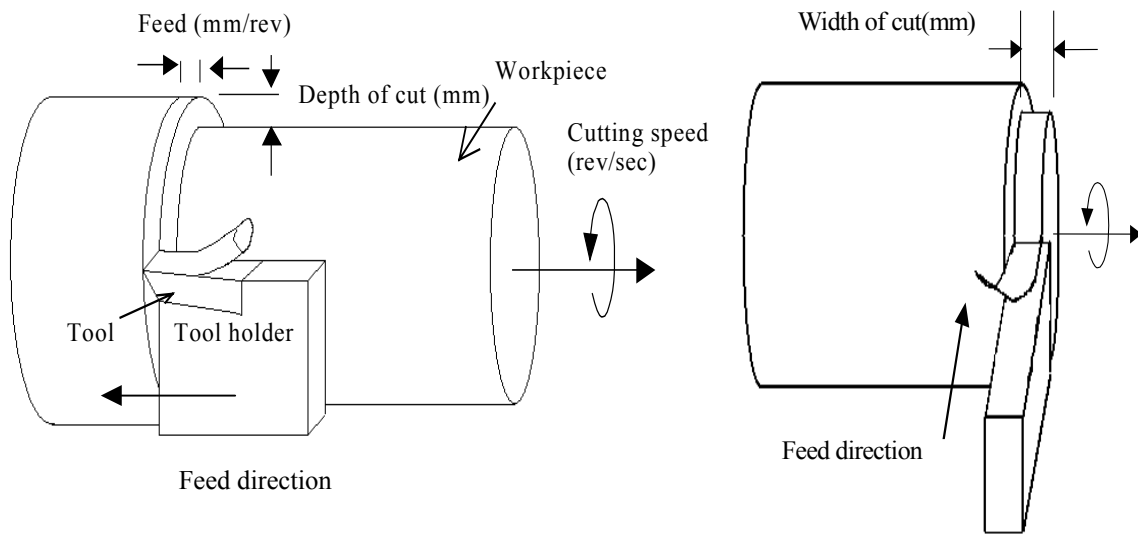
Figure 1-1. Schematic diagrams of straight turning and facing

area such as an inhomogeneous surface condition of the workpiece material.

When chatter occurs, the amplitude of cutting force increases abruptly and the chatter frequency is observed from the Fast Fourier Transform of force data. In addition to the surface damage on the workpiece due to chatter marks, the occurrence of severe chatter results in many adverse effects, which include a poor dimensional accuracy of the workpiece, a reduction of tool life, and a damage to the machine. Certain conservative cutting parameters, which were proposed in other research intended to avoid chatter at the expense of the loss of productivity. As high productivity has become important in many applications, the industry has started seeking less conservative chatter-free cutting parameters without compromising the material removal rate. Although chatter stability

limits for certain cutting conditions can be found through cutting experiments, they are, however, time-consuming and expensive. As an alternative, a theoretical model considering the dynamics in machining processes can be more cost-effective and efficient than the experimental approach. Hence the development of a reliable chatter stability model can significantly contribute to achieving high productivity in machining operations.

Any irregular motion of a tool or a workpiece makes an undulated surface during the machining process. In turning, the waved surface at the previous revolution leads to the deviation in uncut chip thickness from a nominal value at the current revolution. This in turn results in unstable vibration since cutting force is closely coupled with uncut chip thickness. The variation of cutting force due to the variation of uncut chip thickness during consecutive turns in the machining process is called the regenerative effect. It has been considered as a main cause of chatter phenomenon since Tlusty and Polacek (1963) and Tobias (1965) proposed their fundamental chatter theories. Following the pioneering works in the 60's, many studies have achieved some success in predicting stability limits by adding more realistic dynamic aspects of machining operations such as the flank wear effect (Chiou and Liang, 1996) and tool geometry effect (Clancy and Shin, 2002). However, it must be noticed that all research has focused on chatter in mild turning rather than hard turning.

Hard turning is defined as the turning of hardened ferrous metals with Rockwell-C hardness ratings ranging from 45 to 70. The development of more wear-resistant tool materials such as Polycrystalline Cubic Boron Nitride (PCBN) and ceramics have made hard turning more commonly used. Hard turning has the potential to substantially reduce

production costs by replacing more costly and less agile grinding operations on hard materials especially in finishing processes (Konig *et al.*, 1990). However, PCBN tools tend to be damaged more severely than conventional cutting tools of mild turning under violent vibrations because of their relatively brittle property. In addition, the finishing process, which are often involved with hard turning, has a much smaller tolerance of surface precision than other machining processes. Thus, hard turning is affected by the occurrence of chatter more seriously compared with conventional mild turning. As a result, the prevention of chatter has been a very essential element in improving productivity in hard turning. However, due to various technical difficulties at both theoretical and experimental levels, there have been no attempts to develop theoretical models or perform experimental investigations on chatter stability in hard turning.

In comparison with mild turning, hard turning has several unique features. First, the depth of cut is required to be limited since the specific cutting force in hard turning is greater than mild turning due to the high value of hardness. Second, cutting inserts in hard turning have a larger nose radius in order to increase the strength of tools. As a result of the shallow cut and large tool nose, the cutting takes place on the nose of tools. Third, the cutting force decreases more prominently as the cutting speed increases, which generates high temperatures (Dawson, 2002). Therefore, cutting speeds and tool geometry are important elements to be considered in a chatter model for hard turning.

The relative sliding between the tool and the machined surface of the workpiece causes flank wear just behind the cutting zone. As flank wear develops, it tends to increase the friction between the tool and workpiece, which in turn leads to increased cutting forces and temperature. Flank wear has been considered as a significant factor
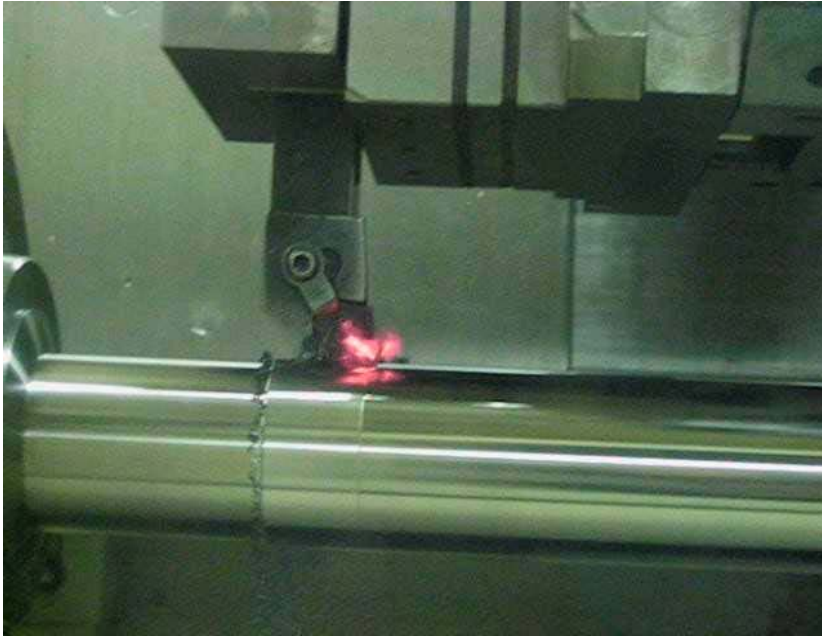
Figure 1-2. Example of the hard turning operation

involved in chatter stability in mild turning since Tlusty (1978) showed the strong

connection between tool wear and chatter stability. However, only a limited number of

published works have endeavored to consider tool wear in modeling chatter stability for

mild turning. Because the relation between flank wear and cutting force in hard turning

shows the same tendency observed in mild turning, it is expected that tool wear is also an

important factor in the modeling of chatter stability in hard turning. Therefore, a

systematic approach to consider flank wear effect on chatter stability is required when

developing a chatter model in hard turning.

Nonlinearity is another challenging factor in developing a chatter model in hard

turning. Although all physical phenomena are nonlinear in nature, often certain simplified

linear models have been used instead of nonlinear models since not only they are easy to

solve but also they provide reasonable results consistent with experiments. However, in the analysis of chattering, the applicability of linear models, which are derived by ignoring nonlinear characteristics of phenomena, is sometimes restricted. According to linear models, the amplitude of chatter should be increased indefinitely if a stability parameter is larger than a critical value. In practice, however, the amplitude of vibration remains at a finite level after a rapid initial increase. In order to explain the finite amplitude phenomenon in chatter, several studies (Hanna and Tobias, 1974, Wu and Liu, 1985, Nayfeh *et al*., 1998) have attempted to include nonlinearity in various sources such as nonlinear cutting force, the nonlinear stiffness of tools and machines, and the friction at the interface between the tool and the workpiece. It is expected that hard turning also has these nonlinearities in the machining process since it involves high specific force, hard materials and rapid tool wear. However, no study on chatter stability considering nonlinearity in hard turning has been reported. The reason includes the difficulty in the modeling of nonlinear phenomenon as well as the deficiency of available experimental data of nonlinearity in hard turning. Therefore, it is important to have reliable measurements of nonlinearity involved in hard turning as well as an appropriate method to deal with nonlinear elements in order to carry out the modeling of nonlinear chatter.

In addition to this, experimental data of chatter stability limits are needed not only for model validation but also for a better understanding of chatter phenomenon. The unique characteristics of chatter in hard turning can be used as a guideline for developing chatter predicting models in the future. Despite its importance, there has been no significant effort devoted to measure critical stability limits in hard turning. Generic research in this area, as documented in this thesis, is believed to be both timely and important.

1.2. Research Objective

The objective of this research is to predict chatter stability limits in hard turning, especially emphasizing the effects of flank wear and nonlinearity. The objective is to be achieved through the steps as follows: (1) Development of a nonlinear chatter models with non-uniform load distribution. (2) Stability analysis for worn tool cases. (3) Theoretical chatter stability predictions based on characteristic parameters, which measured in experiments. (4) Model validation with experimental chatter stability limits for different feed directions and tool wear conditions.

In this study, the effect of material property on chatter stability is considered by measuring the stiffness in the structure and cutting force, which is closely related with the hardness of materials. As a result, the proposed nonlinear chatter model for a worn tool has a capability to predict stability limits for mild turning as well as hard turning. However, the present study focuses on the application to hard turning since it is mainly motivated by the demand for the prediction of chatter-free conditions in hard turning. Less conservative chatter-free cutting conditions from this research can be used to improve productivity in hard turning as a guideline for designing tools and machines as well as a factor in optimizing cutting parameters. Moreover, newly found characteristics of chatter in hard turning can contribute to the broadening of physical understanding of interactions between the tool and the workpiece in hard turning.

1.3. Literature Review

1.3.1. Stability Analysis in Linear Models

Fundamental works in the 60's led a lot of research of chatter modeling for next several decades. Tlusty and Polacek (1963) and Tobias (1965) developed fundamental chatter theories that the regenerative phenomenon and the mode coupling effect caused principal chatter mechanisms. The regenerative phenomenon occurs when the tool is passing a modulated surface caused by the previous revolution. At a critical range of phase values, net energy is provided to the structure by the cutting force. If response is sustained at one of the system's natural frequencies, then chatter incurs.

There have been many attempts to obtain the critical chatter stability limit resolving the complexity caused by the transcendental characteristic of chatter problems. In order to obtain the stability limit, Merritt (1965) simultaneously solved two equations derived from the characteristic equation at $s = j\omega$ to obtain values of the critical stiffness ratio and the chatter frequency, and then determined multiple numbers of spindle speed for each stiffness ratio. Minis *et al*. (1990) used the Nyquist stability criterion as an alternative approach to derive the critical stability parameter by finding the left-most intersection of the Nyquist plot with the negative real axis. Olgac and Hosek (1998) determined the critical parameter from the first pair of roots on the imaginary axis while the others remained in the stable left hand side of the complex plane. The Routh-Hurwitz stability criterion also can be used for time-delayed systems after transforming a transcendental equation to a polynomial equation (Rekasius, 1980).

Stability analyses for chatter models have been extensively studied and some of them have included the flank wear effect on chatter stability.

1.3.2. Flank Wear Effects on Chatter Stability

Tool wear has been considered as a significant factor involving in chatter stability since Tlusty (1978) indicated the strong relation between tool wear and chatter by showing that the contact between the tool and the workpiece caused a positive damping effect. With the presence of flank wear, dynamic cutting force is affected by the physical contact between the workpiece and the tool nose region (Smithey *et al.*, 2001). Two different approaches have been used mainly to consider the flank wear effect on cutting processes (Waldorf *et al.*, 1997). Wu (1988) suggested a contact force model, which is proportional to the displaced volume of a workpiece beneath a tool. Based on the contact force model, Elbestawi *et al.* (1991) showed larger tool flank wear resulted in the increased chatter-free region in numerical simulations. Chiou and Liang (1998) and Clancy and Shin (2002) experimentally verified the same tendency that tool flank wear stabilized chatter vibration in mild turning. But it is hard to extend the contact force model to hard materials because of increased uncertainty in estimating displaced volume. The other approach to explain the flank wear effect is based on a slip-line model, which was originally proposed by Challen and Oxley (1979). This approach has shown good predictions on cutting force including the ploughing force due to the tool nose radius not being zero (Black *et al.*, 1993). Based on the slip-line field and the presence of plastic flow of the workpiece under the flank wear of the tool (Thomsen *et al.*, 1962, Kobayashi and Thomsen, 1960), Waldorf (1996) suggested a method to estimate force on the worn

area introducing non-uniform stress distribution along the flank wear area. He suggested non-uniform stress distribution with a quadratic form on flank wear, which decreases from a nominal value at the front of the cutting edge to 0 at the end of the flank wear area if the length of flank wear is shorter than the critical value. Once the length of flank wear is longer than the critical value, the stress distribution has a constant value in the front part for the exceed of the critical length and then quadratically decreases to zero in the last part of the flank wear area. Furthermore, Stepan (1998) developed a chatter model with non-uniform load distribution on the active face between the workpiece and the tool. However, a chatter model with non-uniform load distribution on the flank wear area has not been developed. Additionally, it should be noticed that all experimental investigations on chatter have been restricted so far to mild turning cases.

1.3.3. Flank Wear in Hard Turning

Because of possible benefits of hard turning as an alternative machining process over grinding (Konig *et al*. 1990), much research related to cutting force and tool wear in hard turning have been actively carried out. The strong relation between the flank wear of tools and cutting processes in hard turning has been reported by Nakayama *et al.* (1988), Wang and Liu (1999) and Chou and Evans (1999). They suggested cutting force increase for larger flank wear in machining hard materials. Kishawy and Elbestawi (1999) showed tool wear also affected on machined surface quality during hard turning. Davies (1998) suggested that the primary sources of vibrational instabilities in hard turning should be the regenerative effect and stick-slip oscillations excited by the rubbing of the tool on the surface of the workpiece as it wears. Dawson (2002) suggested PCBN tools have a rapid

flank wear development at the early stage of hard turning process, which caused the increase of cutting forces. The relation between flank wear and cutting force as well as rapid tool progress in hard turning suggest that tool wear should be an important element to consider in modeling of chatter stability in hard turning.

1.3.4. Nonlinearity in Chatter Stability

Nonlinearity exists in the structure and cutting force of turning processes and it is closely related with chatter stability. Hanna and Tobias (1969) found the dynamic response of the machine structure became nonlinear with increasing force amplitude and proposed a nonlinear structural stiffness in a form of polynomial. In addition, Hanna and Tobias (1974) developed a nonlinear chatter model introducing third-order polynomials for the nonlinear stiffness and cutting force in order to explain a nonlinear phenomenon such as the finite amplitude of chatter, which can not be explained by linear models. As a result of the inclusion of nonlinear terms, three-dimensional stability charts were represented in chatter amplitude, the stiffness ratio and cutting speed instead of typical two-dimensional stability charts in the stiffness ratio and cutting speed from linear models. Furthermore, they attempted to explain the nonlinear behavior of chatter in the stability chart on the plane of chatter amplitude and the stiffness ratio. Saravanja-Fabris and D'Souza (1974) employed the describing function method to predict the stability of nonlinear systems. A stability chart for a fixed value of chatter amplitude was obtained considering the nonlinear relationship between cutting force and uncut chip thickness. Besides, Shi and Tobias (1984) experimentally showed the finite amplitude phenomenon

in chatter and suggested that the temporary absence of the tool contact on the workpiece and the nonlinear cutting stiffness cause this nonlinear behavior.

After these pioneering works, several research have attempted to consider nonlinearity in chatter phenomena by either analytically approximating nonlinear elements (Nayfeh *et al*., 1998, Pratt *et al*., 1999) or solving them numerically (Lin and Weng, 1991, Gradisek *et al.*, 2001, Deshpande and Fofana, 2001, Kalmar-Nagy *et al*., 2001, Litak, 2002).

Most nonlinear chatter models consider either nonlinearity in the structure and cutting force (Hanna and Tobias, 1974, Nayfeh *et al*., 1998, Kalmar-Nagy *et al*., 2001) or nonlinearity due to friction depending on cutting speed (Wu and Liu, 1985, Nosyreva and Molinari, 1997). Berger *et al*. (1992) and Nayfeh *et al*. (1998) showed that nonlinear terms led to qualitatively different stability evolution. In addition, Deshpande and Fofana (2001) showed the effect of the third-order term in the nonlinear cutting stiffness through the difference in resultant phase portraits obtained by a numerical method. These approaches have achieved some success in explaining the nonlinear behavior of chatter. However, it should be noticed that all of them have been based on nonlinearity measured in conventional mild turning.

1.3.5. Nonlinearity in Hard Turning

It is suggested that nonlinearities from various sources clearly exist in hard turning (Davies, 1998). Nonlinearities in hard turning can arise from the geometry of the cutting tool, friction, the cutting mechanics and the mechanical behavior of the machine tool. However, there have been no attempts to measure the nonlinearity in cutting force in hard

turning although it is vital for modeling of nonlinear chatter. If the nonlinearity of cutting force is measured, the effects of tool wear and cutting speed should be considered since there is a strong relation among these factors and cutting force, as pointed out by Dawson (2002).

1.3.6. Chatter Detection

Various methods have been used for detecting the chatter phenomena in cutting tests as follows: First of all, chatter is identified from the time trace and the power spectrum of cutting force, tool acceleration (Chiou and Liang, 1998, Clancy and Shin, 2002) or sound emitted (Chiou and Liang, 1998). Chatter also can be identified from the measurement of surface roughness (Clancy and Shin, 2002) or the visual inspection of chatter marks on the machined surface (Elbestawi *et al*., 1991). In addition, chatter is identified when the ratio of the amplitude of the first revolution to that of the second is greater than one (Kondo *et al*., 1997). Most of experimental investigations on chatter stability have employed multiple methods of chatter detection.

1.4. Approach in This Dissertation

This dissertation presents a chatter model for the purpose of predicting stability limits in hard turning. In order to address completed research, this dissertation is organized based on theoretical predictions from proposed models and model validation through experimental investigations for facing and straight turning, respectively, as shown in Figure 1-3. Chapter 1 is the introduction and background review. Chapter 2–4 are devoted to linear modeling with non-uniform load distribution and stability limit

measurements for chatter in facing. Chapter 5-7 belong to nonlinear chatter modeling considering tool wear and its validation for chatter in straight turning. Finally, Chapter 8 is the closure of this dissertation. Detailed descriptions for each succeeding chapter are given as follows:

In Chapter 2, linear modeling considering flank wear for chatter stability in facing is presented. A non-uniform load distribution is introduced to consider the flank wear effect on stability. The stability analysis for worn tools is described in detail including the effect of a time delay on stability. In order to determine the critical stability parameter for a given time delay, the root locus method is employed.

Chapter 3 provides theoretical predictions of chatter stability in facing. In order to calculate stability limits in the proposed chatter model, characteristic parameters such as the natural frequency, the damping ratio, the structural stiffness and the cutting stiffness are measured. In addition, a converting relation between the stiffness ratio and the width of cut is derived for more practical use of stability charts. Stability charts are obtained for different values of flank wear and the effects of flank wear on stability are discussed.

Chapter 4 investigates chatter stability limits experimentally in order to verify the proposed model. A series of experiments determines the values of the critical width of cut in facing of hardened 52100 steel bars for the first time. The characteristic features of chatter limits in hard turning are discussed. Next, the predicted stability charts are overlapped to experimental stability limits and the validity of the proposed model is discussed. Finally, an empirical model for chatter stability is proposed.

In Chapter 5, a nonlinear chatter model including the flank wear effect is developed. Nonlinearity in cutting force and the structure is considered in modeling combined with

non-uniform load distribution. In order to approximate nonlinear elements, the describing function method is employed. Harmonic balance equations for different nonlinearity and tool wear conditions are derived from describing functions.

In Chapter 6, theoretical stability predictions are carried out based on characteristic parameters of a cutting setup in straight turning. In order to consider the effects of flank wear and cutting speed, multiple sets of experiments are performed to measure cutting force under various cutting conditions. Then, converting relations from the stiffness ratio to the depth of cut or the chatter location are derived for each cutting condition. After that, two different approaches to derive stability charts for opposite feed directions are described. Three-dimensional stability charts are derived as a result of the consideration of nonlinearity. Finally, nonlinear effects and tool wear effects on chatter stability charts are discussed and an explanation of the nonlinear phenomena of chatter is attempted with resultant stability charts.

In Chapter 7, stability predictions from the proposed nonlinear model are verified with experimental stability limits. First, five sets of chatter measurement experiments are performed to obtain experimental chatter limits in straight turning of 52100 bars for the first time. Next, the characteristics of chatter limits in straight turning of 52100 bars are described and discussed. After that, the effects of flank wear on chatter stability are examined by analyzing experimental data. Finally, experimental stability limits are used to verify predictions from the proposed models.

In closing, Chapter 8 reviews the contribution of this dissertation along with recommendations for improvement and concluding marks.

Background review	**Introduction (Chp. 1)**	
Modeling	**Linear chatter modeling for worn tools in facing (Chp. 2)**	**Nonlinear chatter modeling for worn tools in straight turning (Chp. 5)**
Characteristic parameters	**Characteristic parameter measurements (Chp. 3)**	**Characteristic parameters, nonlinear cutting force and stiffness (Chp. 6)**
Theoretical predictions	**Theoretical predictions of chatter stability in facing (Chp. 3)**	**Theoretical predictions of chatter stability in straight turning (Chp. 6)**
Model validations	**Empirical chatter stability in facing (Chp. 4)**	**Empirical chatter stability in straight turning: (Chp. 7)**
Summary	**Summary and recommendations (Chp. 8)**	

Figure 1-3. The organization of the dissertation

16

CHAPTER 2

LINEAR MODELING FOR CHATTER IN FACING

<u>2.1. Introduction</u>

Chatter is a self-excited mechanical vibration during machining processes. It causes

adverse effects such as the poor surface finish of the workpiece, reduced tool life and

eventually the loss of productivity (Tewani *et al.*, 1993). The limit of cutting parameters

to avoid chatter can be less conservative if chatter stability is predicted in terms of cutting

conditions. Therefore the prediction of chatter is one of crucial factors for achieving high

productivity in machining operations.

The prevention of chatter is even more important in hard turning than conventional

mild turning. Recently hard turning has been actively investigated since it has the

potential to replace more costly and less agile grinding processes in finishing hardened

materials of HRC 45-70. Considering the surface quality demand in finishing and the

relatively brittle property of PCBN inserts, hard turning is more sensitive to the

occurrence of chatter. Unfortunately, there have been few theoretical and experimental

investigations on chatter associated with hard turning.

Flank wear is an important factor to consider in the modeling of chatter for hard

turning. The strong relation between flank wear and cutting force has been reported for

hard turning (Wang and Liu, 1999, Chou and Evans, 1999). It was suggested that cutting

force increases for larger flank wear in machining hardened steels. As chatter stability is

clearly affected by flank wear in mild turning (Tlusty, 1978, Elbestawi *et al*. 1991, Chiou

and Liang, 1998), flank tool wear is also suggested as one of primary sources of chatter in

hard turning (Davies, 1998). In addition, Kishawy and Elbestawi (1999) showed tool wear also affected machined surface quality during hard turning. Therefore, it is necessary to introduce an appropriate method to consider the flank wear effect in the modeling of chatter for hard turning.

One of challenging aspects in the modeling of chatter is that there are infinitely many roots of the characteristic equation on the imaginary axis, which correspond to the critical stability parameter. When the regenerative effect is considered as a main mechanism of chatter, a closed loop characteristic equation has a time delay term, which is a period of one revolution in the machining process. Since the time delay results in infinitely many roots on the imaginary axis, it has been a key issue to determine critical values of the stability parameter among infinitely many roots in stability analysis involving chatter problems. In this study, critical stability parameters have been determined explicitly by drawing root loci in terms of the stiffness ratio with the presence of flank wear. Furthermore, the effect of a time delay on chatter stability is also discussed.

In this chapter, linear chatter modeling procedures for facing operations are described. The characteristic equation with non-uniform load distribution is derived to consider the flank wear effect. Then the root locus method for general worn tools, which explicitly decides the critical stability parameter in stability analysis is described.

2.2. Linear Modeling for Chatter in Facing

In this study, a 1-DOF linear chatter model considering the flank wear effect is developed. It is assumed that the workpiece is rigid and the flexible tool is able to vibrate only in the *x* direction as shown in Figure 2-1. The feed direction in facing operations is

the radial direction of the workpiece, which is parallel to the x-direction and the cutting

edge of the tool proceeds normal to the surface of the workpiece. Even though the tool

can be deflected to the tangential or axial direction of the workpiece, the machining

performance is only sensitive to the radial vibration of the tool. Therefore, it is valid to

assume a 1-DOF chatter model instead of a 3-DOF model. Since grooving inserts used in

facing operations have a very small tool nose radius compared with the value of uncut

chip thickness, the tool geometry effect in hard turning is assumed to be negligible. The

zero value of the coordinate x of the tool edge position is set in a way that the x-

component F_x of cutting force F is in balance with spring's force while chip thickness is

just the prescribed value, which corresponds to the nominal value of feed. The equation

of motion in the feed direction x is

$$m\ddot{x}(t) + c\dot{x}(t) + k_m x(t) = \Delta F_x(t) \tag{2-1}$$

where m is the mass of the tool, c is the damping coefficient, k_m is the structural stiffness,

and $\Delta F_x(t)$ is the amount of variation in the x-component of cutting force.
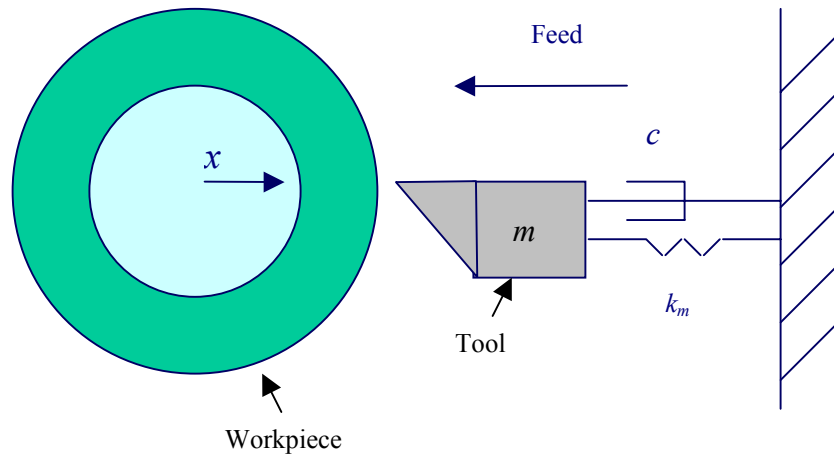
Figure 2-1. Schematic diagram of the tool-workpiece system

The variation of cutting force ΔF_x in equation (2-1) is caused by the variation of uncut chip thickness during consecutive turns in the machining process, as shown in Figure 2-2. Any irregular motion of a tool makes an undulated surface during machining process and it leads the deviation in uncut chip thickness from a nominal value at the next revolution, which results in the variation of cutting force. This phenomenon is called the regenerative effect, which induces ΔF_x for a sharp tool as the following:

$$\Delta F_x(t) = k_c[x(t) - x(t - T_p)] \tag{2-2}$$

where k_c is cutting stiffness, $x(t)$ and $x(t\text{-}T_p)$ are deviations from the equilibrium position of the tool edge at the current turn and the previous turn, respectively, and T_p is the period of a turn.
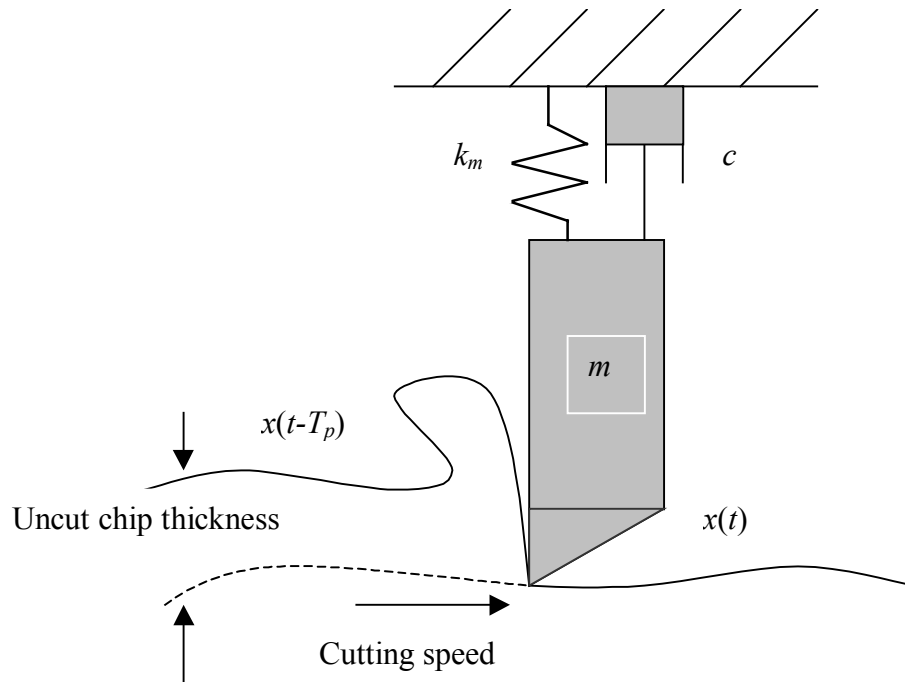
Figure 2-2. Schematic diagram of the regenerative effect in facing

In the present study, non-uniform load distribution on the flank wear area is introduced to consider the flank wear effect in the chatter model. Two different approaches have been used mainly to include the effect of flank wear (Waldorf *et al.*, 1997). Wu (1988) suggested a method to represent the flank wear effect by employing contact force, which is proportional to the displaced volume of the workpiece beneath the tool. Based on the contact force model, Elbestawi *et al.* (1991) predicted an increased chatter-free region in numerical simulations for larger tool flank wear. The same tendency that tool flank wear stabilized chatter vibration was experimentally verified in mild turning by Chiou and Liang (1998) and Clancy and Shin (2002). However, it is difficult to extend the contact force model to hard materials since the uncertainty in estimating displaced volume increases. Another way to consider the flank wear effect is based on the slip-line model, which was originally proposed by Challen and Oxley (1979). Cutting force including ploughing force due to the existence of flank was predicted by this method (Black *et al.*, 1993). Considering the slip-line field and the presence of plastic flow of the workpiece under the tool flank (Kobayashi and Thomsen, 1960, Thomsen *et al.*, 1962, Smithey *et al.*, 2001), Waldorf (1996) introduced non-uniform stress distribution along the flank wear area to estimate force on the worn area. Furthermore, Stepan (1998) suggested a chatter model with non-uniform load distribution on the active face between the workpiece and the tool. However, a chatter model with non-uniform load distribution on the flank wear area has not been attempted. In this study, the method to integrate non-uniform load distribution on flank wear has been employed for considering the flank wear effect to avoid the uncertainty in estimating the displaced volume of hard materials.

In the present study, non-uniform load distribution $\sigma(z_l)$ is assumed in the local coordinate z_l along flank wear as the following (see Figure 2-3):

$$\sigma(z_l) = \frac{1}{l}\left[1 + \cos\left(\pi\left(\frac{z_l}{l}\right)^{n_s}\right)\right], \quad z_l \in [-l,0] \tag{2-3}$$

where l is the length of flank wear. The exponent n_s is to determine how much plastic deformation occurs and is assumed to be inversely proportional to the flank wear length l as the following :

$$n_s = \frac{\alpha}{l} \tag{2-4}$$

where α is a positive constant. As shown in Figure 2-4, this load distribution has the maximum value at the beginning of flank wear and becomes zero at the end of flank wear. This form of load distribution has ability to reflect the effects of the flank wear length as well as the degree of plastic deformation of the workpiece under flank wear. As a result, the effect of plastic deformation and flank wear on chatter stability can be examined through this load distribution.

Let us introduce h which is the duration to pass the interface of length l between the tool and the workpiece at the speed of υ :

$$h = \frac{l}{\upsilon} \tag{2-5}$$

Converting non-uniform load distribution of equation (2-5) into the form in local time θ yields

$$\sigma(\theta) = \frac{1}{h}\left[1 + \cos\left(\pi\left(\frac{\theta}{h}\right)^{n_s}\right)\right], \quad \theta \in [-h,0]. \tag{2-6}$$
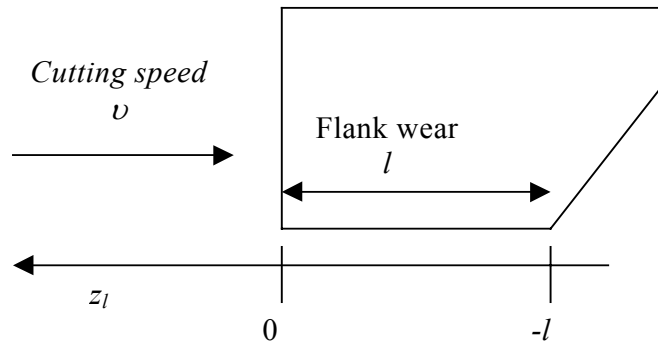
Figure 2-3. Schematic diagram of the tool tip with the flank wear length of l and local coordinate z_l along flank wear
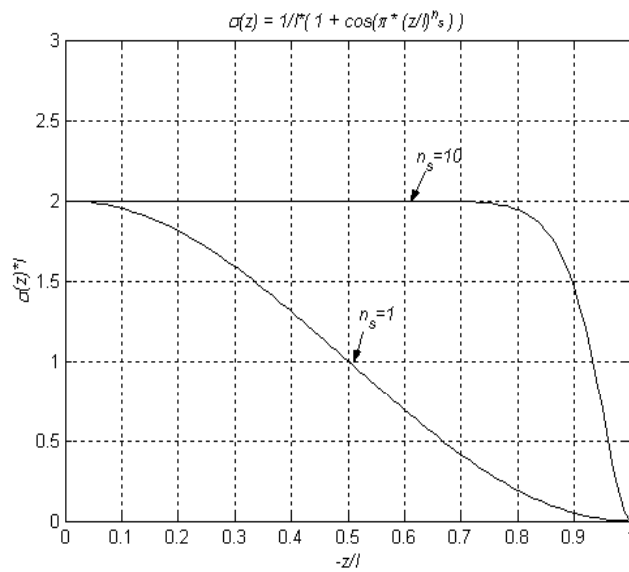
Figure 2-4. Non-uniform load distribution along flank wear

When load distribution on a finite length of the tool as well as the regenerative effect are considered, $\Delta F_x(t)$ in equation (2-2) becomes as the following:

$$\Delta F_x(t) = k_c \int_{-T_p - h}^{-T_p} \sigma(T_p + \theta) x(t + \theta) d\theta - k_c \int_{-h}^{0} \sigma(\theta) x(t + \theta) d\theta \tag{2-7}$$

where k_c is the cutting stiffness, and T_p is the period of the workpiece. Substituting the cutting force variation in equation (2-7) into the differential equation (2-1) and dividing the both sides by m yields

$$\ddot{x}(t) + 2\omega_n \zeta \dot{x}(t) + \omega_n^2 x(t) = \frac{k_c}{k_m} \omega_n^2 \int_{-T_p - h}^{-T_p} \sigma(T_p + \theta) x(t + \theta) d\theta - \frac{k_c}{k_m} \omega_n^2 \int_{-h}^{0} \sigma(\theta) x(t + \theta) d\theta$$

$$\tag{2-8}$$

where $\omega_n = (k_m/m)^{1/2}$ is the natural frequency of the system and $\zeta = c/(2m\omega_n)$ is the damping ratio of the system. The regenerative effect which reflects the position difference between the previous turn and the present turn yields two terms on the right side of equation (2-8) and the flank wear effect is considered by integrating load distribution $\sigma(\theta)$ for each term. Performing the Laplace transform of equation (2-8) with zero initial conditions and rearranging resulting terms yield the characteristic equation for a worn tool with non-uniform load distribution:

$$s^2 + 2\zeta\omega_n s + \omega_n^2 + \frac{k_c}{k_m} \omega_n^2 \int_{-h}^{0} \sigma(\theta) e^{s\theta} d\theta (1 - e^{-sT_p}) = 0 \tag{2-9}$$

When the value of n_s is 1 and l is negligibly small, load distribution $\sigma(\theta)$ becomes the Dirac delta function corresponding to the load distribution of an ideal sharp tool. The Dirac delta function $\delta(\theta)$ has the following filtering property. Suppose $\gamma > 0$ and let f be integrable on $[0, \infty)$ and continuous at γ. Then

$$\int_0^\infty f(x)\delta(x - \gamma) dx = f(\gamma) \tag{2-10}$$

24

Therefore, the value of integral in equation (2-9) becomes unity so that

$$\int_{-h}^{0} \sigma(\theta) e^{s\theta} d\theta = \int_{-h}^{0} \delta(\theta) e^{s\theta} d\theta = 1 \tag{2-11}$$

The characteristic equation for a sharp tool is derived from equation (2-9) and (2-11) and is shown as

$$s^2 + 2\zeta\omega_n s + \omega_n^2 + \frac{k_c}{k_m}\omega_n^2(1 - e^{-sT_p}) = 0 \tag{2-12}$$

<div align="center">2.3. Stability Analysis for Worn Tools</div>

2.3.1. Determination of the Critical Stability Parameter

The system is stable if all of roots of the closed loop characteristic equation have negative real values. If any of roots have zero real values, the rest having negative real values, then this represents the critical condition of stability. Because the closed loop characteristic equation with a time delay has infinitely many roots on the imaginary axis, it has been a crucial issue in stability analysis to derive the critical parameter among infinitely many roots which determines the stability of the system. In chatter stability problems that also include a time delay, the stiffness ratio, k_c/k_m is a commonly used parameter when stability is decided for a given time delay.

There have been many attempts to obtain the critical k_c/k_m resolving the complexity in stability analyses caused by the transcendental nature of the characteristic equation for chatter problems. For example, Tlusty and Polacek (1963) and Merritt (1965) developed fundamental chatter theories that determined the chatter frequency and the stiffness ratio for a time delay by simultaneously solving two equations at $s = j\omega$, which were derived

from the characteristic equation. Nyquist stability criterion was employed by Minis *et al*.

(1990) as an alternative approach to derive the critical stability parameter. In addition, the

root locus method determined the critical stiffness by finding the first pair of roots on the

imaginary axis while the others remained in the stable left hand side of the complex plane

(Olgac and Hosek, 1998). The Routh-Hurwitz stability criterion also can be used for

time-delayed systems after transforming a transcendental equation to a polynomial

equation (Rekasius, 1980).

In the present study, critical parameters for chatter stability are explicitly determined

by drawing root loci in terms of the stiffness ratio. Even though the methodology is not

new, this is the first attempt to expand the root locus method in stability analyses to more

general worn tool cases. The condition of root loci to have the minimum stiffness ratio as

the critical parameter is derived after finding poles and zeros and categorizing branches

in the root locus plot.

First of all, locations of roots with zero and infinite values of the stiffness ratio, which

correspond to poles and zeros of the open loop system, are found analytically (see

Appendix A.1). There are an infinite number of poles at $s = -\infty \pm j\, 2n\pi/T_p$ ($n = 0, 1, 2,\ldots$

) as well as two finite poles at $s = -\zeta\omega_n \pm \sqrt{\zeta^2\omega_n^2 - \omega_n^2}$. The closed loop system also has an

infinite number of zeros on the imaginary axis at $s = \pm j2n\pi/T_p$ ($n = 0, 1, 2,\ldots$). Therefore,

the gap between branches decreases as the amount of time delay increases.

In addition to locations of poles and zeros of the open loop system, it is necessary to

know if any root of the closed loop characteristic equation has a positive real part, which

induces chatter for given cutting conditions. In this study, whether roots of the closed

loop characteristic equation have a positive sign is determined analytically (see Appendix

A.2). According to the results, there are two kinds of branches in the root locus diagram

following these criteria:

1) One always remains in the left-hand side of the s-plane and ends at one of zeros

on the imaginary axis,

$$if \int_{-h}^{0} \sigma(\theta)\cos(2n\pi\theta/T_p)d\theta > 0 \ for \ \omega_n > 2n\pi/T_p, \qquad \text{(2-13a)}$$

$$if \int_{-h}^{0} \sigma(\theta)\cos(2n\pi\theta/T_p)d\theta < 0 \ for \ \omega_n < 2n\pi/T_p \qquad \text{(2-13b)}$$

2) The other crosses the imaginary axis only once from the left-hand side to the right-

hand side of the s-plane and ends at one of zeros on the imaginary axis,

$$if \int_{-h}^{0} \sigma(\theta)\cos(2n\pi\theta/T_p)d\theta < 0 \ for \ \omega_n > 2n\pi/T_p \qquad \text{(2-14a)}$$

$$if \int_{-h}^{0} \sigma(\theta)\cos(2n\pi\theta/T_p)d\theta > 0 \ for \ \omega_n < 2n\pi/T_p. \qquad \text{(2-14b)}$$

Because roots have positive real parts, the second type of branches is related to the

instability of the closed loop system. Whether a branch has an unstable root or not

depends on the value of the zero of the branch as well as the amount of a time delay and

load distribution. Since in this study values of $\int_{-h}^{0} \sigma(\theta)\cos(2n\pi\theta/T_p)d\theta$ are always

positive for a given load distribution, the natural frequency, the amount of a time delay

and the order of a branch determine if it has unstable roots. If $\omega_n > 2n\pi/T_p$, n = 0, 1, 2,...,

then branches remain in the stable left hand side of the s-plane. On the contrary, if $\omega_n <$

$2n\pi/T_p$, n = 0, 1, 2,..., then branches approach to zeros on the imaginary axis with

positive real parts.

For instance, the root loci of the closed loop system are found for different values of n

when T_p = 0.1 sec, ω_n = 111 Hz and ς = 0.054 as shown in Figure 2-5. Branches are
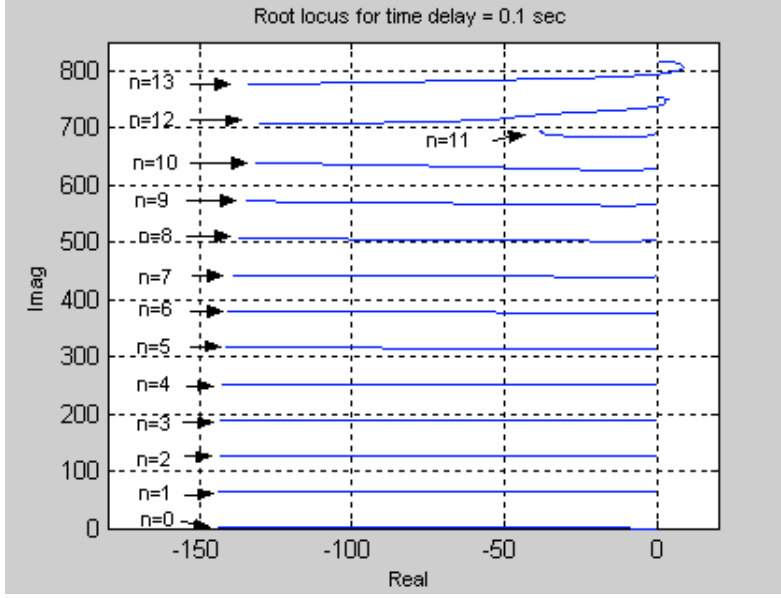
Figure 2-5. Root locus plot for the system with non-uniform load distribution when $T_p =$ 0.1 sec, $\omega_n = 111$ Hz and $\varsigma = 0.054$

apart from each other by $2\pi/T_p$ as expected. When the branch identifier n is larger or equal to 12, branches cross the imaginary axis. The results agree with the condition of $\omega_n < 2n\pi/T_p$.

When a fair of branch reach the imaginary axis in the root locus plot, the other branches being in the left hand side of the s-plane, the value of the stiffness ratio at the imaginary axis corresponds to the instability of the system. *If branches crossing the imaginary axis never return to the left-hand side of the s-plane and it is possible to find the minimum value of the stiffness ratio on the imaginary axis, then the minimum stiffness ratio is the critical parameter to determine the stability of the closed loop system.* In the present study, branches remain in the right hand side of the s-plane as the stiffness ratio is increased to infinite once crossing the imaginary axis. Therefore, the critical stiffness ratio is the minimum value of the stiffness ratio among infinitely many branch crossings

on the imaginary axis. Procedures to obtain the minimum k_c/k_m in the root locus of the

closed loop system are summarized as follows:

1) For a given value of a time delay, determine the value of branch identifier n,

    which satisfies $\omega_n < 2n\pi / T_p$.

2) The nth branch of the root locus plot is drawn as the gain k_c/k_m changes from zero

    to infinity. Detail numerical procedures to find the root in the complex plane for a

    value of k_c/k_m are described in Appendix A.3.

3) The value of k_c/k_m on the imaginary axis is calculated by an interpolation method.

4) The above procedures are repeated for increasing n until the minimum value of

    k_c/k_m on the imaginary axis is found.

For instance, the minimum k_c/k_m is found in the root locus of the closed loop system

when $T_p = 0.1$ sec, $\omega_n = 111$ Hz and $\varsigma = 0.054$ as shown in Figure 2-6. The condition of

$\omega_n < 2n\pi/T_p$ is satisfied when n is larger or equal to 12. The value of the stiffness ratio on

the imaginary axis is calculated for an increased value of n starting from 12. In this case,

the branch of $n = 12$ has the minimum value of the stiffness ratio on the imaginary axis

according to numerical calculations. The frequency corresponding to the minimum

stiffness ratio is the chatter frequency and it is larger than the natural frequency of the

system.

2.3.2. Time Delay Effect on Chatter Stability

The effect of a time delay T_p on the stability has been found for a worn tool. If the

real part of (ds/dT_p) at $s = j\omega$ is positive, then it means the root crosses the imaginary axis
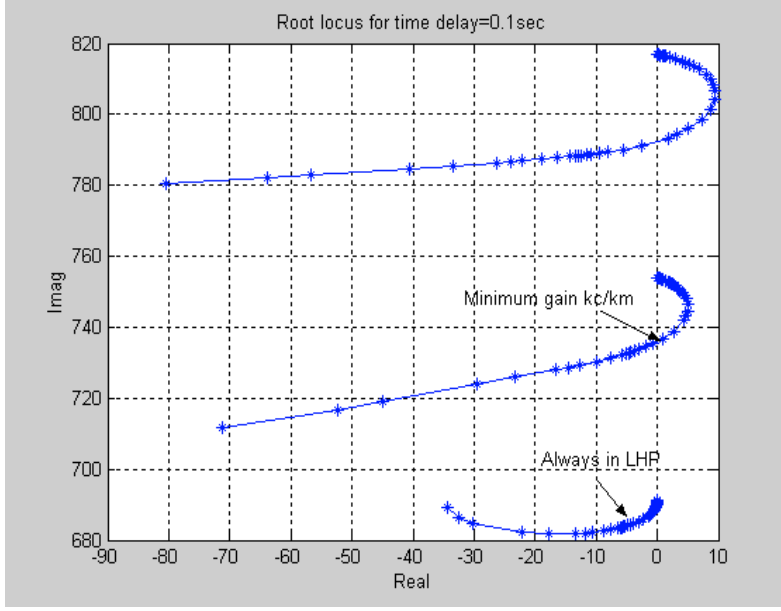
Figure 2-6. Determination of the minimum stiffness ratio in the root locus plot when $T_p =$ 0.1 sec, $\omega_n = 111$ Hz and $\varsigma = 0.054$

from the left side to the right side parallel to the real axis. Therefore, an increase in the time delay makes the system unstable with the positive real part of (ds/dT_p) at $s = j\omega$. For a worn tool with the flank wear length of l and load distribution $\sigma(\theta)$, the real part of (ds/dT_p) at $s = j\omega$ has the sign in accordance with (see Appendix A.4.):

$$\text{sgn}\left[\text{Re}\left(\frac{ds}{dT_p}\bigg|_{s=j\omega}\right)\right] = \text{sgn}\left\{\frac{1}{\omega}\left|\begin{array}{l}\left[(\frac{k_c}{k_m}\omega_n^2)^2(I_{tc}I_s - I_c I_{ts}) + (2\zeta\omega_n + \frac{k_c}{k_m}\omega_n^2 I_{tc})(2\zeta\omega_n + \frac{k_c}{k_m}\omega_n^2 I_s)\right] \\ -(2w + \frac{k_c}{k_m}\omega_n^2 I_{ts})(-\omega^2 + \omega_n^2 + \frac{k_c}{k_m}\omega_n^2 I_c)\end{array}\right|\right\}$$

(2-15)

where

30

$$I_c = \int_{-h}^{0} \sigma(\theta) \cos\theta \, d\theta, \qquad\qquad I_{tc} = \int_{-h}^{0} \sigma(\theta)\theta \cos\theta \, d\theta \qquad\qquad \text{(2-16a- b)}$$

$$I_s = \int_{-h}^{0} \sigma(\theta) \sin\theta \, d\theta, \qquad\qquad I_{ts} = \int_{-h}^{0} \sigma(\theta)\theta \sin\theta \, d\theta \qquad\qquad \text{(2-16c-d)}$$

Therefore, if the sign of equation (2-15) is positive, the high cutting speed region has more aggressive cutting conditions remaining chatter-free environment than the low cutting speed region since the time delay is the inverse of cutting speed.

2.3.3. Stability Analysis for Sharp Tools

A stability analysis for a sharp tool can be derived as a special case of a stability analysis for a worn tool. When n_s is equal to 1 and flank wear length l is negligibly small in non-uniform load distribution $\sigma(\theta)$, load distribution becomes the Dirac delta function $\delta(\theta)$. This is the load distribution corresponding to chatter stability models for a sharp tool, which have been studied for several decades (Merritt, 1965, Minis *et al.*, 1990, Olgac and Hosek, 1996). Characteristics of the root locus and the time delay effect on stability for a sharp tool can be obtained by substituting $\delta(\theta)$ into $\sigma(\theta)$ of above results. It turned out that the locations of poles and zeros for a sharp tool case are the same as those for a worn tool. In addition, branches in the root locus plot of a sharp tool have positive real parts for $\omega_n < 2n\pi/T_p$ since the integrals in equation (2-13) have the unity value. Furthermore, if $\omega^2 - \omega_n(1 + k_c/k_m) + 2\zeta^2 \omega_n^2 > 0$, the system becomes unstable as the time delay T is increased (see Appendix A.5).

2.4. Conclusion

A new modeling of chatter for facing has been developed considering the flank wear effect through non-uniform load distribution on flank wear. Having a more realistic load distribution reflecting the change of the flank wear length as well as the degree of the plastic deformation, a stability analysis has been carried out to determine the critical stability parameter for worn tools. The minimum stiffness ratio is the critical stability parameter based on characteristics of branches in the root locus found in stability analysis. It is shown that stability is affected by a time delay, characteristic parameters and the load distribution. Stability charts for sharp tools are obtained as a special case of the present chatter model.

CHAPTER 3

PREDICTIONS OF CHATTER STABILITY IN FACING

3.1. Introduction

Theoretical predictions of chatter stability are attempted with the linear modeling of

chatter in facing of hardened materials, which considers the flank wear effect through

non-uniform load distribution on a worn area of tools. In order to achieve more realistic

predictions, the unique features of hard turning such as the cutting speed effect involved

with high temperature should be considered in the predicting processes. In the present

study, the effect of the cutting speed is considered through measuring the cutting stiffness

at different cutting speed values.

After conducting a series of experiments to measure characteristic parameters

required in the proposed modeling of chatter, critical stiffness ratios are predicted for a

given range of cutting speed. In addition, a converting relation between the stiffness ratio

and the width of cut is obtained reflecting the effect of cutting speed. The flank wear

effect is examined and discussed based on resultant stability charts for different flank

wear values. A tangential stability line is proposed for more practical use of stability

charts especially in the low cutting speed range.

3.2. Measurements of Characteristic Parameters

Characteristic parameters of the tool system are determined by a series of experimental measurements. Since it is assumed that the tool system is the only flexible component in the model, the natural frequency, the damping ratio, the structural stiffness and the cutting stiffness of the tool system should be measured for the theoretical prediction of chatter stability in machining processes. The tool system in experiments consists of a top-notch type PCBN grooving insert (Kennametal NG3125R) and a tool holder (Kennametal MSR-123B) installed on a very rigid lathe (Hardinge Conquest T42SP). Furthermore, the relation between the stiffness ratio and the width of cut is obtained to plot the stability chart in terms of the width of cut instead of the stiffness ratio. Results of characteristic parameter measurements are summarized in Table 3-1.

Table 3-1. Characteristic parameters of the tool system

Workpiece	52100 hollow bar (HRC 62±1)
	Length = 76.2 mm
	Outer diameter = 41.2 mm,
	Inner diameter = 26.9 mm
Tool system	Kennametal PCBN grooving insert (NG3125R)
	Kennametal tool holder (MSR-123B)
Machine	Hardinge CNC lathe
Natural frequency	111 Hz
Damping ratio	0.054
Structural stiffness	5600 N/mm
Cutting stiffness	985 N/mm (at the width of cut = 0.508 mm and the cutting speed = 14 rps)
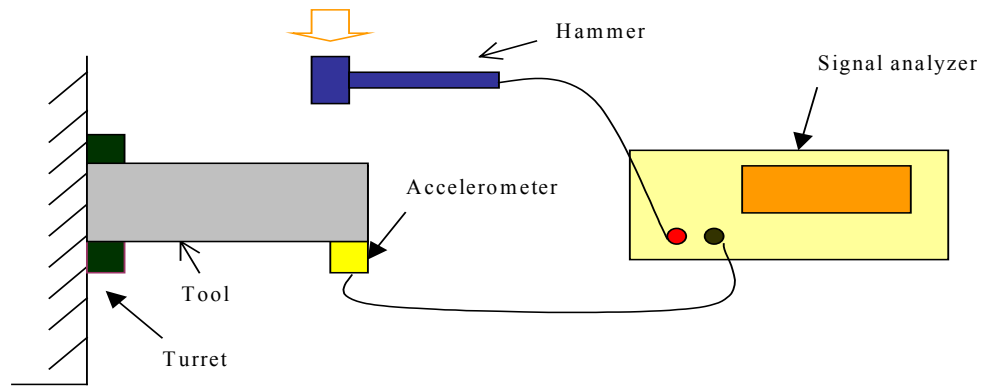
Figure. 3-1. Schematic diagram of impact testing for measuring the natural frequency ω_n and the damping ratio ζ

The natural frequency and the damping ratio of the tool system are determined by impact testing. Attaching an accelerometer on a side of the tool, frequency responses are obtained by applying an impact with a hammer at the opposite side of the tool system as shown in Figure 3-1. The peak at the lowest frequency is chosen as the natural frequency of the tool system in the averaged frequency response. The damping ratio is decided by observing how fast the magnitude of the peak of the natural frequency diminished along with frequency variation. The main processes to obtain the damping ratio of the tool system are finding two points corresponding to 0.707 times the maximum magnitude of the peak and then calculating frequency difference between these two points. As a result of impact testing, it turned out that the natural frequency of the tool system is 111 Hz and the damping ratio is 0.054.

The structural stiffness is obtained by simultaneous measurements of displacement and static force applied at the end of the workpiece through the tool. The workpiece is

76.2 mm long and assumed as a rigid body. The displacement of the tool system relative

to the 52100 hollow bar is measured by a dial gage and static force exerted on the tool tip

is measured by a dynamometer as shown in Figure 3-2. A carbide insert is used instead of

the PCBN insert for experiments of measuring the structural stiffness because the PCBN

tool tip is too brittle to endure applied static force. The structural stiffness of the tool

system is determined as 5320 N/mm.
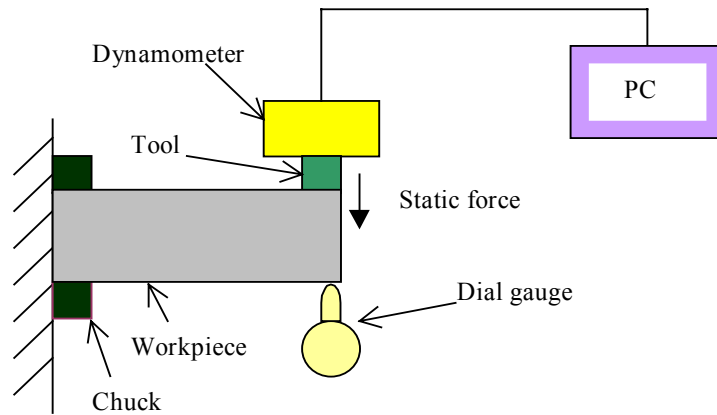
Figure 3-2. Schematic diagram of the experimental setup for measuring the structural
stiffness k_m

The cutting stiffness is found by measuring thrust force for given cutting conditions

in the cutting operation. As seen in Figure 3-3, the dynamometer connected to the tool

system of the machine measured thrust force as the cutting process is performed at the

end of the 76.2mm long work piece. In the present study, thrust force is assumed to be

linearly proportional to uncut chip thickness or the feed rate and the proportionality

constant is the cutting stiffness. Thrust force is measured for three different values of the width of cut in the range of the feed rate from 0.0127 to 0.0508 mm/rev and results are shown in Figure 3-4. All facing operations are operated with "slightly worn" tools, which have flank wear in the range from 40 to 60 μm. The slope of the curves corresponding to the cutting stiffness is increased slightly along with an increase of the width of cut. Thrust force measurements as a function of the feed rate for two different values of cutting speed are represented in Figure 3-5. Thrust force and the cutting stiffness decrease for higher cutting speed. These tendencies in force measurements are well matched with existing experimental investigations on hard turning (Chou and Evans, 1999). The cutting stiffness is determined as 985 N/mm from those cutting force data when the width of cut is 0.508 mm and the cutting speed is 14 rps.
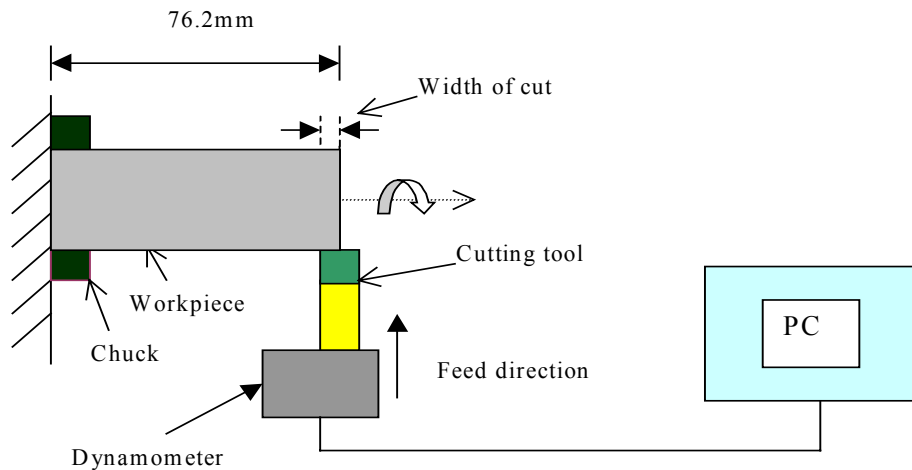
Figure 3-3. Schematic diagram of the experimental setup for measuring the cutting stiffness k_c in facing
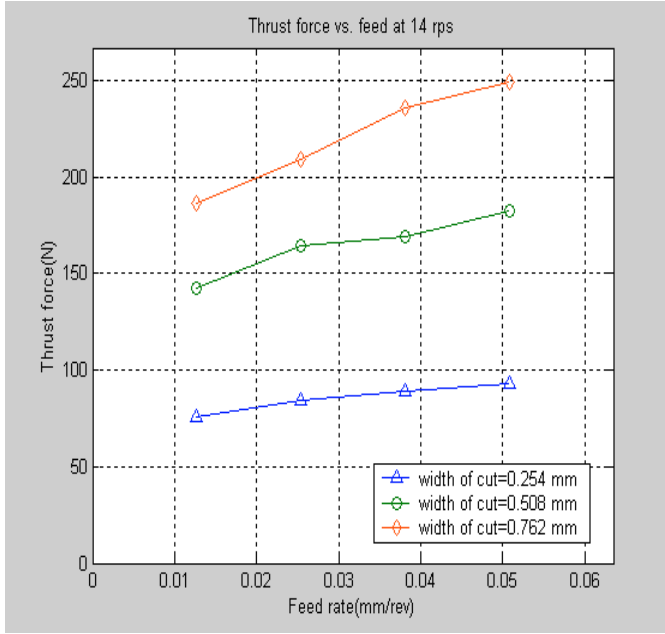
Figure 3-4. Thrust force versus the feed rate at the cutting speed of 14 rev/sec

The relation between the stiffness ratio and the width of cut is obtained from cutting

force data of machining of hardened 52100 steels. In this study, the stability chart is

plotted in terms of the width of cut instead of the stiffness ratio since the width of cut is a

more practical parameter in machining operations. Chiou and Liang (1998) converted the

stiffness ratio to the width of cut by multiplying a constant, which is derived from force

measurements. Here, the converting relation is obtained as a function of cutting speed to

reflect the dependence of the cutting stiffness on cutting speed, which is clearly shown in

Figure 3-5. The converting relation is derived as:

$$woc = (0.031\Omega + 2.6)\left(\frac{k_c}{k_m}\right) + (0.02\Omega - 0.3) \tag{3-1}$$

where *woc* is the width of cut.
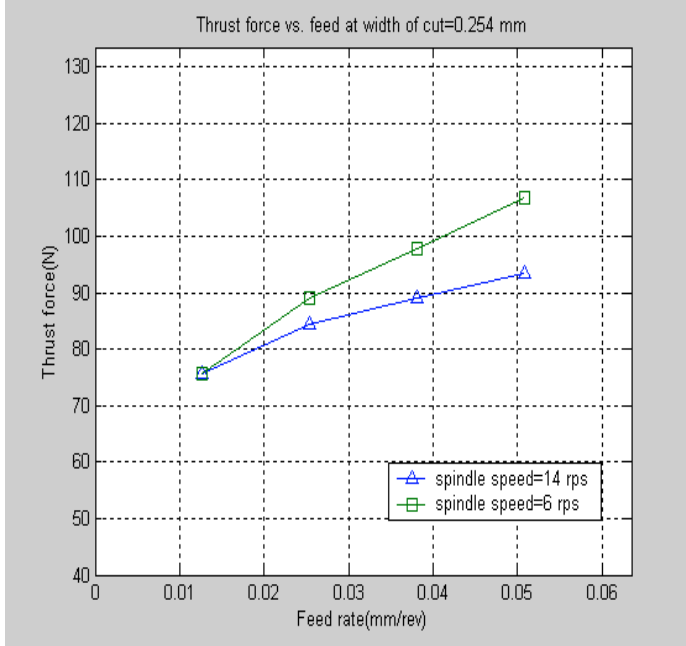
Figure 3-5. Thrust force versus the feed rate at the width of cut of 0.254 mm

3.3. Predictions of Stability Limit in Facing

Based on the stability analysis and parameter measurements in previous sections, the stability chart is obtained to predict chatter-free cutting conditions. The minimum stiffness ratio k_c/k_m is obtained in the root locus for a given time delay and the same procedures are repeated for the range of cutting speed. Since the minimum k_c/k_m is the critical stability parameter as shown in the stability analysis, the region above the minimum stiffness ratio is called the unstable region. The region below the minimum stiffness ratio is called the stable region where there is no chatter for a given cutting speed. Values of the width of cut corresponding to minimum stiffness ratios are obtained by means of the converting relation derived from force measurement data. For example,

stability lines for worn tools with different flank wear length are shown in Figure 3-6, when characteristic parameters in Table 3-1 are used. For non-uniform load distribution, the values of flank wear length l are 0.0254, 0.0762 and 0.127 mm and the value of n_s are assumed as 0.5. As shown in Figure 3-6, flank wear causes the increased stable region under the stability line. Moreover, the flank wear effect on stability predictions is examined by comparing the overall size of the stable region under the stability line for 0.0254, 0.0762 and 0.127 mm of flank wear. In order to show the dependency of the flank wear effect on cutting speed, the area of the stable region is calculated for 4 different speed divisions, respectively. As shown in Figure. 3-7, the total area under the stability line is increased as the length of flank wear is increased and the stabilizing effect is most dominantly appeared in the high-speed range ($12 < \Omega < 15$ rps).
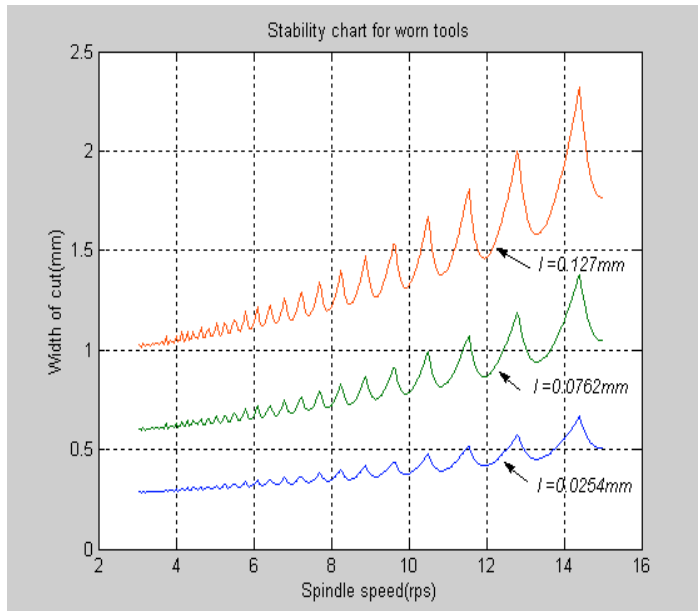
Figure 3-6. Stability chart for worn tools with different values of flank wear
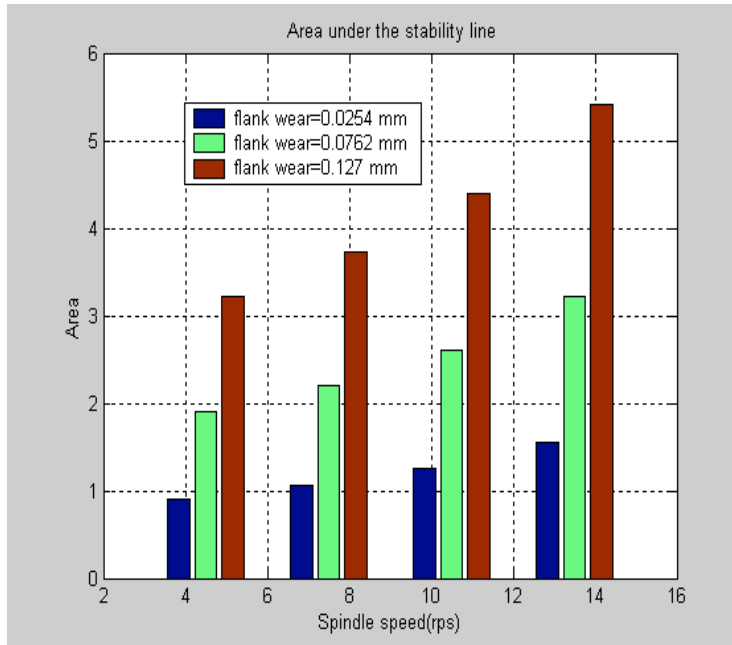
Figure 3-7. Area under the stability line for different values of flank wear.

The question of whether a stability line with more conservatism can be used as an alternative to the original stability line for more practical use of the stability chart is now examined. Because a small change in cutting speed causes a large variation in the predicted stability line in the low cutting speed range and the length of flank wear can change during machining processes, it is necessary to apply a conservative prediction for proper machining operations. In order to introduce a new stability line, the lowest points of the original stability line are connected as shown in Figure 3-8. This stability line is called a tangential stability line and it provides more conservative chatter prediction in the stability chart. As seen in Figure 3-9, the tangential stability line shows the same tendency as is shown by the original stability line for different values of flank wear. Therefore, the tangential stability line can be used as an alternative stability line,

reflecting the stabilizing effect due to flank wear. Another conservative stability line can be derived from stability charts for sharp tools. Having the same parameters, except with a load distribution of $\delta(\theta)$, the stability chart for a sharp tool is obtained as shown in Figure 3-10. In stability charts for sharp tools, the closed loop system is always stable regardless of the amount of time delay when k_c/k_m is less than $2\zeta(\zeta+1)$. This stability line is called an absolute stability line. Since a worn tool has larger stable region than a sharp tool in the stability chart as shown in Figure 3-10, the absolute stability line can be used for a worn tool as the most conservative stability guideline. In addition, the prediction for a sharp tool provides very similar stability limits compared with the stability line for the worn tool with flank wear of 0.0254 mm. Therefore, the flank wear effect can be negligible when the length of flank wear is less than 0.0254 mm.
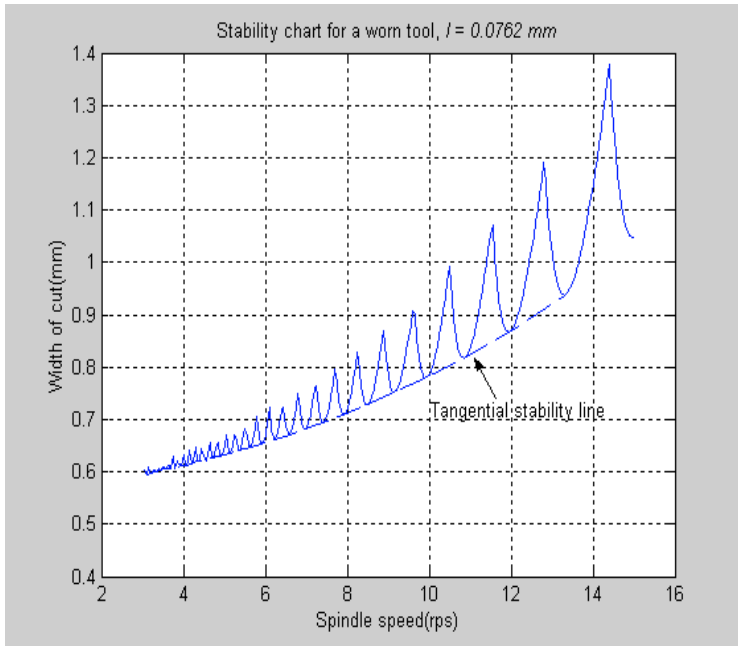
Figure 3-8. Tangential stability line in the stability chart for a worn tool with the flank wear of 0.0762 mm
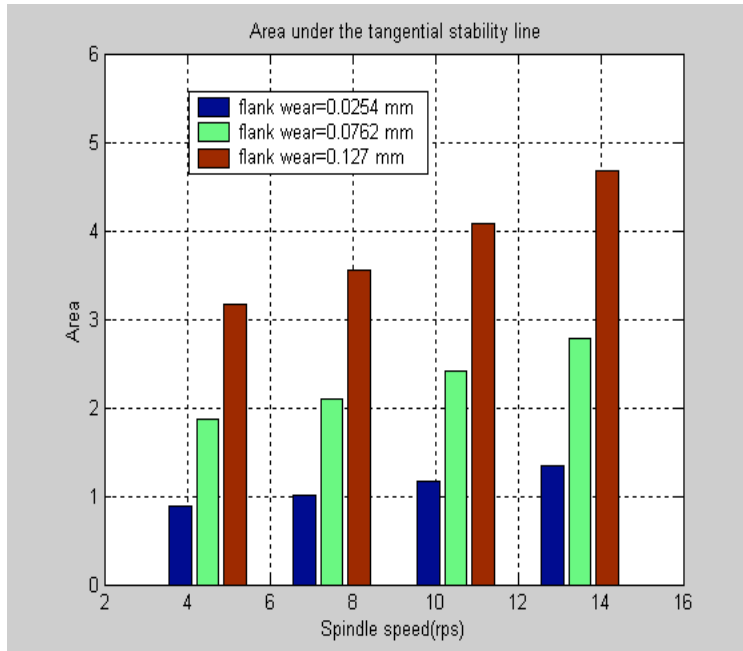
Figure 3-9. Area under the tangential stability lines for different values of flank wear
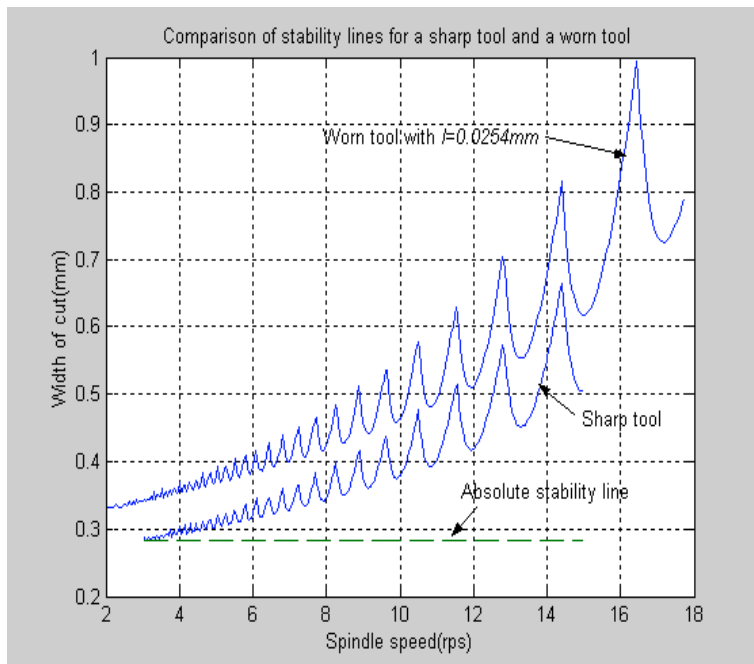
Figure 3-10. Comparison of stability lines for a sharp tool and a worn tool

3.4. Conclusion

Characteristic parameters of a tool system have been measured for predicting stability limits in facing from the proposed model. In order to consider the cutting speed effect, the values of the cutting stiffness are measured at two cutting speeds while the range of flank wear is between 40 and 60 μm. Theoretical predictions of stability have been obtained from measured characteristic parameters. The minimum stiffness ratios are obtained for a range of speed with the root locus method and then stability charts in the width of cut are plotted employing the converting relation. The stabilizing effect of flank wear is clearly shown in tangential stability lines as well original stability lines from theoretical predictions. The absolute stability line is derived as the most conservative stability guideline.

CHAPTER 4

EXPERIMENTAL RESULTS AND MODEL VALIDATION FOR FACING

4.1. Introduction

Even though there have been numerous experimental studies on chatter in mild turning, no experimental investigations regarding chatter stability in hardened steels has been attempted so far. Empirical chatter stability limits can be used not only for model validation but also for evaluating effects of various cutting parameters on stability, which allows a more reasonable consideration of physical factors in the modeling of chatter stability. Therefore, it is very important to measure chatter stability limits in order to provide reliable predictions of chatter stability for various cutting conditions. In the present study, an attempt is made to measure chatter stability limits in hard turning for the first time by conducting a series of facing operations of 52100 hollow bars. The experimental results are overlapped to predicted stability lines to validate the proposed modeling of chatter.

4.2. Chatter Stability in Facing

Experimental procedures to determine stability limits are described in detail as follows. 52100 hollow bars with the overall length of 304.8mm, which are also used in characteristic parameter measurements, are used as the workpiece in the present experiments. A top-notch type PCBN grooving insert is applied at the end of the

workpiece whose overhang length from the collar is 76.2 mm long. The width of cut is increased by 0.254 mm from the initial value of 0.508 mm under a given cutting speed over the range from 4 to 14 rev/sec until chatter is observed. The feed rate of 0.0508 mm/rev is fixed for all experiments and the feed direction is radial. In order to see the effect of flank wear, sets of tools with known flank wear length between 40 and 60 μm are prepared. The onset of chatter is identified by detecting more than 40% of the abrupt force amplitude increase in the force trace, which is collected by the dynamometer during cutting operations. Because of the radial feed direction in experiments, the structural stiffness continued to decrease as the tool advanced to the center of the workpiece. As a result, the use of a constant structural stiffness is limited to only the very early stage of the cutting process. Therefore, any detection of chatter is ignored in experiments unless it started from the early stage of the cutting process, which is limited to the first 25% of overall machining time.

The feature of chatter in hard turning has been found from experimental results. Results of the chatter stability experiments are summarized in Figure 4-1. The cross and the circle symbols correspond to no chatter and the existence of chatter, respectively. In experiments, chatter occurred as the width of cut is increased over a certain critical value under given cutting conditions. It is consistent with the result of the stability analysis that instability is induced as the stiffness ratio is larger than a critical value. The width of cut where chatter is induced is called the critical width of cut. As shown in Figure 4-1, chatter stability in machining 52100 steels has the tendency that the critical width of cut is decreased along with an increase of the cutting speed when the speed is less than 6 rev/sec (rps). After reaching the minimum value of the critical width of cut
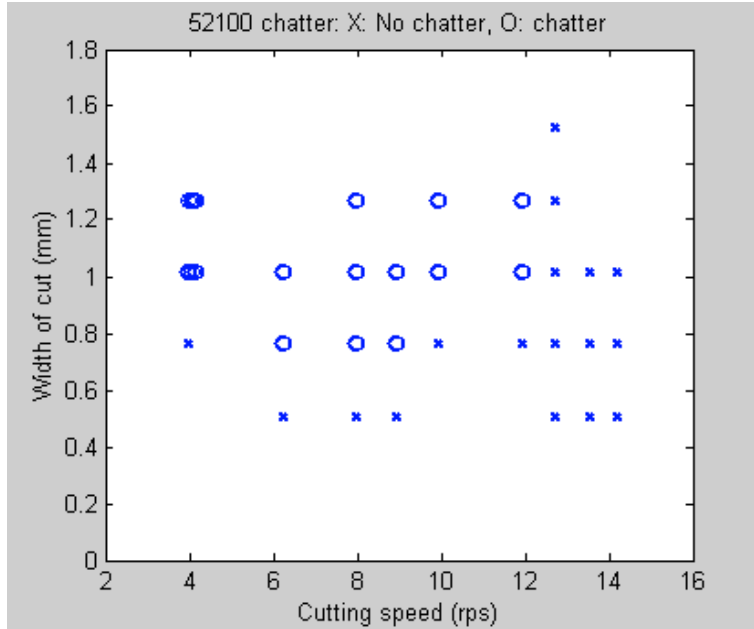
Figure 4-1. Chatter stability limits in facing

(0.762 mm) in the range of the cutting speed between 6 and 8.5 rps, the critical width of cut increases as the cutting speed increases. The critical width of cut is observed as 1.016 mm at cutting speeds between 10 and 11.5 rps. At the speed of 12.5 rps, there is no chatter observation even when the width of cut is 1.524 mm. At speeds higher than 12.5 rps, no chatter is found in experiments until the width of cut is 1.016 mm. Since instant tool failures occurred for the width of cut larger than 1.016 mm at cutting speeds higher than 12.5 rps, no data are collected for the width of cut larger than 1.016 mm. However, it is clearly seen that the critical width of cut increases rapidly in the high-speed region. This characteristic of chatter found in machining 52100 steels contrasts with that of chatter in mild turning. Chiou and Liang (1998) and Clancy and Shin (2002) performed chatter experiments with worn tools in mild turning and commonly found that the critical width of cut decreased in the high cutting speed range as the cutting speed increased.

Therefore, the abrupt increase of the stable region at a high cutting speed (> 12.5 rps) is a characteristic of hard turning chatter in contrast to that of mild turning. In addition, the standard deviation of the critical width of cut is 0.15 mm at the speed of 6 rps, which ensures the repeatibility of experiments.

4.3. Predictions versus Experimental Results

The validity of the proposed chatter model is examined by comparing experimental data with theoretical stability predictions as shown in Figure 4-2. The solid line corresponds to the predicted stability line and the region above the solid line is the unstable region. The region under the solid line is the stable region, where no chatter is predicted. Crosses represent experimental data having no chatter and circles represent chatter detection. There is good agreement between the prediction and experimental results especially in the cutting speed range between 6 and 10 rps. However, the proposed model expects a little smaller stable region in both the low (< 6 rps) and the high (>10 rps) cutting speed range. As an alternative way, an empirical model is proposed to match experimental data points for the full range of the cutting speed. The new stability line can be obtained by means of the following relation:

$$woc_{new} = [-1.5\sin(10.0/\Omega) + 2.3]woc \qquad (4\text{-}1)$$

The new stability line of the empirical model is compared with experimental data in Figure. 4-3. Since the empirical model provides a larger stable region in the low and the high-speed range, predictions of the critical width of cut are in very good agreement for the full range of the speed. Even though there is a slight deviation from experimental
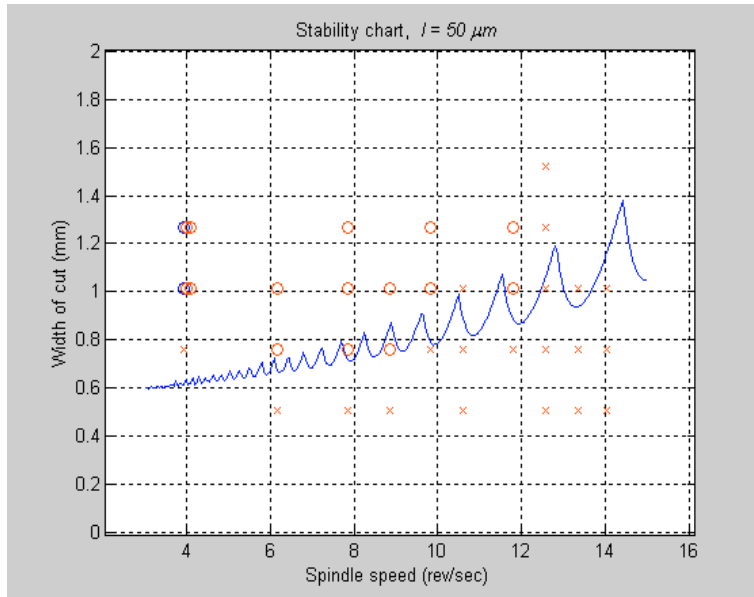
Figure 4-2. Verification of the proposed model by experimental data in facing
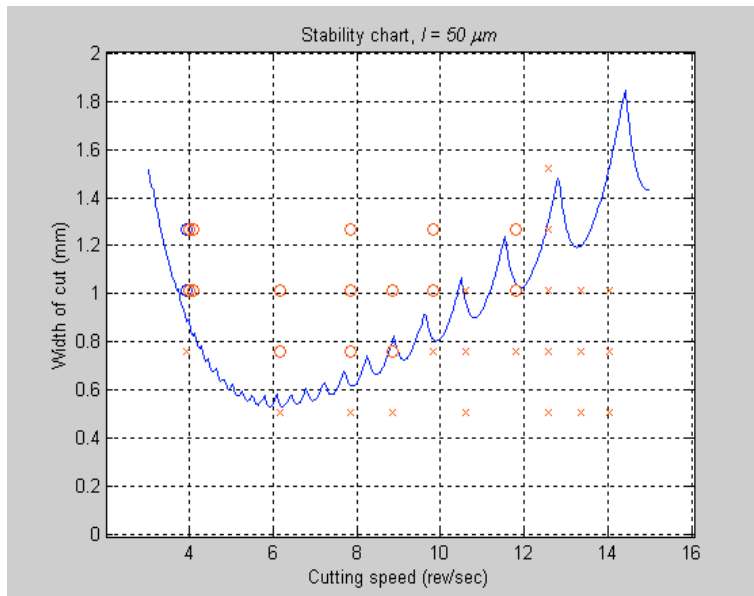
Figure 4-3. Verification of the empirical model by experimental data in facing

results at the cutting speed of 12.5 rps, the accuracy of the prediction is certainly

improved.

4.4. Conclusion

The characteristics of chatter in facing operations of 52100 steels are found through a

series of cutting tests. An abrupt increase of the stable region at high speed (>12.5 rps)

and a large stable region at very low speed (< 6rps) are discovered. The proposed model

is validated by experimental data and very good agreement is confirmed especially in the

middle range of cutting speed (6-10 rps). Furthermore, an empirical stability model is

proposed as an alternative way to predict chatter stability.

CHAPTER 5

NONLINEAR CHATTER MODELING WITH FLANK WEAR EFFECT IN

STRAIGHT TURNING

5.1. Introduction

Linear chatter models have a fundamental limit in describing nonlinear chatter

behaviors observed in practice. In addition, the amplitude of chatter is indeterminate in

the stability predictions of linear models. Furthermore, it is expected hard turning is

involved with strong nonlinearity caused by the high hardness of the workpiece and

severe wear of the tool, there is a limitation of the linear approximation of the cutting

process. Therefore, it is necessary to develop nonlinear chatter model to predict more

reliable stability limits in hard turning.

Several researchers have attempted to investigate nonlinear chatter in order to explain

nonlinear phenomena of chatter. Most of them have considered either the nonlinearity in

the structure and cutting force (Hanna and Tobias, 1974, Nayfeh *et al.,*1998) or

nonlinearity caused by friction (Wu and Liu, 1985, Nosyreva and Molinari, 1997) of

conventional mild turning. Analytical methods approximating nonlinear elements

(Nayfeh *et al.,*1998, Pratt *et al.,*1999) or direct numerical methods (Lin and Weng, 1991,

Gradisek *et al.,*2001, Deshpande and Fofana, 2001, Litak, 2002) have been employed for

nonlinear models. Both approaches have achieved some success in accounting for

nonlinear chatter behaviors. Nevertheless, all of theoretical or experimental investigations

for nonlinear chatter have been limited to conventional mild turning. In the present study, an attempt is made to develop a nonlinear chatter model for hard turning.

According to Davies (1998), nonlinearity in hard turning can arise from the geometry of the cutting tool, friction, the cutting mechanics and the mechanical behavior of the machine tool. In the present study, the structure and cutting force are considered as primary sources of nonlinearity in hard turning. Each nonlinearity is assumed to be of the form of a third-order polynomial, similar to what Hanna and Tobias (1974) suggested. In addition, since cutting force depends on cutting speed and flank wear in hard turning, the nonlinearity of cutting force is measured for different cutting speed and tool wear conditions. As friction depends on speed and tool wear, the effect of friction is taken into account implicitly in the model by measuring cutting force as a function of speed and flank wear.

Flank wear has been considered as a significant factor affecting chatter stability limits in conventional turning operations. Recently the strong relation between flank wear and cutting force in hard turning has been reported by Nakayama *et al.* (1988), Wang and Liu (1999) and Chou and Evans (1999). They suggested an increase in cutting force for larger flank wear in machining hard materials. Kishawy and Elbestawi (1999) showed tool wear also affected machined surface quality during hard turning. Davies (1998) suggested that tool wear be related with the occurrence of unstable vibration in hard turning. Therefore, it is necessary to consider the flank wear effect in the modeling of chatter to obtain more reasonable stability predictions in hard turning. In the present study, the flank wear effect on chatter stability is considered by introducing non-uniform load distribution on the flank wear area.

Traditional analytical tools for dealing with the stability analysis of nonlinear systems include describing function, phase plane, and Lyapunov stability. These simplifications may be satisfactory so long as the resulting solutions agree with experimental results. In the present study, the describing function method is used to simplify nonlinearity for stability analysis.

5.2. Modeling for Nonlinear Chatter in Straight Turning

There have been successful applications of 1-DOF chatter models, which agreed well with experimental results and are mathematically simple (Chiou and Liang, 1998). Considering mathematical complexity due to a time delay and nonlinearity in the present study, a 1-DOF model is selected for the modeling of nonlinear chatter for a worn tool. Furthermore, since the performance of machining process is most sensitive to the radial vibration, chatter is assumed to move only in the radial direction.

The cutting edge of an insert does not move normal to the surface of the workpiece in straight turning. As a result, the orthogonal cutting condition where tangential and radial direction forces are dominant is no longer valid. Thus, oblique cutting conditions should be considered in the modeling process for straight turning. In addition, the direction of cutting force is affected by the tool geometry such as the side cutting edge angle since the radius of tool nose is larger than the depth of cut. For cutting tools with substantial tool nose radius, the side cutting edge angle C_s of the tool is calculated as the angle between the centerline and the tool nose tangential line, which is tangential to the intersection point between the half depth of cut and the tool. Figure 5-1 is drawn based on the

proportion between the tool nose radius and the depth of cut, which are used in the present study. The tool nose radius of the insert (Kennametal CNGA 432T) is about 6 times larger than the most frequently used depth of cut, 0.127 mm. It is turned out that the value of C_s is larger than 45° due to the large nose radius and the small depth of cut. Hence, radial chatter is still valid in straight turning cases.

In the present study, the workpiece is assumed to be a mass-spring-damper system, which is able to move only in the radial direction x as shown in Figure 5-2. The cutting tool with a certain C_s is moving along the axial direction of the workpiece, which is defined as the z coordinate in Figure 5-2. In order to consider the regenerative effect for radial chatter in oblique cutting, the relationship between C_s and the radial displacement of the bar is taken into account. If there is a displacement variation $\Delta\delta$ for two consecutive revolutions of the workpiece in the radial direction, then the displacement variation along the direction normal to the side cutting edge is $\Delta\delta \sin(C_s)$ as shown in Figure 5-2. Because the feed direction in straight turning is axial, the radial cutting stiffness k_c corresponds to the variation of radial force divided by the displacement in the feed direction. Consequently, the radial force due to the variation $\Delta\delta$ in the radial direction is $k_c\Delta\delta \sin C_s \cos C_s$.

Considering the nonlinearity in structure as a third-order polynomial, the equation of motion in the x direction is given as the following:

$$m\ddot{x}(t) + c\dot{x}(t) + k_m[x(t) + \beta_1 x^2(t) + \beta_2 x^3(t)] = \Delta F_x(t) \tag{5-1}$$

where m is the mass of the workpiece, c is the damping coefficient, k_m is the structural stiffness, and $\Delta F_x(t)$ is the amount of variation in the x-component of cutting force. In addition β_1 and β_2 are the coefficients for the quadratic and the cubic terms, respectively,
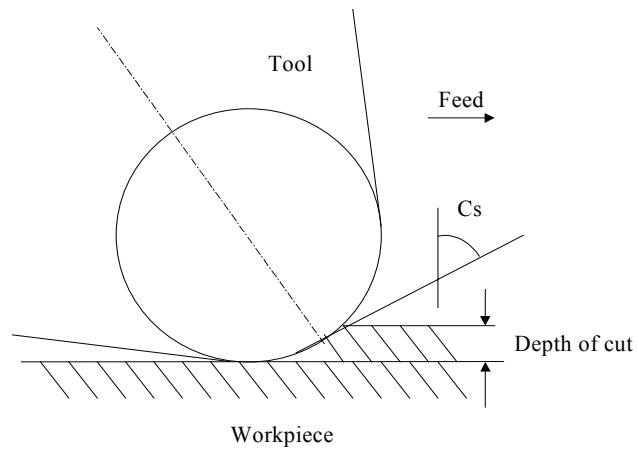
Figure 5-1. Schematic diagram of the tool geometry in hard turning
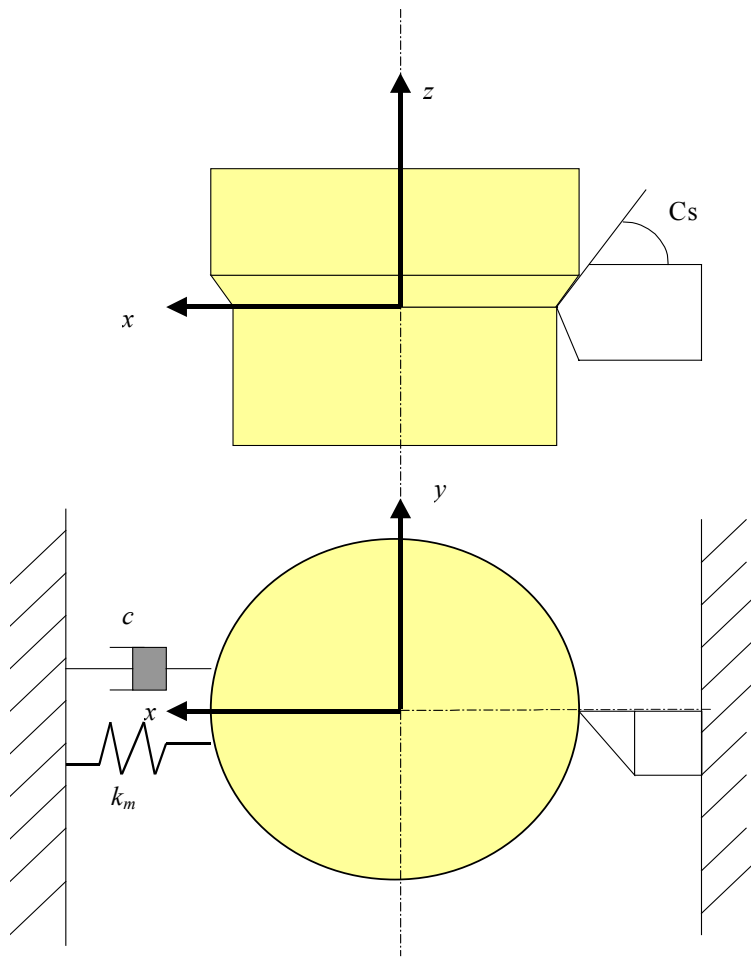
Figure 5-2. Schematic diagram of the tool-workpiece system in straight turning

in the nonlinear structural stiffness. In the present study, it is assumed that each

coefficient linearly depends on the stiffness ratio k_c/k_m so that

$$\beta_1 = \lambda_1 \frac{k_c}{k_m} + \eta_1 \qquad\qquad (5\text{-}2a)$$

$$\beta_2 = \lambda_2 \frac{k_c}{k_m} + \eta_2 \qquad\qquad (5\text{-}2b)$$

where λ_1, λ_2, η_1, and η_2 are constants.

Combining the regenerative effect and the nonlinear cutting stiffness, nonlinear

cutting force $\Delta F_x(t)$ is given as

$$\Delta F_x(t) = k_c \left\{ x(t) - x_T + c_1 [x(t) - x_T]^2 + c_2 [x(t) - x_T]^3 \right\} \sin C_s \cos C_s \qquad (5\text{-}3)$$

where x_T is $x(t\text{-}T_p)$, which is the displacement from the equilibrium position at the

previous rotation, T_p is the period, k_c is the cutting stiffness in the radial direction, c_1 and

c_2 are the coefficients for the quadratic and the cubic terms, respectively, in the nonlinear

cutting stiffness term. Each coefficient is assumed to be linearly proportional to the

stiffness ratio k_c/k_m as

$$c_1 = \lambda_3 \frac{k_c}{k_m} + \eta_3 \qquad\qquad (5\text{-}4a)$$

$$c_2 = \lambda_4 \frac{k_c}{k_m} + \eta_4 \qquad\qquad (5\text{-}4b)$$

where λ_3, λ_4, η_3, and η_4 are constant coefficients.

Furthermore, the non-uniform load distribution on flank wear in equation (2-6) is

introduced to add the flank wear effect in the chatter model. As a result, $\Delta F_x(t)$ in

equation (5-3) is expressed as the following:

$$\Delta F_x = -k_c \int_{-h}^{0} \begin{cases} x(t+\theta) - x(t-T_P+\theta) \\ +c_1[x(t+\theta) - x(t-T_P+\theta)]^2 \\ +c_2[x(t+\theta) - x(t-T_P+\theta)]^3 \end{cases} \sigma(\theta)d\theta \sin C_s \cos C_s \qquad (5\text{-}5)$$

The cutting system can be represented as a closed loop including a nonlinear element

as shown in Figure 5-3. In the present study, the nonlinear element of the system is

approximately represented by the describing function. It is assumed that higher-frequency

harmonics can be neglected, compared with the fundamental component. If even

nonlinearity is considered, it is necessary to introduce a bias term in the input signal to

the nonlinear element in order to keep the harmonic balance through the closed loop.

Consequently, the input $x(t)$ consists of bias u_0 and a sinusoidal signal u_1 such that

$$x(t) = u_0 + u_1 = A_0 + A_1 \sin(\omega t) \qquad (5\text{-}6)$$

In the present study, it is assumed that the nonlinear output $W(t)$ from the nonlinear

element can be approximated by the first three terms in a Fourier series, viz.,

$$W(t) \approx a_0 + a_1 \cos(\omega t) + b_1 \sin(\omega t) \qquad (5\text{-}7)$$

where $\quad a_0 = \dfrac{1}{2\pi} \int_0^{2\pi} W(t)d(\omega t) \qquad (5\text{-}8\text{a})$

$$a_1 = \frac{1}{\pi} \int_0^{2\pi} W(t)\cos(\omega t)d(\omega t) \qquad (5\text{-}8\text{b})$$

$$b_1 = \frac{1}{\pi} \int_0^{2\pi} W(t)\sin(\omega t)d(\omega t) \qquad (5\text{-}8\text{c})$$

Describing functions for the signal consisting of the bias and the pure sinusoidal are

$$N_0 = \frac{a_0}{A_0} = \frac{1}{2\pi A_0} \int_0^{2\pi} W[A_0 + A_1 \sin(\omega t)]d(\omega t) \qquad (5\text{-}9)$$

$$N_1 = \frac{(b_1 + ja_1)}{A_1} = \frac{1}{\pi A_1} \int_0^{2\pi} W[A_0 + A_1 \sin(\omega t)][\sin(\omega t) + j\cos(\omega t)]d(\omega t) \qquad (5\text{-}10)$$
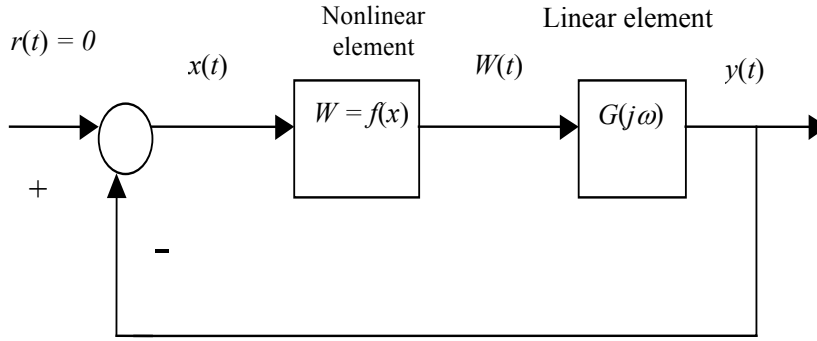
Figure 5-3. Closed loop system with a nonlinear element

When the time delay T_p exists, the delayed input $x_T(t)$ is given as the following:

$$x_T(t) = x(t - T_p) = A_0 + A_1 \sin \omega(t - T_p) = u_0 + u_{1T} \tag{5-11}$$

Substituting equation (5-5) for the right hand side of equation (5-1), the equation of

motion, including the non-uniform load distribution and nonlinearity, is given as

$$
\begin{aligned}
& m\ddot{x} + b\dot{x} + k_m(x + \beta_1 x^2 + \beta_2 x^3) \\
& = -k_c \int_{-h}^{0} \left\{ \begin{array}{l} x(t + \theta) - x(t - T_p + \theta) \\ + c_1[x(t + \theta) - x(t - T_p + \theta)]^2 \\ + c_2[x(t + \theta) - x(t - T_p + \theta)]^3 \end{array} \right\} \sigma(\theta) d\theta \sin C_s \cos C_s
\end{aligned}
\tag{5-12}
$$

After moving the nonlinear terms into the right hand side of the above equation, the

nonlinear output $W(t)$ is found to be

$$
W(t) = k_c \int_{-h}^{0} \left\{ \begin{array}{l} x(t + \theta) - x(t - T_p + \theta) \\ + c_1[x(t + \theta) - x(t - T_p + \theta)]^2 \\ + c_2[x(t + \theta) - x(t - T_p + \theta)]^3 \end{array} \right\} \sigma(\theta) d\theta \sin C_s \cos C_s + k_m \beta_1 x^2 + k_m \beta_2 x^3
$$

$$\tag{5-13}$$

After approximating the nonlinear output $W(t)$ as in equation (5-7), the describing function for the bias term in equation (5-9) is derived as

$$N_0 = \int_{-h}^{0} k_c c_1 \left[\frac{A_1^2}{A_0} - \frac{A_1^2}{A_0} \cos(\omega T_p) \right] \sigma(\theta) d\theta \sin^2 C_s + k_m \beta_1 \left(A_0 + \frac{A_1^2}{2A_0} \right) + k_m \beta_2 \left(A_0^2 + \frac{3}{2} A_1^2 \right)$$

(5-14)

The real part of the describing function N_1 in equation (5-10), which corresponds to the first harmonics of $W(t)$ is given as

$$N_{1_{real}} = \int_{-h}^{0} \left\{ \begin{array}{l} k_c [\cos(\omega\theta) - \cos(\omega\theta - \omega T_p)] \\ + \frac{3}{4} k_c c_2 A_1^2 \left[\begin{array}{l} \cos(\omega\theta) - 3\cos(\omega T_p)\cos(\omega\theta) \\ -\sin(\omega T_p)\sin(\omega\theta) + 3\cos(\omega T_p)\cos(\omega\theta - \omega T_p) \\ -\sin(\omega T_p)\sin(\omega\theta - \omega T_p) - \cos(\omega\theta - \omega T_p) \end{array} \right] \end{array} \right\} \sigma(\theta) d\theta \sin C_s \cos C_s$$
$$+ 2k_m \beta_1 A_0 + k_m \beta_2 \left(3A_0^2 + \frac{3}{4} A_1^2 \right)$$

(5-15)

The imaginary part of the describing function N_1 is found as

$$N_{1_{imag}} = \int_{-h}^{0} \left\{ \begin{array}{l} k_c [\sin(\omega\theta) - \sin(\omega\theta - \omega T_p)] \\ + \frac{3}{4} k_c c_2 A_1^2 \left[\begin{array}{l} \sin(\omega\theta) - 3\cos(\omega T_p)\sin(\omega\theta) \\ +\sin(\omega T_p)\cos(\omega\theta) + 3\cos(\omega T_p)\sin(\omega\theta - \omega T_p) \\ +\sin(\omega T_p)\cos(\omega\theta - \omega T_p) - \sin(\omega\theta - \omega T_p) \end{array} \right] \end{array} \right\} \sigma(\theta) d\theta \sin C_s \cos C_s$$

(5-16)

With these describing functions in the equations (5-14), (5-15) and (5-16), the two harmonic balance equations are

$$N_0 G(0) = N_0 \frac{1}{k_m} = -1$$

(5-17)

$$N_1 G(j\omega) = -1$$

(5-18)

where the linear element $G(j\omega)$ shown in Figure 5-3 is

$$G(s) = \frac{Y(s)}{W(s)} = \frac{-X(s)}{W(s)} = \frac{1}{ms^2 + bs + k_m} \tag{5-19}$$

Substituting equations (5-14) and (5-19) into equation (5-17), one obtains the first

harmonic balance equation as

$$A_1^2 \int_{-h}^{0} \frac{k_c}{k_m} c_1 \left[1 - \cos(\omega T_p)\right] \sigma(\theta) d\theta \sin C_s \cos C_s + \beta_1 \left(A_0^2 + \frac{A_1^2}{2}\right) + \beta_2 \left(A_0^3 + \frac{3}{2} A_1^2 A_0\right) + A_0 = 0$$

$$\tag{5-20}$$

Substituting equations (5-15) and (5-19) into equation (5-18), the second harmonic

balance equation is found to be

$$\int_{-h}^{0} \left\{ \begin{array}{l} \frac{k_c}{k_m}\left[\cos(\omega\theta) - \cos(\omega\theta - \omega T_p)\right] \\ \\ + \frac{3}{4}\frac{k_c}{k_m} c_2 A_1^2 \begin{bmatrix} \cos(\omega\theta) - 3\cos(\omega T_p)\cos(\omega\theta) \\ -\sin(\omega T_p)\sin(\omega\theta) + 3\cos(\omega T_p)\cos(\omega\theta - \omega T_p) \\ -\sin(\omega T_p)\sin(\omega\theta - \omega T_p) - \cos(\omega\theta - \omega T_p) \end{bmatrix} \end{array} \right\} \sigma(\theta) d\theta \sin C_s \cos C_s$$

$$+ 2\beta_1 A_0 + \beta_2 \left(3A_0^2 + \frac{3}{4} A_1^2\right) = \frac{\omega^2}{\omega_n^2} - 1$$

$$\tag{5-21}$$

Substituting equations (5-16) and (5-19) into equation (5-18), the third harmonic balance

equation can be found as

$$\int_{-h}^{0} \left\{ \begin{array}{l} \frac{k_c}{k_m}\left[\sin(\omega\theta) - \sin(\omega\theta - \omega T_p)\right] \\ \\ + \frac{3}{4}\frac{k_c}{k_m} c_2 A_1^2 \begin{bmatrix} \sin(\omega\theta) - 3\cos(\omega T_p)\sin(\omega\theta) \\ +\sin(\omega T_p)\cos(\omega\theta) + 3\cos(\omega T_p)\sin(\omega\theta - \omega T_p) \\ +\sin(\omega T_p)\cos(\omega\theta - \omega T_p) - \sin(\omega\theta - \omega T_p) \end{bmatrix} \end{array} \right\} \sigma(\theta) d\theta \sin C_s \cos C_s = -\frac{2\zeta\omega}{\omega_n}$$

$$\tag{5-22}$$

The nonlinear chatter model for sharp tools is derived from that of worn tools for the purpose of examining the flank wear effect on predictions. When tools are ideally sharp, the non-uniform load distribution corresponds to the Dirac delta function as shown in equation (2-11). In that case, the equation of motion in the x direction is

$$m\ddot{x} + b\dot{x} + k_m(x + \beta_1 x^2 + \beta_2 x^3) = -k_c[(x - x_T) + c_1(x - x_T)^2 + c_2(x - x_T)^3]\sin C_s \cos C_s$$

(5-23)

After rearranging equation (5-23), the nonlinear output $W(t)$ becomes

$$W(t) = k_c[(x - x_T) + c_1(x - x_T)^2 + c_2(x - x_T)^3]\sin C_s \cos C_s + k_m\beta_1 x^2 + k_m\beta_2 x^3 \quad (5\text{-}24)$$

After approximating $W(t)$ in equation (5-24) by the describing functions method, the three harmonic balance equations are

$$\frac{A_1^2}{A_0}\left(k_c c_1(1 - \cos\omega T)\sin C_s \cos C_s + \frac{1}{2}k_m\beta_1 + \frac{3}{2}k_m\beta_2 A_0\right) + k_m + k_m\beta_1 A_0 + k_m\beta_2 A_0^2 = 0$$

(5-25)

$$\frac{k_c}{k_m}(1 - \cos\omega T)\left[1 + \frac{3}{2}c_2 A_1^2(1 - \cos\omega T)\right]\sin C_s \cos C_s + 2\beta_1 A_0 + \beta_2(3A_0^2 + \frac{3}{4}A_1^2) = \frac{\omega^2}{\omega_n^2} - 1$$

(5-26)

$$\frac{k_c}{k_m}\sin\omega T\left[1 + \frac{3}{2}c_2 A_1^2(1 - \cos\omega T)\right]\sin C_s \cos C_s = \frac{-2\zeta\omega}{\omega_n} \quad (5\text{-}27)$$

Furthermore, a nonlinear chatter model without even nonlinearity is developed as a special case of the model for sharp tools. Without the bias term coming from even nonlinearity, much simpler harmonic balance equations are derived. If only odd nonlinearity exists in the structure and cutting force, the equation of motion is simply

$$m\ddot{x} + b\dot{x} + k_m x + k_m\beta_2 x^3 = -k_c(x - x_T)\sin C_s \cos C_s - k_c c_2(x - x_T)^3 \sin C_s \cos C_s \quad (5\text{-}28)$$

The harmonic balance equations corresponding to equation (5-28) can be found by substituting the zero value for β_1 and c_1 into equations (5-26) and (5-27), yielding

$$\frac{k_c}{k_m}(1-\cos\omega T)\left[1+\frac{3}{2}c_2 A_1^2(1-\cos\omega T)\right]\sin C_s \cos C_s + \frac{3}{4}A_1^2 k_m \beta_2 = \frac{\omega^2}{\omega_n^2}-1 \qquad (5\text{-}29)$$

$$\frac{k_c}{k_m}\sin\omega T\left[1+\frac{3}{2}c_2 A_1^2(1-\cos\omega T)\right]\sin C_s \cos C_s = \frac{-2\zeta\omega}{\omega_n} \qquad (5\text{-}30)$$

5.3. Stability Analysis

There are four nonlinear coefficients β_1, β_2, c_1, and c_2 in the harmonic balance equations (5-20), (5-21) and (5-22). In the present study, either the nonlinear structural stiffness or the nonlinear cutting stiffness is assumed to be constant depending on the feed direction of the turning operation. As a result, two nonlinear coefficients remain as unknowns, which depend on the stiffness ratio as shown in equations (5-2a), (5-2b), (5-4a) and (5-4b). Therefore, the harmonic balance equations as well as two equations for nonlinear coefficients are required to be solved simultaneously. As a result, the values of the stiffness ratio k_c/k_m, the chatter frequency ω, offset amplitude A_0 and two nonlinear coefficients are determined as a solution of the equations for given values of cutting speed Ω and sinusoidal input amplitude A_1. However, the presence of the time delay results in infinitely many solutions of the equations. Hence, it is necessary to determine the critical stability parameter among infinitely many solutions. In the present study, the minimum stiffness ratio is found as the critical stability parameter. Newton's method is employed in order to find solutions satisfying the five equations simultaneously. The procedures to determine the stability limits are represented as a flow chart in Figure 5-4.
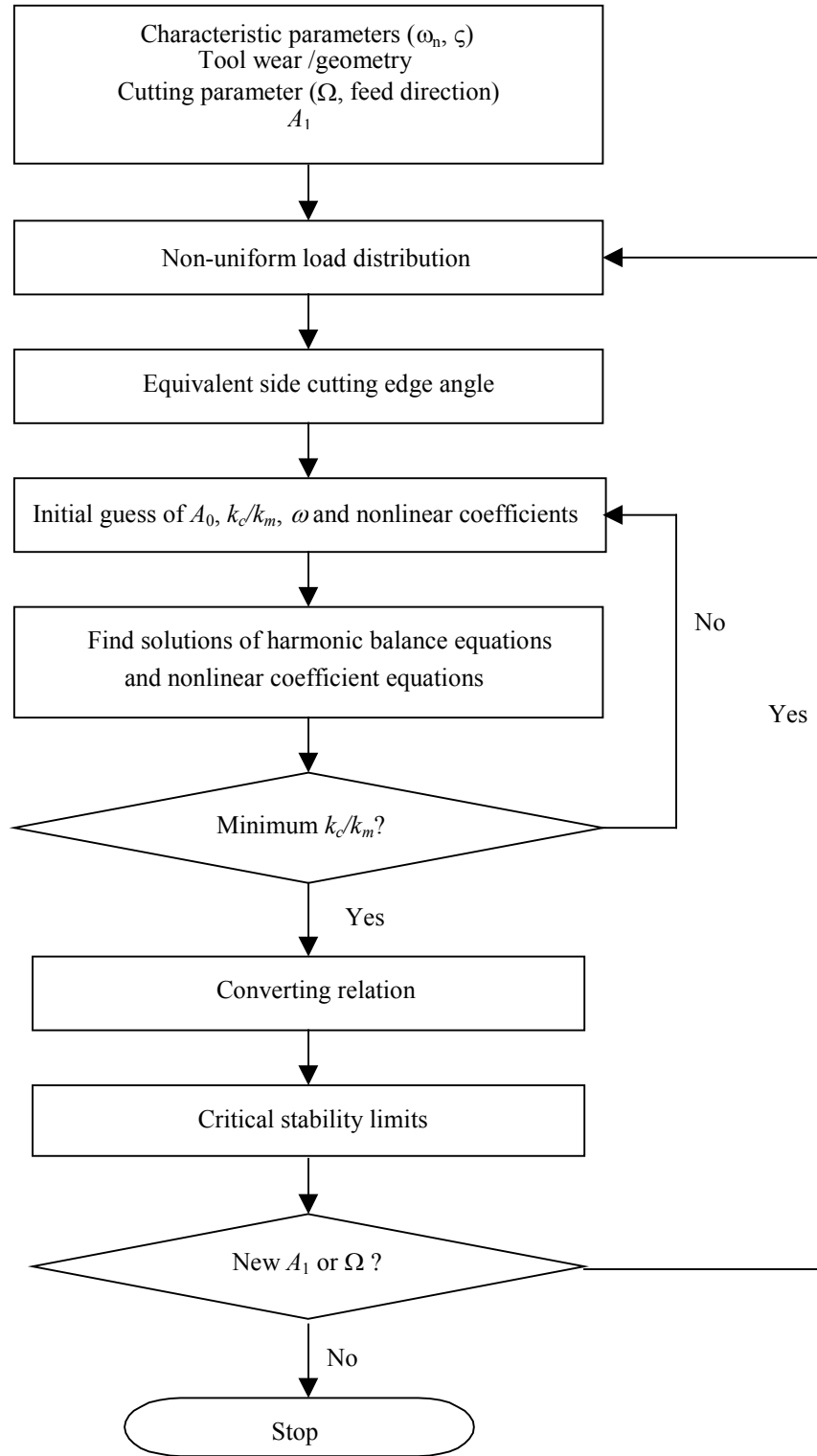
Figure 5-4. Flow chart of the procedures to determine critical stability limits

After deciding critical stability parameters, stability charts are plotted in the axes of A_1, k_c/k_m, and Ω. The stability chart on the plane of k_c/k_m and Ω corresponds to the conventional stability chart from linear models except the finite value of A_1 is designated. Furthermore, the stability chart on the plane of A_1 and k_c/k_m is convenient to predict the evolution of a limit cycle. Each solution obtained from harmonic balance equation is a limit cycle, which has the amplitude of A_1 and the frequency of ω.

When the even terms of nonlinearity are ignored, equation (5-20) is vanished. As a result, the minimum k_c/k_m for given values of A_1 and Ω is obtained from equations (5-21), (5-22) and the equation for one of odd nonlinear coefficients.

5.4. Conclusion

The modeling of chatter has been carried out considering nonlinearity and flank wear in hard turning. Three harmonic balance equations are derived as a result of approximating nonlinear elements with describing functions. Adding two equations for nonlinear coefficients, critical cutting parameters are determined by solving five equations simultaneously for given cutting conditions. The values of of k_c/k_m, ω, A_0 and two nonlinear coefficients are determined as a solution for given values of A_1 and Ω. As a special case, the nonlinear model without even nonlinearity is developed for sharp tools.

CHAPTER 6

MEASUREMENTS OF CHARACTERISTIC PAREMETERS AND REDICTIONS OF

CHATTER STABILITY IN STRAIGHT TURNING

6.1. Introduction

There are two available feed directions in straight turning. One is called "outward

turning" (feeding toward the end of the workpiece); the other is called "inward turning"

(feeding toward the collar). Each feed direction has characteristics to take into account.

Since the critical stability limit can be found for a fixed depth of cut for outward turning,

the nonlinearity in cutting force is required to measure only for the corresponding depth

of cut. However, it should be noticed that the feed direction of outward turning is rarely

used in practice. In contrast, inward turning has the conventional feed direction.

However, laborious works are required to measure the nonlinearity of cutting force for

various values of the depth of cut. In the present study, both feed directions of straight

turning are considered in chatter predictions compromising these features. Outward

turning is carried out to predict stability limits based on completely measured

nonlinearity. Inward turning is performed for the practical use of the chatter model

although the variation of nonlinearity with the depth of cut is assumed to be negligible.

Nonlinearity in the chatter model is considered through the structural stiffness and the

cutting stiffness. Thus, accurate measurements of the nonlinear stiffness are crucial for

reliable theoretical stability predictions. Even though there have been some published

theoretical attempts (Nayfeh *et al*., 1998, Kalmar-Nagy *et al*., 2001) to consider the nonlinear stiffness in chatter stability problems, most research has relied on a limited number of existing experimental data of nonlinearity in mild turning. Unfortunately, there have been no experimental results of the nonlinear cutting and structural stiffness in hard turning. Hence, it is very significant to conduct reliable measurements of the nonlinear stiffness not only for the accurate predictions of the current study, but also for possible applications in other nonlinear models in the future.

Based on characteristic parameters, three-dimensional stability charts are obtained for various tool conditions and nonlinearities The effects of each nonlinearity and flank wear on stability limits are discussed.

6.2. Measurements of Characteristic Parameters

6.2.1. Natural Frequency and Damping Ratio

The natural frequency and the damping ratio of the flexible workpiece are derived through impact testing. The same experimental setup shown in Figure 3-1 is used for the test. A hardened 52100 steel bar 203.2 mm in length, which is used in experiments for chatter stability limits, is also examined in impact testing. It is assumed that the workpiece is flexible in the radial direction. The hammer generated an impact on the bar in the radial direction and the output signal is collected through an accelerometer attached on the opposite side of the bar. As a result, a frequency response is obtained from a signal analyzer after averaging ten repeated hammer tests as shown in Figure 6-1. The natural frequency corresponds to the highest peak of the frequency response, and the damping
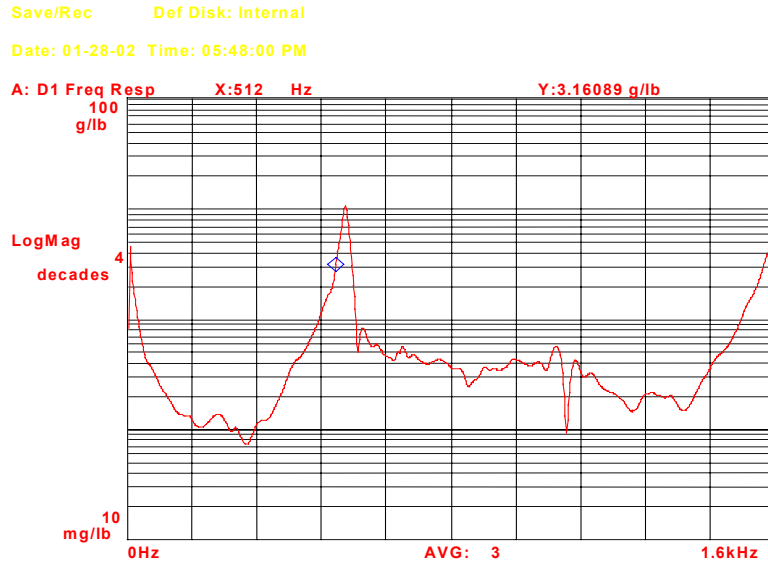
Figure 6-1. Averaged frequency response from impact testing.

ratio is obtained by measuring the variation of frequency for a nominal amplitude change of the peak. The natural frequency and the damping ratio of the workpiece are determined from the frequency response as 540 Hz and 0.013, respectively.

6.2.2. Cutting Stiffness

The cutting stiffness is determined by measuring the variation of cutting force with the feed rate. The proposed models implicitly consider the hardness of material through the cutting stiffness, since hardness is strongly related with cutting force. In the present study, the cutting stiffness is measured through a series of experiments for both feed directions of straight turning. Furthermore, since cutting force in hard turning is influenced by flank wear and cutting speed (Dawson, 2002), the variation of cutting force is measured for the separate ranges of flank wear and cutting speed.

The cutting stiffness for outward turning is measured by conducting cutting operations for a given range of the feed rate with a fixed value of the depth of cut, which correspond to condition index 1 – 4 in Table 6-1. On the other hand, the cutting stiffness for inward turning is measured for various values of the depth of cut by performing cutting tests corresponding to condition indices between 5 and 12.

Table 6-1. Conditions of cutting experiments for the cutting stiffness.

Condition index	The depth of cut (mm)	The range of flank wear (µm)	Cutting speed (rev/min)	The range of feed (mm/rev)
1	0.1270	40 – 60	450	0.0254 – 0.102
2	0.1270	40 – 60	800	0.0254 – 0.102
3	0.1270	140 – 160	450	0.0254 – 0.102
4	0.1270	140 – 160	800	0.0254 – 0.102
5	0.0635	40 – 60	450	0.0254 – 0.102
6	0.0635	40 – 60	700	0.0254 – 0.102
7	0.1270	40 – 60	450	0.0254 – 0.102
8	0.1270	40 – 60	700	0.0254 – 0.102
9	0.1905	40 – 60	450	0.0254 – 0.102
10	0.1905	40 – 60	700	0.0254 – 0.102
11	0.2540	40 – 60	450	0.0254 – 0.102
12	0.2540	40 – 60	700	0.0254 – 0.102

6.2.2.1. Nonlinear Cutting Stiffness for Outward Turning

The proposed models reflect the effects of nonlinearity as well as material hardness on chatter stability by the nonlinear cutting stiffness. Furthermore, nonlinearity caused by friction, which is a function of cutting speed and tool wear is implicitly considered in the model by measuring the cutting stiffness for the separate range of cutting speed and flank wear. In this study, cutting tests are performed at 450 rpm and 800 rpm with two groups

of tools. The first group is called "slightly worn tools" with the flank wear range between 40 and 60 μm. The second "very worn tools" group has the flank wear range between 140 and 160 μm.

The schematic experimental set up to determine the value of the cutting stiffness is shown in Figure 6-2. The specifications of the workpiece and the tool are summarized in Table 6-2. Cutting operations are conducted at the end of a workpiece for the cutting range of 7.62 mm. The depth of cut is fixed to 0.127 mm. The overhang length of the workpiece is fixed to 101.6 mm. Each set of experiments determined the value of the cutting stiffness measuring the variation of radial force over the feed rate in the range of [0.0254 0.102] mm/rev. Cutting tests are repeated for the same cutting condition to improve the precision of cutting force measurements. The results of measured cutting forces are summarized in Table 6-3.

The 95% confidence interval means the average value is found within the interval for a 95% chance. The confidence interval is then

$$\text{Confidence interval} = \left[M - t_\alpha \frac{\sigma_p}{\sqrt{n_p}}, M + t_\beta \frac{\sigma_p}{\sqrt{n_p}} \right] \tag{6-1}$$

where M is the mean, n_p is the sample size, σ_p is the standard deviation, and t_α is a constant corresponding to the sample size and the expected confidence level. The 95% confidence interval of cutting force is calculated for each cutting test to examine the precision of experiments. The results are also summarized in Table 6-3, which are in the reasonable range considering that both rapid tool wear and high temperature occurred in hard turning.
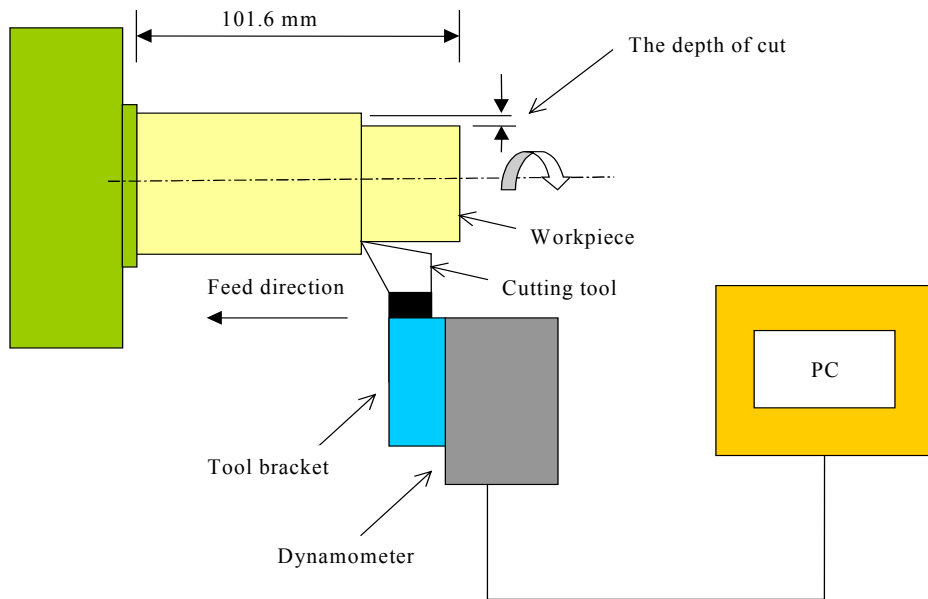
Figure 6-2. Schematic diagram of the experimental setup for the cutting stiffness measurement

Table 6-2. Specifications of the cutting system for experiments

Workpiece	52100 hollow bar (HRC 59±1)
	Outer diameter: 41mm
	Inner diameter: 30.5mm
	Overall length: 304.8mm
Insert	Kennametal PCBN insert CNGA432T (KB5635)
Tool holder	Kennametal DCLNR-124B
Machine	Hardinge Conquest T42
Dynamometer	Kistler 9257B

Table 6-3. Summary of radial cutting force data for condition index 1 – 4

Condition index	Feed (mm/rev)	Average radial force (N)	95% confidence interval (N)	Number of cutting operations
1	0.0254	64.9	61.1 – 68.8	5
	0.0508	75.9	75.0 – 76.7	6
	0.0762	96.5	91.5 – 101.0	4
	0.1016	109.3	105.0 –113.7	5
2	0.0254	64.1	55.8 – 72.5	3
	0.0508	75.1	72.3 – 77.8	6
	0.0762	89.4	87.8 – 90.9	6
	0.1016	101.7	96.7 – 106.8	5
3	0.0254	67.0	58.9 – 75.0	4
	0.0508	87.7	86.8 – 88.9	4
	0.0762	104.5	101.1 – 107.9	5
	0.1016	124.3	121.9 – 126.6	4
4	0.0254	66.9	60.2 – 73.6	4
	0.0508	86.6	78.1 – 95.1	4
	0.0762	102.9	100.9 – 104.8	4
	0.1016	112.7	111.9 – 113.6	4

As shown in Figure 6-3 and Figure 6-4, the radial cutting force is proportional to the feed rate and inversely proportional to cutting speed for both tool wear conditions. The decreased amount of radial force with the cutting speed increase is proportional to the feed rate. Therefore, the cutting speed effect caused by high temperature is proportional to the material removal rate. Moreover, it is found that radial cutting force increases as flank wear increases regardless of cutting speed, comparing Figure 6-3 with Figure 6-4. These tendencies in force measurements are in good agreement with existing experimental investigations on hard turning (Chou and Evans, 1999, Dawson, 2002). The nonlinear cutting stiffness in turning is derived from curve fitting the radial force data, which are measured over the range of the feed rate. Experimental data are fitted in with a cubic curve, whose origin coincides with a nominal feed rate and the corresponding radial force. The feed rate is 0.0762 mm/rev, which is used in subsequent
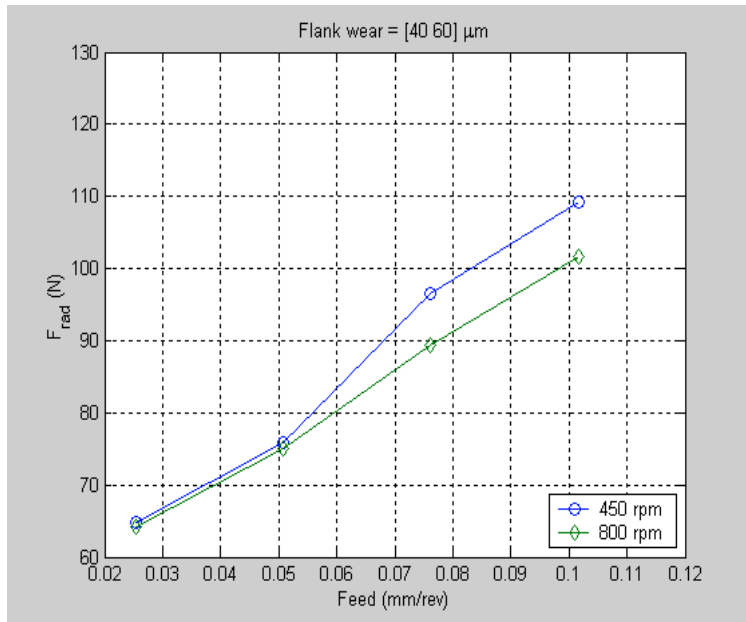
Figure 6-3. Radial cutting force of slightly worn tools versus the feed rate for different cutting speeds
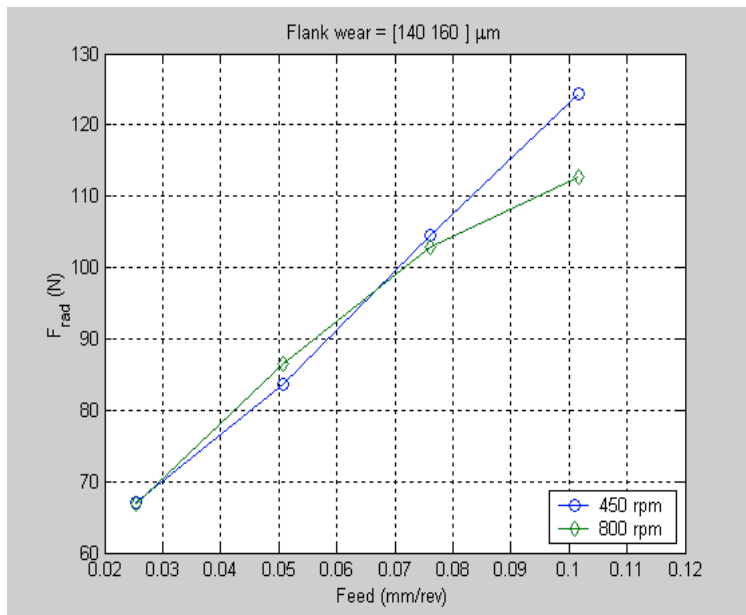
Figure 6-4. Radial cutting force of very worn tools versus the feed rate for different cutting speeds

chatter experiments. In that case, the variation of radial force due to the variation of the uncut chip thickness, i.e. the feed rate is given as

$$\Delta F_x(\Delta s) = k_c[(\Delta s) + c_1(\Delta s)^2 + c_2(\Delta s)^3] \qquad (6-2)$$

where Δs is the variation of the feed rate with respect to the nominal feed. The values of each term in equation (6-2) obtained through curve fittings as shown in Figure 6-5. The results are summarized in Table 6-4. The value of the cutting stiffness k_c is determined as 772 N/mm for slight worn tools and a cutting speed of 450 rpm. The value of k_c of slightly worn tools decreases to 558 N/mm for a cutting speed of 800 rpm. The same tendency is observed in very worn tools as the value of k_c decreases from 833 N/mm to 534 N/mm. While the cutting stiffness increases as tool wear develops at the low cutting speed range, this tendency does not remain at the high cutting speed range since the softening effect due to high temperature is possibly counterbalancing the flank wear effect.

The variations of the nonlinear cutting stiffness k_c, c_1, and c_2 along the axial direction of the bar are assumed to be negligible. As shown in Table 6-4, the average ratio of the square coefficient c_1 to the cubic coefficient c_2 is 0.02 and 0.23 at 450 rpm and 800 rpm, respectively. Furthermore, the ratio of the square term to the cubic term decreases for very worn tools at each cutting speed. Therefore, the importance of the square term relatively decreases as cutting speed decreases or flank wear increases. Ignoring the second term in the stiffness results in a much simpler modeling process. Stability limit predictions without the square term in nonlinear stiffness are to be examined later as a special case of nonlinear chatter models in order to determine whether the simplification can be justified.
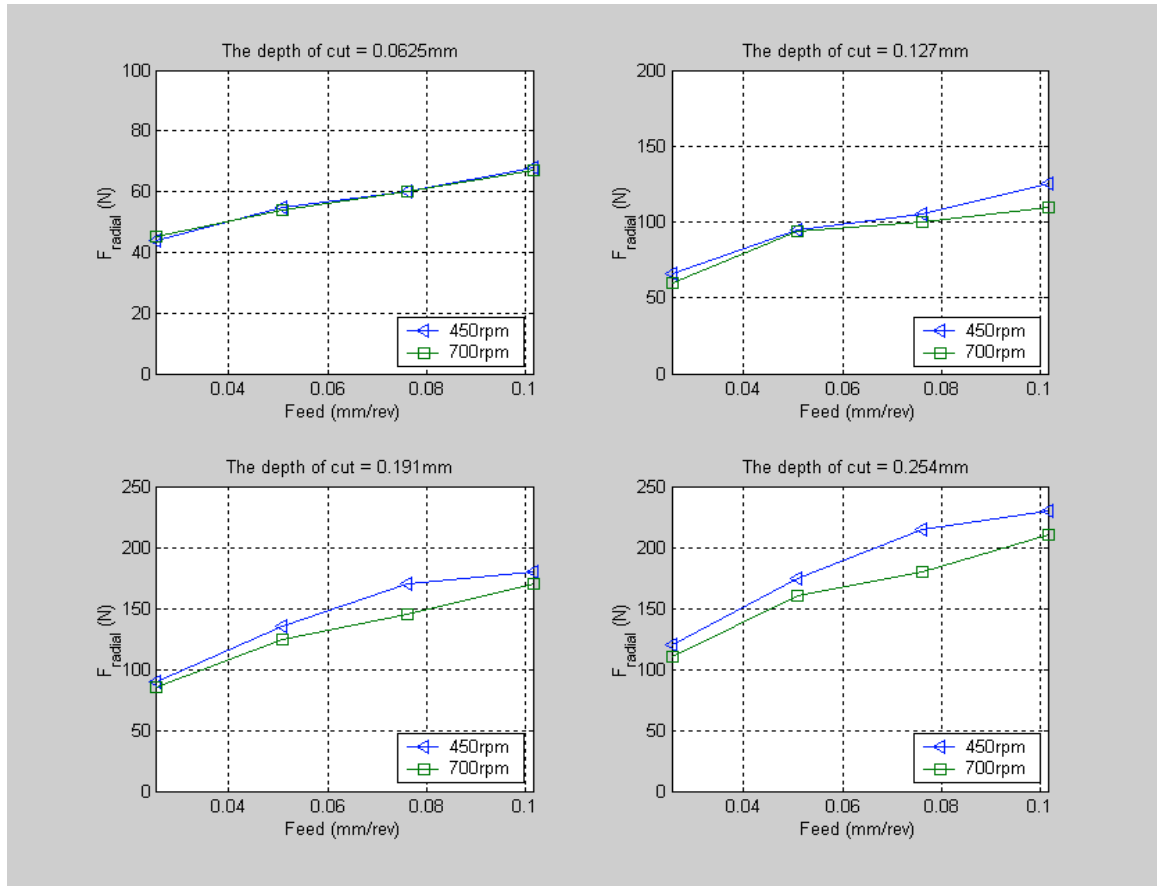
Figure 6-5. Curve fittings of radial cutting force data to a cubic curve and a straight line

Table 6-4. Summary of the nonlinear cutting stiffness for condition index $1-4$

Condition index	Flank wear (μm)	Speed (rpm)	k_c (N/mm)	c_1 (N/mm^2)	c_2 (N/mm^3)	c_1/c_2
1	40 - 60	450	772	-7.8	-229	0.034
2	40 - 60	800	558	-28	-96.5	0.29
3	140 - 160	450	833	-0.93	-96.5	0.010
4	140 - 160	800	534	-9.4	-59.0	0.16

If the nonlinear relation between cutting force and the feed rate is ignored, then the linear cutting stiffness k_c can be derived for each cutting condition as shown in Table 6-5. The linear cutting stiffness decreases as cutting speed increases for both wear conditions. In addition, the linear cutting stiffness increases as flank wear progresses. As a consequence, the linear cutting stiffness shows the same tendencies as the nonlinear cutting stiffness. The linear cutting stiffness is used in the proposed linear modeling of chatter in straight turning.

6.2.2.2. Linear Cutting Stiffness for Inward Turning

The linear cutting stiffness is measured for various values of the depth of cut in inward turning. Radial cutting force is measured over the range of the depth of cut, which correspond to condition indices 5 – 12 in Table 6-1. The overhang length of the workpiece is 76.2 mm during cutting tests. The cutting speed effect is considered by conducting a series of cutting tests at two different values of cutting speed while the range of flank wear is remained between 40 and 60 μm.

It is found radial cutting force is proportional to the depth of cut. In addition, the cutting speed effect, which induces lower force at the high-speed range is shown more prominently at a larger value of the depth of cut as shown in Figure 6-6. The results of the linear cutting stiffness are summarized in Table 6-6.

Table 6-5. Summary of the linear cutting stiffness for condition index 1 – 4

Condition index	Flank wear (μm)	Speed (rpm)	k_c (N/mm)
1	40 - 60	450	606
2	40 - 60	800	500
3	140 - 160	450	759
4	140 - 160	800	605
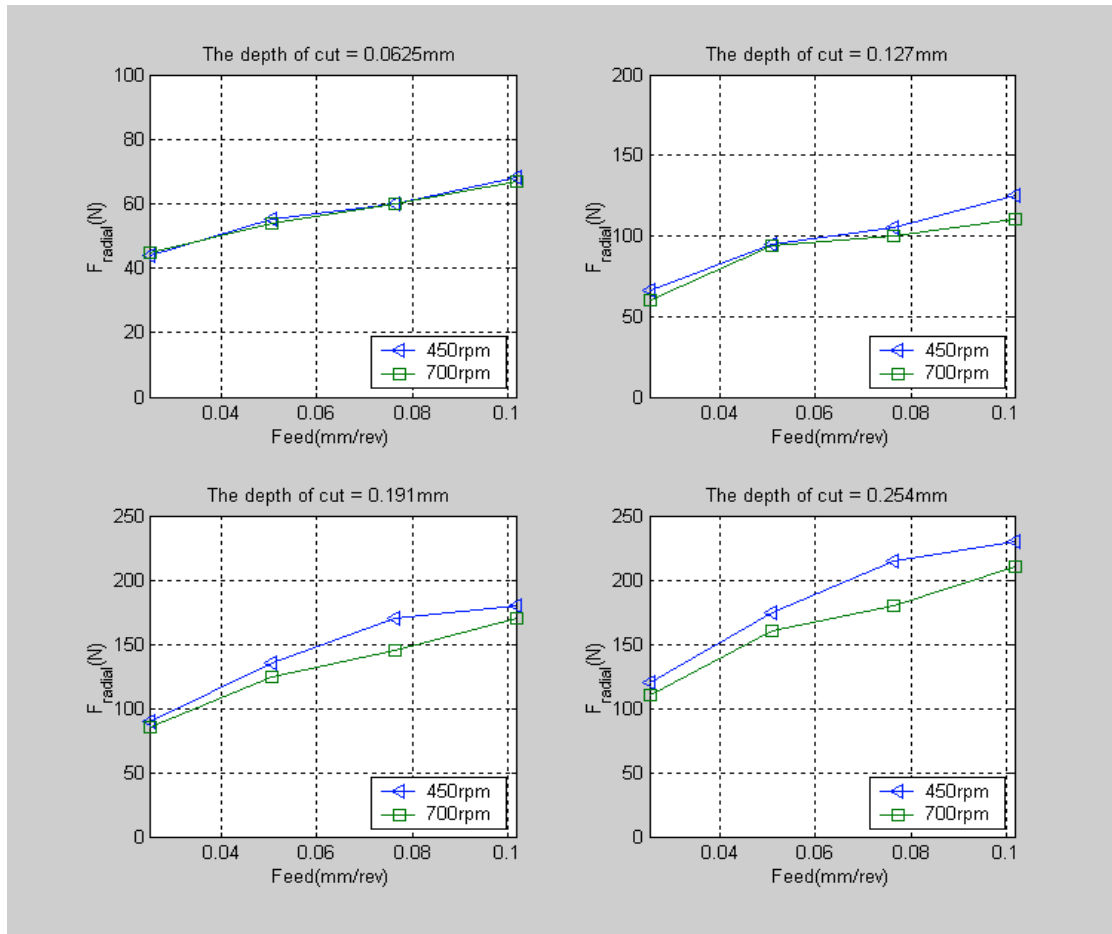
Figure 6-6. Radial cutting force versus the feed rate for the depth of cut = [0.0625 0.254] mm, cutting speed = [450 700] rpm, and flank wear = [40 60] μm

Table 6-6. Summary of the linear cutting stiffness for condition index 5-12

		The depth of cut (mm)			
		0.0625	0.1250	0.1875	0.254
Cutting speed (rpm)	450	303	736	1200	1460
	700	284	685	1080	1260

6.2.3. Structural Stiffness

The nonlinear structural stiffness along the 52100 hollow bar has been obtained through a series of experiments. Similar to the cutting stiffness, the nonlinear structural stiffness is used not only as one of main sources of nonlinearity in the modeling for chatter but also as the converting relation between the stiffness ratio and the critical chatter location.

Simultaneous measurements of the radial displacement of the workpiece and the static force exerted on the bar are carried out for deriving the structural stiffness. The experimental set up for measuring the structural stiffness is the same as shown in Figure 3-2 except the overhang length of the workpiece became 203.2mm. Static force data are collected by a dynamometer installed at the tool post. Static force is exerted through a carbide tool tip on the surface of workpiece since they are relatively less brittle and cheaper than PCBN tools. In addition, the radial displacement of the workpiece is measured by the dial gage attached on the opposite side of the bar.

Similar displacement measurements for different values of static force are repeated at least four times per position on the bar to derive nonlinearity of the structural stiffness as

a third-order polynomial. These procedures are performed at seven different positions along the bar in the longitudinal direction and experimental data of displacement and static force are summarized in Table 6-7.

The data of static force for the variations of the radial displacement of the bar can be approximately fitted to a cubic curve at each measured position as

$$\Delta F_x(\Delta x) = k_m[(\Delta x) + \beta_1(\Delta x)^2 + \beta_2(\Delta x)^3] \qquad (6\text{-}3)$$

where Δx is radial displacement, k_m is the structural stiffness, β_1 and β_2 are the coefficients of the nonlinear structural stiffness, respectively. The values of k_m, β_1 and β_2 are obtained as a result of curve fittings as shown in Figure 6-7, and the results are summarized in Table 6-8. The variations of k_m, β_1 and β_2 along the workpiece are shown in Figure 6-8. Nonlinear squar and cubic terms decrease to zero as the location on the workpiece proceeds to its end. In conclusion, nonlinearity in the structural stiffness is less significant as the overhang length of the workpiece increases.

When the same data are fitted to a straight line with the least square method, the values of the linear structural stiffness are obtained as shown in Table 6-9. The variation of the linear structural stiffness is shown in Figure 6-9.

6.2.4. Converting Relations

In order to plot stability charts while varying a more practical cutting parameter, the converting relations between the stiffness ratio and a cutting parameter are derived. For outward turning with a fixed depth of cut, the cutting stiffness is assumed to be independent of the location on the workpiece while the structural stiffness is varied along it. Thus there is a direct relation between the structural stiffness and the location on the

Table 6-7. Summary of displacement and static force data along the workpiece

Location (mm)	Displacement (mm)	Force (N)
51	0.020	317.0
	0.033	425.0
	0.051	542.0
	0.056	564.0
76	0.028	233.0
	0.048	311.0
	0.064	374.0
	0.071	415.0
102	0.023	140.0
	0.036	217.0
	0.058	306.0
	0.084	370.0
127	0.023	86.0
	0.043	140.0
	0.069	200.0
	0.094	284.0
152	0.084	196.0
	0.122	260.0
	0.152	312.0
	0.183	347.0
178	0.076	163.0
	0.137	242.0
	0.206	367.0
	0.312	432.0
203	0.064	103.0
	0.127	152.0
	0.254	292.0
	0.356	323.0
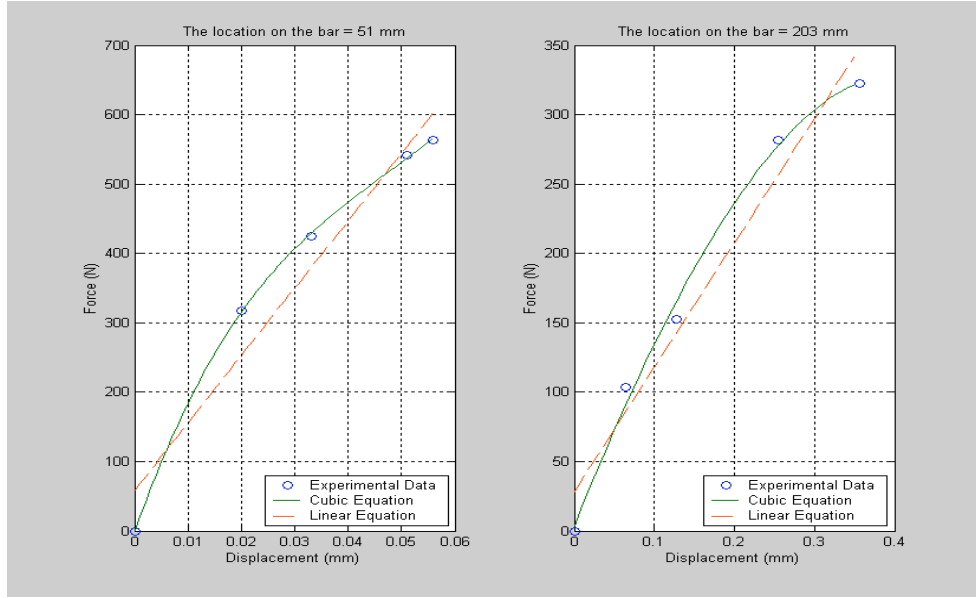
Figure 6-7. Curve fittings of experimental data for the structural stiffness to a cubic curve and a straight line at two different locations on the workpiece.

Table 6-8. Summary of the nonlinear structural stiffness along the workpiece

Location (mm)	k_m (N/mm)	β_1 (N/mm^2)	β_2 (N/mm^3)
50.8	22000	111	-16
76.2	13000	120	-16
101.6	6600	-21	-2
127	4800	70	-10
152.4	2600	-1	-1
177.8	1600	-11	3
203.2	1400	-1	-1
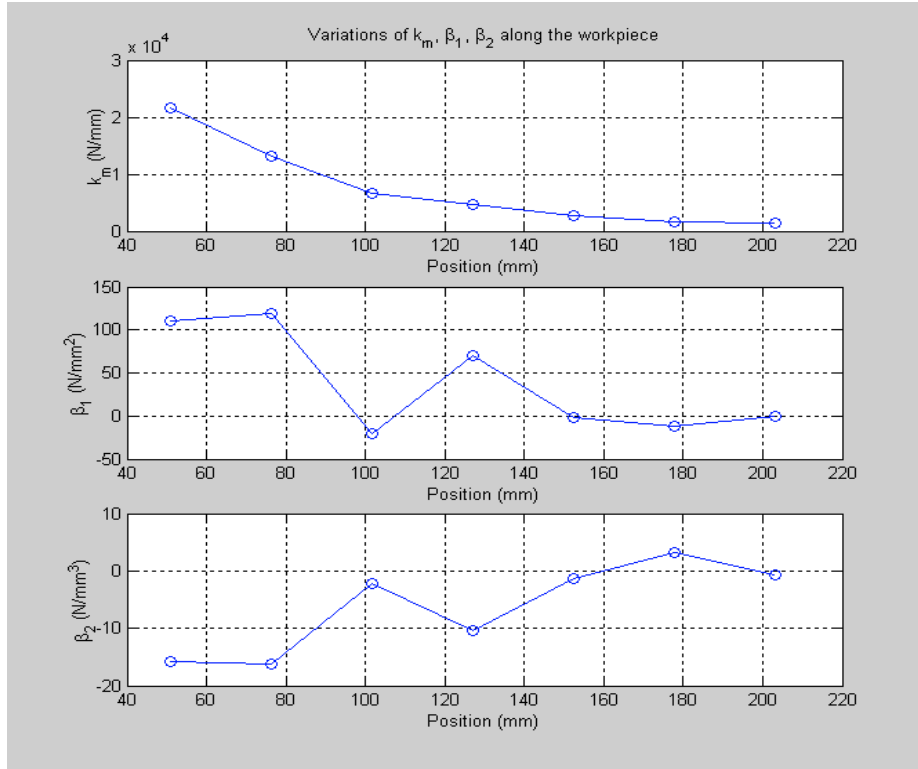
Figure 6-8. Variations of the nonlinear structural stiffness along the workpiece

Table 6-9. Summary of the linear structural stiffness along the workpiece

Location (mm)	k_m (N/mm)
50.8	9700
76.2	5600
101.6	4400
127	2900
152.4	1900
177.8	1400
203.2	900
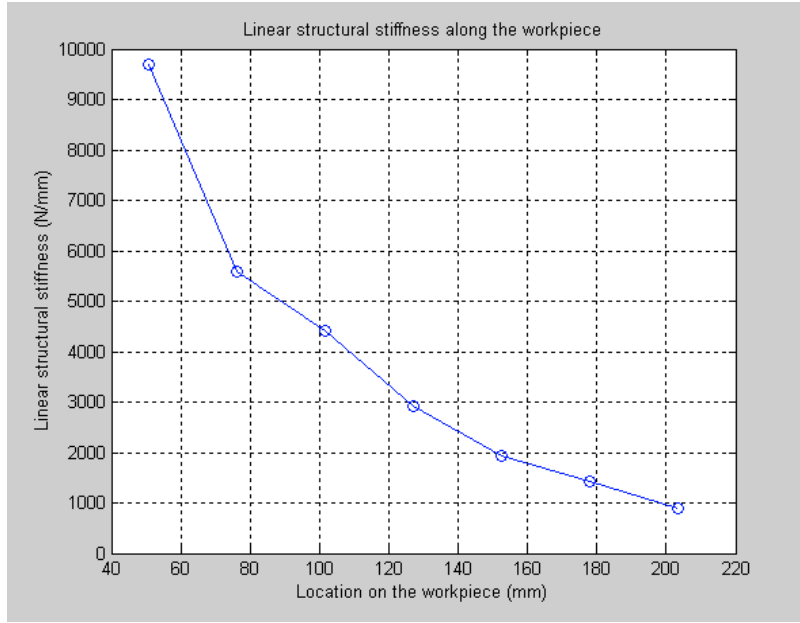
Figure 6-9. Linear structural stiffness along the workpiece

bar. In the present study, the converting relation between the stiffness ratio and the
position on workpiece is derived based on the variation of the linear structural stiffness
along the workpiece shown in Figure 6-9. In order to obtain the structural stiffness at an
arbitrary position between measured locations, a linear proportionality of the structural
stiffness to the location is assumed. For example, the structural stiffness in the range of
[50.8 76.2] mm is obtained as a function of the location

$$k_m(z) = -161z + 17900 \tag{6-4}$$

where z is the location on the workpiece in the longitudinal direction.

   Since the linear cutting stiffness depends on cutting speed effect as well as flank wear,
the converting relation are derived as a function of cutting speed for each tool wear
condition. For example, the relation between the cutting stiffness and cutting speed for
slightly worn tools is

$$k_c(\Omega) = -18\Omega + 741 \tag{6-5}$$

where Ω is cutting speed in rev/sec. Therefore, the resultant converting relation for slightly worn tools is given as

$$z = \left(\frac{k_c}{k_m}\right)^{-1}(0.11\Omega - 4.6) + 110 \tag{6-6}$$

Similarly, the converting relation for very worn tools over the same range of the structural stiffness is obtained as the following:

$$z = \left(\frac{k_c}{k_m}\right)^{-1}(0.016\Omega - 4.9) + 110 \tag{6-7}$$

Converting relations for other ranges of the structural stiffness can be obtained by repeating above procedures for each tool wear condition.

For inward straight turning with a short cutting range, the structural stiffness is assumed to be constant, and the cutting stiffness is varied with the depth of cut. Thus, there is a direct relation between the cutting stiffness and the depth of cut. In the present study, the converting relation between the stiffness ratio and the depth of cut is derived based on the experimental data of the linear cutting stiffness over the range of the depth of cut. Since the linear cutting stiffness depends on cutting speed, a converting relation is derived as a function of cutting speed. The converting relation between the stiffness ratio and the depth of cut is given as followings:

$$doc = (0.035\Omega + 0.63)\frac{k_c}{k_m} - 0.0016\Omega + 0.023 \tag{6-8}$$

where *doc* is the depth of cut.

6.3. Chatter Stability Predictions in Straight Turning

6.3.1. Stability Predictions from the Linear Chatter Model

Without the consideration of nonlinear elements, the minimum stiffness ratios for fresh tools as well as very worn tools are obtained over the range of cutting speed as shown Figure 6-10. The tangential stability line for fresh tools is called the absolute stability line, which corresponds to $2\zeta(1+\zeta)/[\sin(C_s)\cos(C_s)]$. This stability line guarantees a stable machining process regardless of cutting speed according to the linear modeling. Applying the converting relation, the stability chart is presented in the chatter location versus cutting speed as shown in Figure 6-11. The region below the solid line corresponds to the stable region and chatter is expected in the unstable region above the solid stability line. The predicted chatter location is proportional to cutting speed and the stabilizing effect of flank wear is shown in the stability prediction for different flank wear length.

The theoretical predictions of chatter in inward turning are also attempted for both fresh tools and very worn tools. In order to find the critical depth of cut where chatter occurs, the converting relations shown in equation (6-8) are applied to the values of the minimum stiffness ratio. As shown in Figure 6-12, the variation of critical depth of cut with cutting speed shows the increasing tendency. The stabilizing effect of flank wear is also observed in the stability chart.
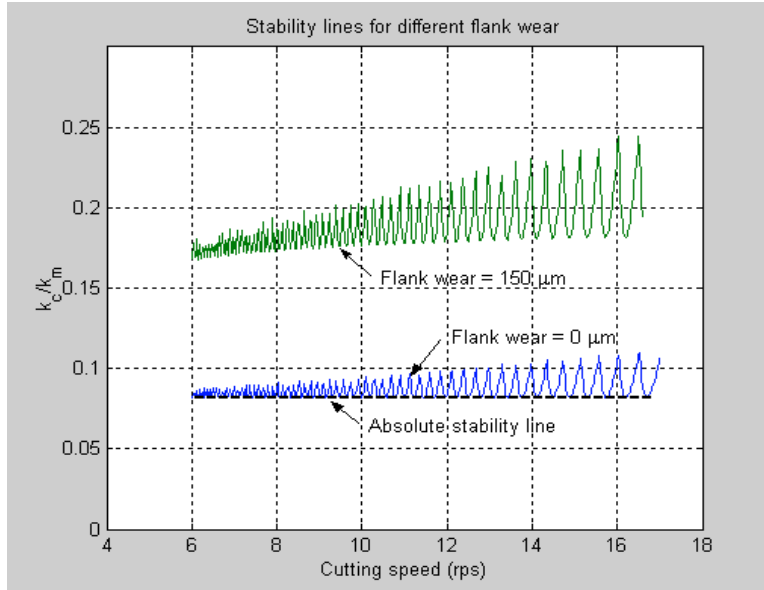
Figure 6-10. Comparison of the minimum stiffness ratio for fresh tools and very worn tools in outward turning
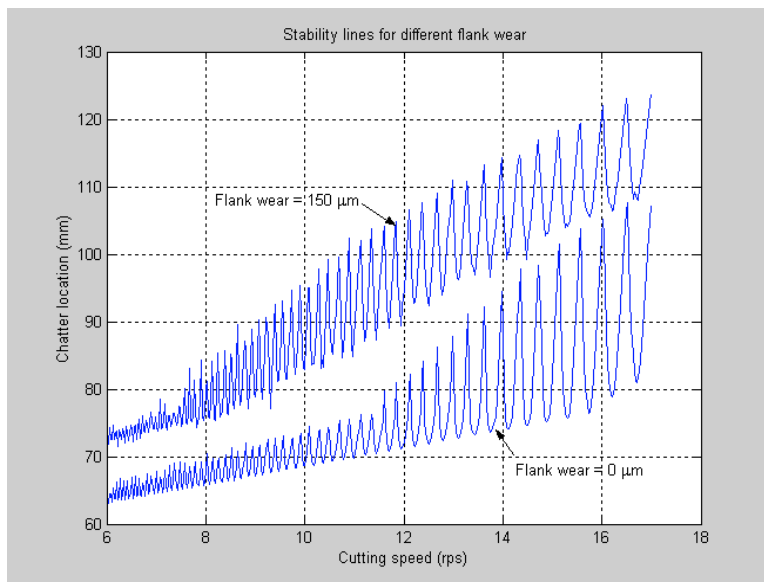
Figure 6-11. Stability chart for fresh tools and very worn tools in outward turning
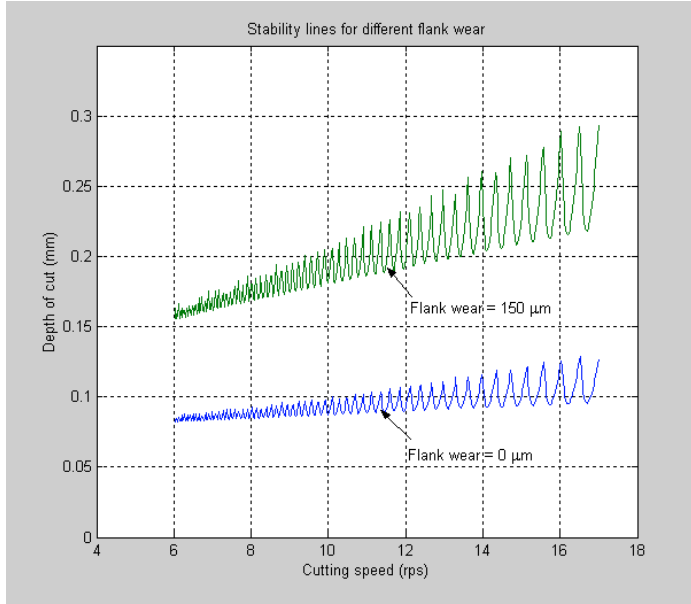
Figure 6-12. Stability chart for fresh tools and very worn tools in inward turning

6.3.2. Stability Predictions from the Nonlinear Chatter Model

6.3.2.1. Stability Charts of the Nonlinear Model

The three-dimensional stability chart in Figure 6-13 is obtained from the nonlinear model by expanding the numerical procedures described in Appendix A.2 to the system of three harmonic equations. Since the minimum stiffness ratio k_c/k_m is the critical stability parameter, the region below the plane of the minimum stiffness ratio is called "the stable region". The region above the plane of the minimum the stiffness ratio is called "the unstable region" where chatter is expected for given values of cutting speed and sinusoidal input amplitude. Employing an appropriate converting relation, stability charts are plotted in terms of a more practical parameter instead of the stiffness ratio.

The stability line of the linear model corresponds to that of the nonlinear model with the zero value of A_1. Furthermore, the amplitude of oscillation at the critical stability

86
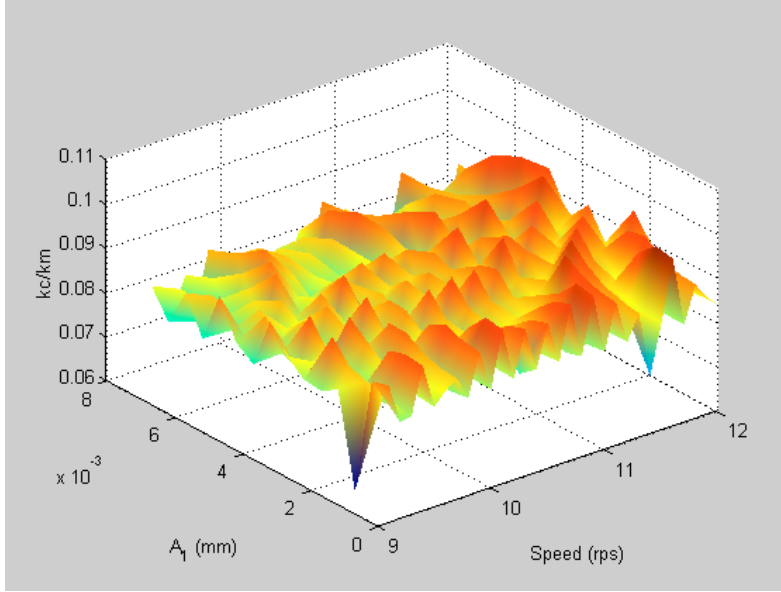
Figure 6-13. Example of the three-dimensional stability chart for the nonlinear chatter model

limit is indeterminate in the linear model. As a result, the stability charts from the linear model can be represented in the 3-D space as a series of straight cylinders extending the stability line normal to the k_c/k_m and Ω plane.

6.3.2.2. Evolution of Chatter

In contrast to linear models, which have the same stability line on the plane of k_c/k_m and Ω regardless of A_1, nonlinear models have distinct stability lines for different values of A_1. The stability line of the linear model corresponds to that of the nonlinear model with the zero chatter amplitude. Figure 6-14 shows the stability charts for fresh tools obtained from the nonlinear model. When the chatter amplitude is 0.004 mm, it predicts a larger stable region than the linear model shown in Figure 6-12. However, when the chatter amplitude increases from 0.004 to 0.01mm, the stable region decreases.
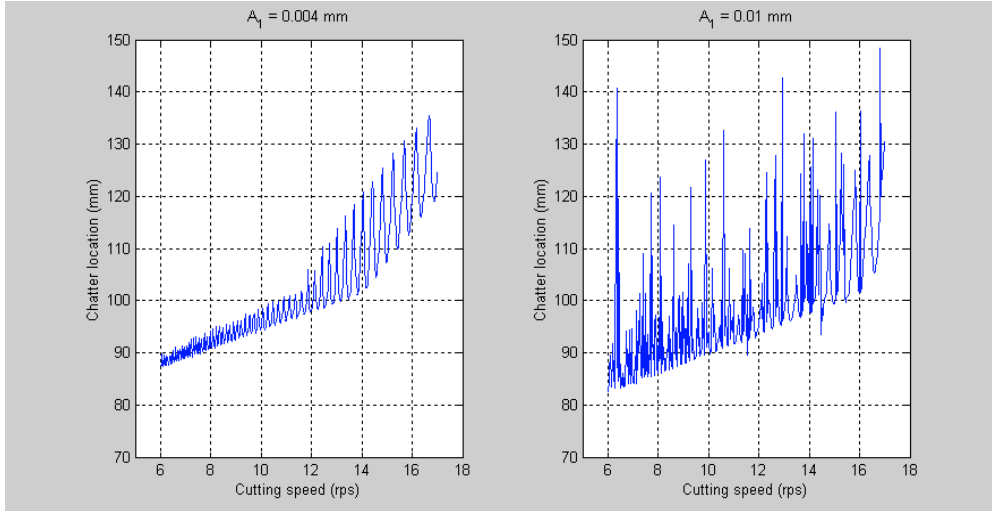
Figure 6-14. Variation of the stability line for different A_1 values

In order to explore this feature in the nonlinear model, it is convenient to introduce the cross-sectional view on the A_1 and k_c/k_m plane parallel to the Ω axis as shown in Figure 6-15. The stability line is obtained at the cutting speed of 12 rps when fresh tools are used in outward turning. The solid line corresponds to the critical stability limit and the right side of the line is the unstable region since the minimum k_c/k_m is the critical stability parameter.

As the value of k_c/k_m is increased along the stiffness ratio axis in Figure 6-15, no chatter is observed as long as it remains in the left side of the solid line. Chatter starts when the stiffness ratio reaches the value at the point A, and it follows the solid line as the value of k_c/k_m is increased. If the initial value on the stiffness ratio axis is larger than the value at A, then unstable chatter occurs. Therefore, there are three types of solutions available near the point A: stable chatter on following the solid line, no chatter and unstable chatter on the k_c/k_m axis.
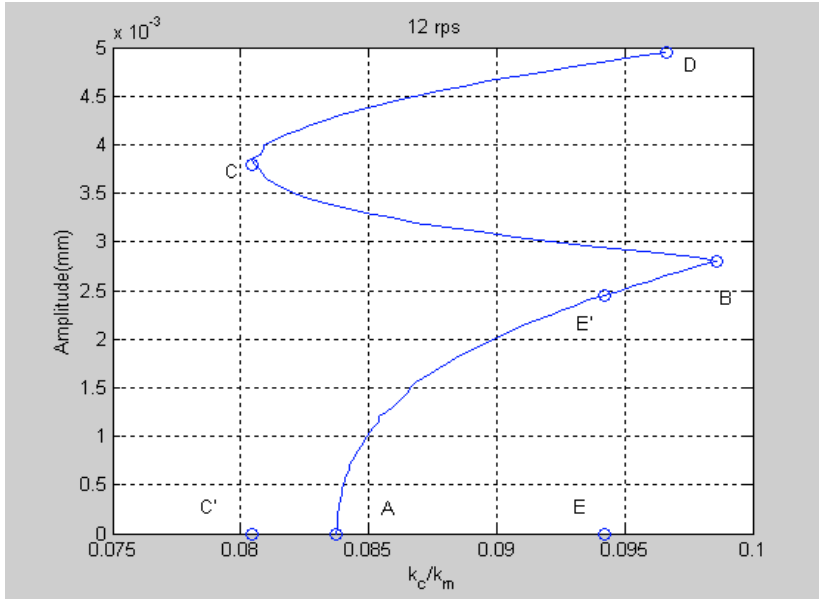
Figure 6-15. Stability line on the plane of A_1 and k_c/k_m at the cutting speed of 12 rps

The oscillation at the critical stability limit, which corresponds to a point on the solid line in the stability chart, is a limit cycle with constant amplitude and frequency. The stability of a limit cycle can be examined by investigating the variation of amplitude with a disturbance. As the amplitude of oscillation returns to an original value after experiencing disturbances, it is called stable; but if otherwise it is said to be unstable.

The solid line between A and B corresponds to the stable branch of limit cycles. When the amplitude of chatter increases, it reaches the stable region departing from the line. As a result, amplitude decreases and it returns to the line and vice versa for the decrease of amplitude. In the branch between the points B and C, unstable chatter is expected. Hence, the amplitude of chatter grows infinitely or jumps to the next available stable branch once the point B is met. The CD branch is for stable chatter with the similar argument of the AB branch.

If the value of k_c/k_m at the point E in the unstable region is chosen without passing the point A, then it becomes unstable and the amplitude of chatter immediately grows to the point E'. After jumping to the point E', the amplitude of chatter is slowly increased with the increase of k_c/k_m along the stable branch AB, which corresponds to the finite amplitude phenomenon observed in practice. If the value of k_c/k_m is decreased on the branch CD, chatter is predicted for the value of k_c/k_m smaller than the critical stiffness ratio at $A_1 = 0$. Thus, the absolute stability line suggested in the linear model is not valid any more. At the point C, the amplitude of chatter abruptly decreases to zero by dropping to the point C'. Therefore, nonlinear phenomena of chatter such as the finite amplitude phenomenon and the jump can be explained in the stability chart of the nonlinear model. Furthermore, not only the existence but also the evolution of chatter can be predicted from the nonlinear modeling.

The variations of amplitude A_1 with the stiffness ratio for the four values of cutting speed are shown in Figure 6-16. As cutting speed increases from 6 to 9 rps, the range of A_1 for the unstable branch is suppressed from 0.002 to 0.001 mm. At 12 rps, the stable branch is observed until amplitude reaches 0.0028 mm. The slope of the stable branch decreases as cutting speed increases from 12 to 15 rps. The variations of amplitude with the chatter location are obtained in Figure 6-17 after applying the converting relation to the results in Figure 6-16. The chatter location monotonously increases proportional to cutting speed for the same value of A_1.
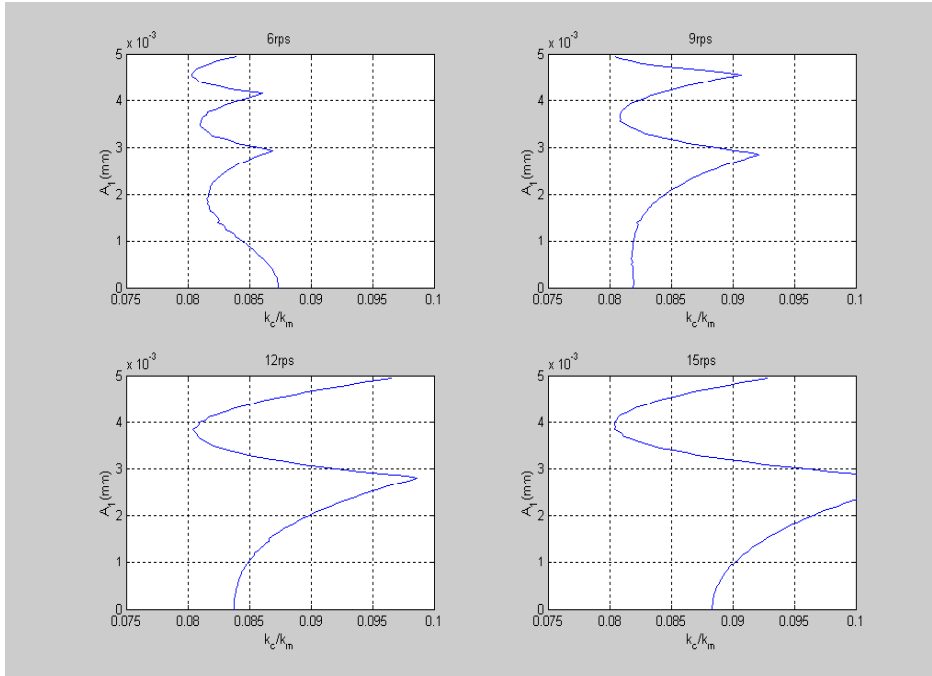
Figure 6-16. Comparison of stability charts for fresh tools at different cutting speeds
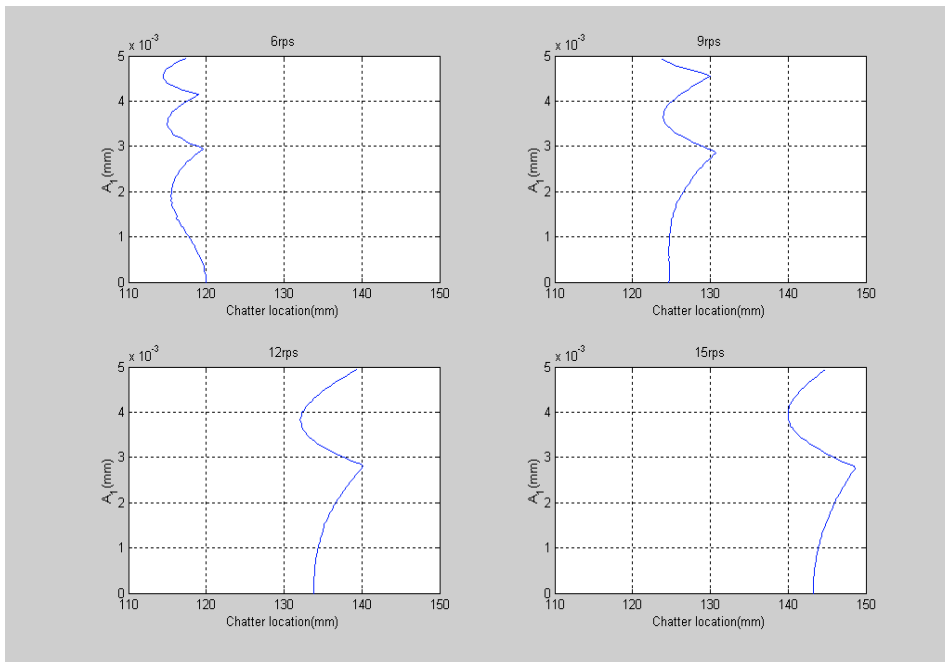
Figure 6-17.Variation of the critical chatter location with amplitude for fresh tools at different cutting speeds

6.3.2.3. Flank Wear Effect

In order to see the flank wear effect on chatter predictions from nonlinear chatter modeling, the stability chart on the plane of A_1 and k_c/k_m are obtained for four different values of cutting speed for slightly worn tools as shown in Figure 6-18. Comparing with the results from fresh tool cases in Figure 6-17, the solid lines for slightly worn tools are shifted to right and it shows the stabilizing effect of flank wear. The amount of the shift is proportional to cutting speed. Therefore, the flank wear effect is more prominently shown in the high cutting speed range. In addition, it should be noticed that the overall shape of the curve, which determines the evolution of chatter, is maintained for each cutting speed regardless of the tool wear condition.
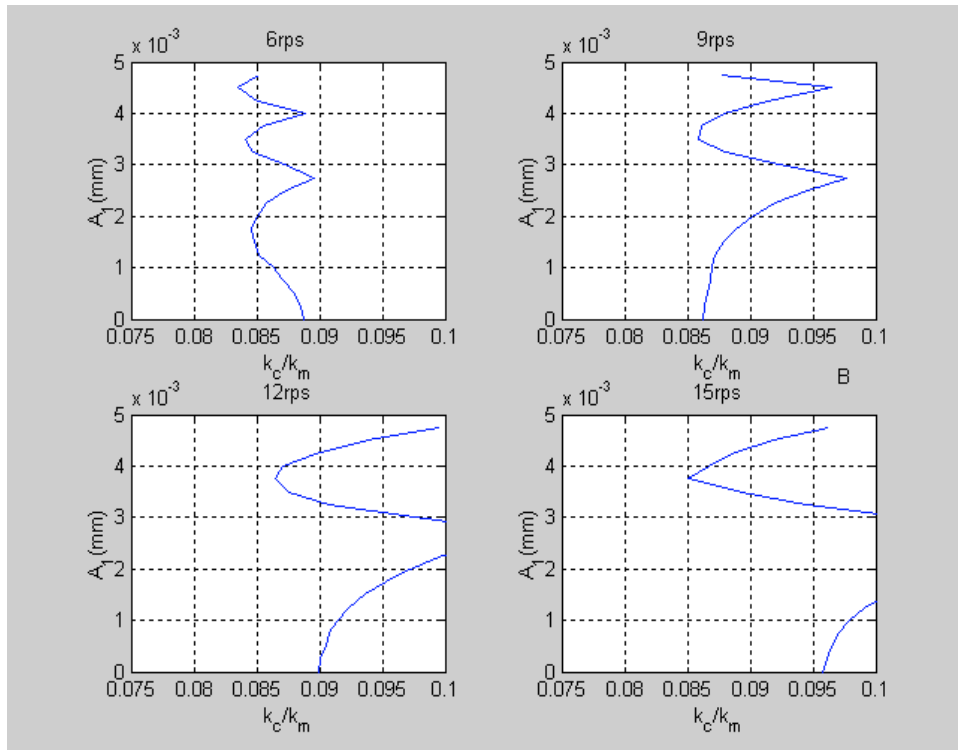
Figure 6-18. Variation of the critical chatter location with amplitude for slightly worn tools at different cutting speeds

6.3.2.4. Nonlinear Effect

In order to investigate the effect of nonlinearity from the structure and cutting force on chatter stability, stability limits for the various combination of the linear and nonlinear stiffness are obtained. The area under the stability line for $A_1 = 0.004$ mm is calculated for fresh tools in outward turning in order to examine the effect of each nonlinear condition quantitatively and the results are summarized in Table 6-10. It is found the nonlinear structural stiffness causes a larger variation of the area than the cutting stiffness. Therefore, the nonlinear structural stiffness is a more dominant factor than the nonlinear cutting stiffness in the chatter stability predictions of this study.

Table 6-10. Area of the stable region for various nonlinearity

Conditions	Area
Linear stiffness	1472
Linear structural stiffness and nonlinear cutting stiffness	1474
Nonlinear structural stiffness and linear cutting stiffness	1463
Nonlinear stiffness	1464

6.3.2.5. Effect of Even Nonlinearity

Since even terms in nonlinearity introduce a bias term of the input to keep harmonic balance conditions, the modeling of chatter with mathematical simplicity is available if the assumption of negligible even nonlinearity is justified. The effect of even terms is examined by considering the variation of the area under the stability line when one of

even terms of the stiffness is ignored. According to the results are summarized in Table 6-11, the effect of the even term is negligible in the cutting stiffness. However, the even term in the structural stiffness should not be ignored since it results in a noticeable variation of the stability line. Thus, the bias term of the input should be introduced in the nonlinear modeling processes.

Table 6-11. Effect of even nonlinearity on the stable region

Ignored term	Area
None	1464
Even cutting stiffness	1464
Even structural stiffness	1475

6.4. Conclusion

The natural frequency and the damping ratio of the workpiece are measured through impact testing. A series of cutting tests is carried out to measure the force variation with the feed rate considering the effect of cutting speed and flank wear. The nonlinear cutting stiffness is obtained through curve fitting of force data to a cubic equation. The nonlinear structural stiffness of the workpiece is also determined as the form of a third-order polynomial. Based on experimental data, converting relations between the stiffness ratio and a cutting parameter are derived for both feed directions in turning.

The nonlinear model is able to predict not only the existence of chatter but also the evolution of chatter at given cutting conditions. The finite amplitude phenomenon and the jump are predicted for certain cutting conditions from the stability chart. It is predicted that flank wear has a stabilizing effect, which depends on cutting speed. In addition, the effect of the nonlinear structural stiffness on the prediction is more prominent than that of the nonlinear cutting stiffness. Finally, it is found that the even term of the structural stiffness should be considered in the modeling process.

CHAPTER 7

EXPERIMENTAL RESULTS AND MODEL VALIDATION FOR STRAIGHT

TURNING

7.1. Introduction

The measurement of chatter stability limits through cutting tests is one of the most

important parts in chatter investigations since it provides not only the practical guideline

for machining operations but also useful information which future modeling research can

rely on. The importance of empirical stability limits is even bigger in hard turning. The

reason includes the poor understanding of the interaction between the workpiece and the

tool, which is affected by dynamic tool wear and high temperature. Nevertheless, there

has been no attempt to measure stability limits in hard turning. In this study, chatter

stability limits in straight turning of hardened 52100 steels are measured for the first time.

In the present study, critical stability limits are measured for both feed directions

available in straight turning. The power spectrum and the time trace of force data as well

as visual inspection are employed as chatter detection criteria. In order to examine the

flank wear effect on stability limits, tools with different flank wear ranges are used for

cutting tests. The characteristics of chatter stability limits in hard turning are discussed,

and the validity of the proposed nonlinear modeling for chatter in straight turning is

examined.

7.2. Measurements of Chatter Stability in Straight Turning

7.2.1. Chatter Detection Methods

Various methods have been used for detecting chatter phenomena in cutting tests (Elbestawi *et al*., 1991, Kondo *et al*., 1997, Chiou and Liang, 1998, Clancy and Shin, 2002). In cutting operations, chatter can be identified from the time trace and the power spectrum of cutting force, tool acceleration and sound emitted. The typical example of cutting force trace shows the steady state of force as shown in Figure 7-1 when chatter does not exist. However, the abrupt change of force is observed when chatter starts and the chatter frequency is found in the power spectrum of the corresponding force data as shown in Figure 7-2. The surface roughness measurement or the visual inspection of the machined surface also serves as a chatter detecting method. Most experimental investigations on chatter stability have employed multiple identification methods to verify chatter phenomenon.
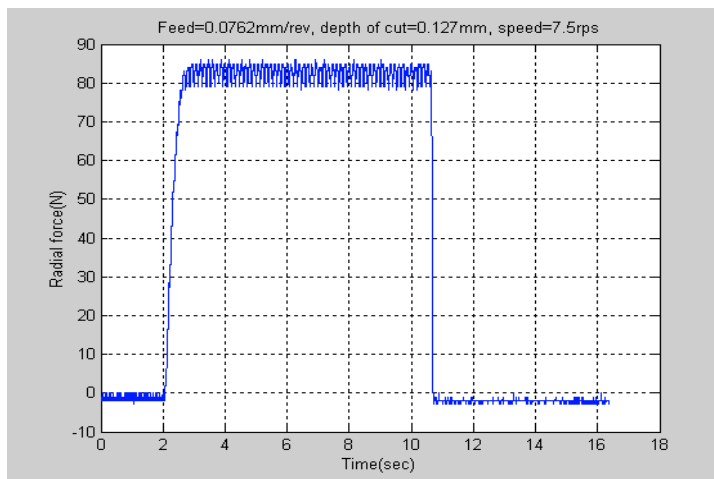
Figure 7-1. Example of the cutting force trace without chatter
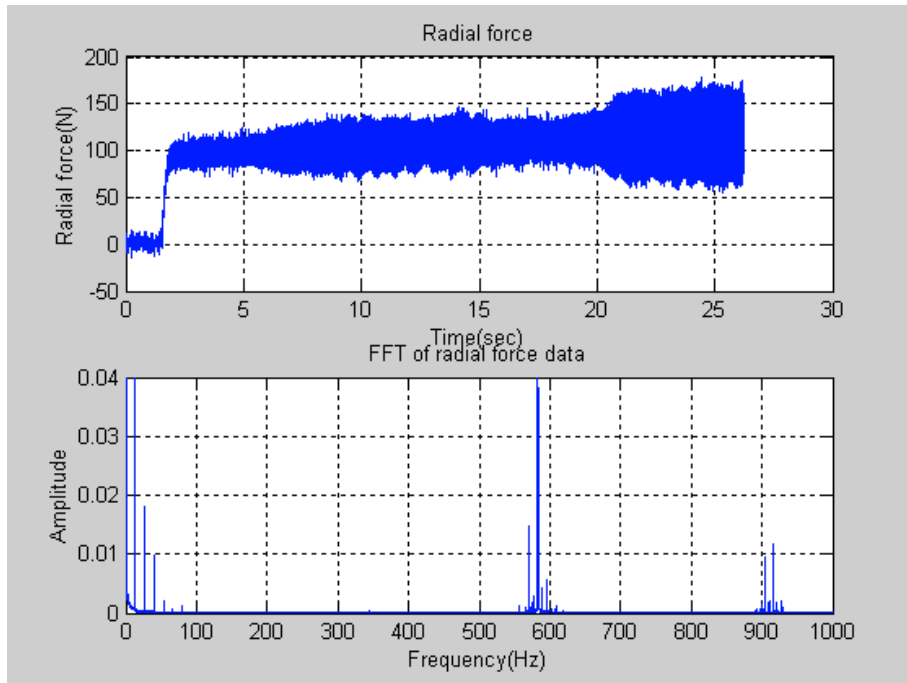
Figure 7-2. Example of the cutting force trace under chatter and the corresponding power spectrum of force data

In this study, the time trace and the spectrum of cutting force data as well as the visual inspection of chatter marks on the machined surface are employed for chatter detection. Chatter is identified only if following three conditions are satisfied at the same time. First, more than a 40% increase in cutting force amplitude is observed in the time trace of cutting force. Second, the chatter frequency is observed in the spectrum from the Fast Fourier Transform (FFT) of cutting force data. Third, chatter marks on the surface of the workpiece are visually identified. Figure 7-3 shows an example of chatter marks on the surface of the workpiece.
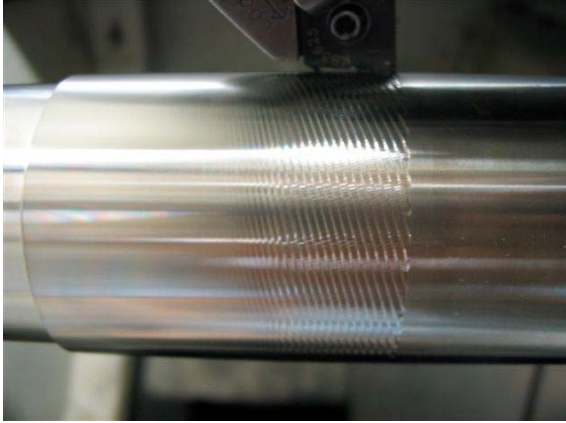
Figure 7-3. Example of chatter marks on the surface of a 52100 bar

The data of cutting force from chatter experiments are collected by a Kistler 9257B dynamometer, which is mounted on the tool post as shown in Figure 7-4. In order to avoid the aliasing of the frequency spectrum, the sample rate of the low pass filter is chosen as 1500 Hz considering the natural frequency of the workpiece.

Figure 7-4. Dynamometer setup mounted on the tool post

7.2.2. Workpiece and Tool

Hardened 52100 steel hollow bars (HRC 59 ± 1) are used as the workpiece of experiments for chatter stability measurements. The inner diameter and the outer diameter of the workpiece are 30.5 mm and 41 mm, respectively. The overall length of the workpiece is 304.8 mm. A kenloc type Kennametal PCBN insert (KB5625) is used for cutting experiments. A tool holder Kennametal DCLNR-124B is used for inward turning and DCLNL-124B for outward turning. All cutting operations in experiments are performed in a Hardinge Conquest T42 Super Precision Lathe.

All bars are finished before chatter experiments to remove the scale due to heat treatment since it causes out of roundness in the bar. All finishing operations prior to chatter experiments are performed with carbide cutting inserts in order to avoid unnecessary tool wear of PCBN tools.

Three groups of tools with different wear conditions are prepared for cutting operations. The first group is called "fresh tools," which are tools used for the first time. The flank wear is assumed to be zero for this group. "Slightly worn tools" with the flank wear range between 40 and 60 μm belong to the second group. The last "very worn tools" group has the flank wear range between 140 and 160 μm. Since the tool wear rate follows a logarithmic curve in hard turning (Dawson, 2002), flank wear proceeds relatively slowly after rapid growth at the early stage of machining process. Accordingly, the flank wear of a fresh tool reaches the range of the second group just after a few machining runs. In contrast, the second group is well separated from the third group.

7.2.3. Experimental Procedures

7.2.3.1. Determination of Stability Limits in Outward Turning

Chatter stability limits are determined for outward turning with the feed direction toward the end of the workpiece as shown in Figure 7-5. Because the low structural stiffness causes chatter, cutting operations must proceed from the high stiffness part to the low stiffness part in order to find a chatter location on the workpiece. According to the experimental investigation described in Chapter 6, the structural stiffness of the workpiece has its maximum value at the collar, and then decreases as it advances to the end of the bar. Therefore, cutting operations should be carried out from the collar side feeding axially to the end of the bar to find where chatter starts.

Figure 7-5. Experimental set up for the stability limit measurements in outward turning

In order to avoid tool tip breaks when the tool is applied on the middle of the bar, a step is introduced at the middle of the workpiece. The workpiece is machined to have the outer diameter of 38.1 mm for the half portion of the workpiece and 40.2 mm for the other portion in order to make a 1.27 mm high step at the middle of the bar. The overhang length of the workpiece is 203.2 mm.

The outward turning operation starts from the step, which is 50.8 mm apart from the collar and then it continues to proceed to the end of bar until chatter is detected. The depth of cut and the feed rate are fixed as 0.127 mm and 0.0762 mm/rev, respectively. The location where chatter is induced is called "the critical chatter location". Referring to the time trace of force data and chatter marks on the workpiece, the critical chatter location is determined for a given cutting speed. The same procedures are repeated over the range of cutting speed from 6 to 17 rps for each group of tools. The experimental procedures in outward turning are represented as a flow chart in Figure 7-8.

In order to maintain the tool wear range for experimental procedures, the length of flank wear is regularly examined with a Zygo microscope or an electronic microscope. For example, flank wear of 145 μm is measured in the image of the tool tip obtained by the Zygo microscope as shown in Figure 7-6. Flank wear is also observed by the electronic microscope as shown in Figure 7-7. The light colored portion in the upper part of the picture corresponds to the flank wear of 40 μm. When the size of flank wear is not uniform, averaged flank wear is derived after measuring the flank wear length at a multiple number of positions in the flank wear area.
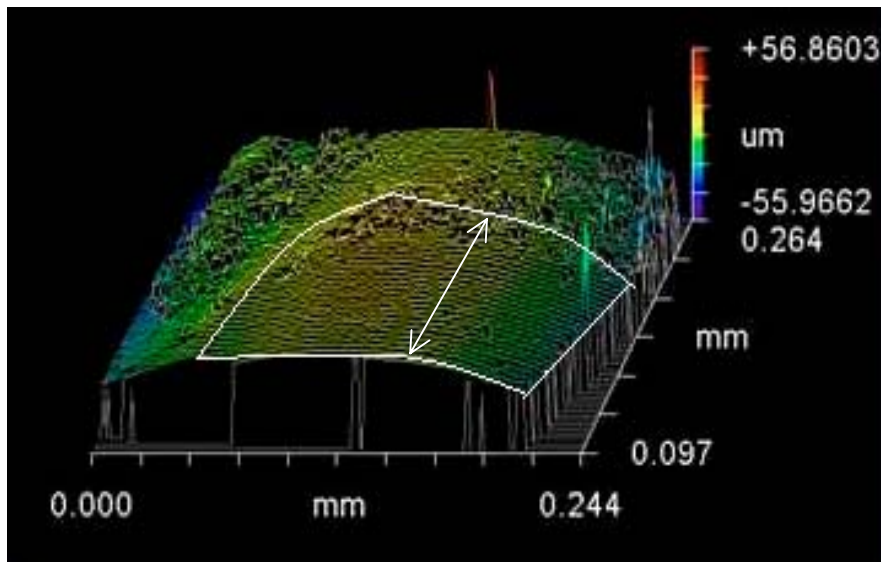
Figure 7-6. Measurement of the size of flank wear with Zygo
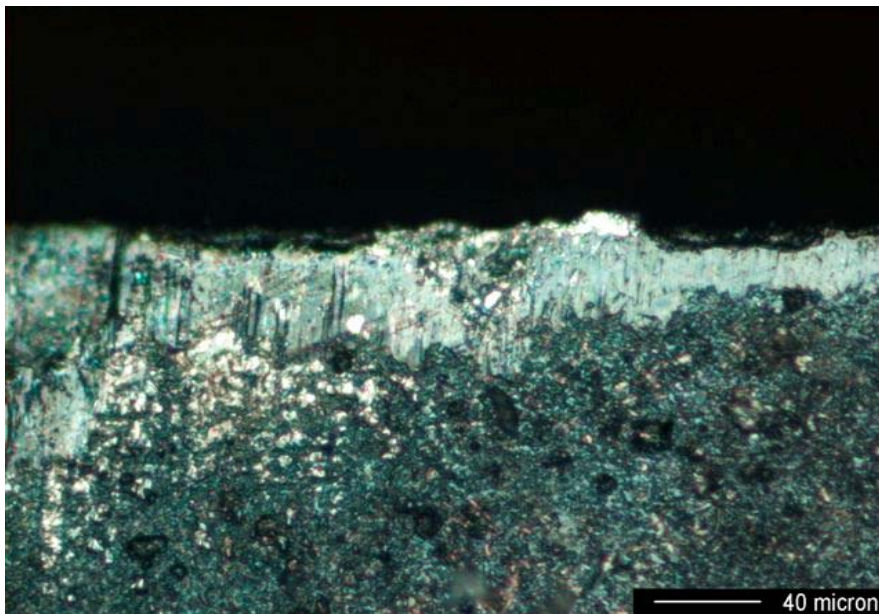
Figure 7-7. Measurement of the size of flank wear with an electronic microscope
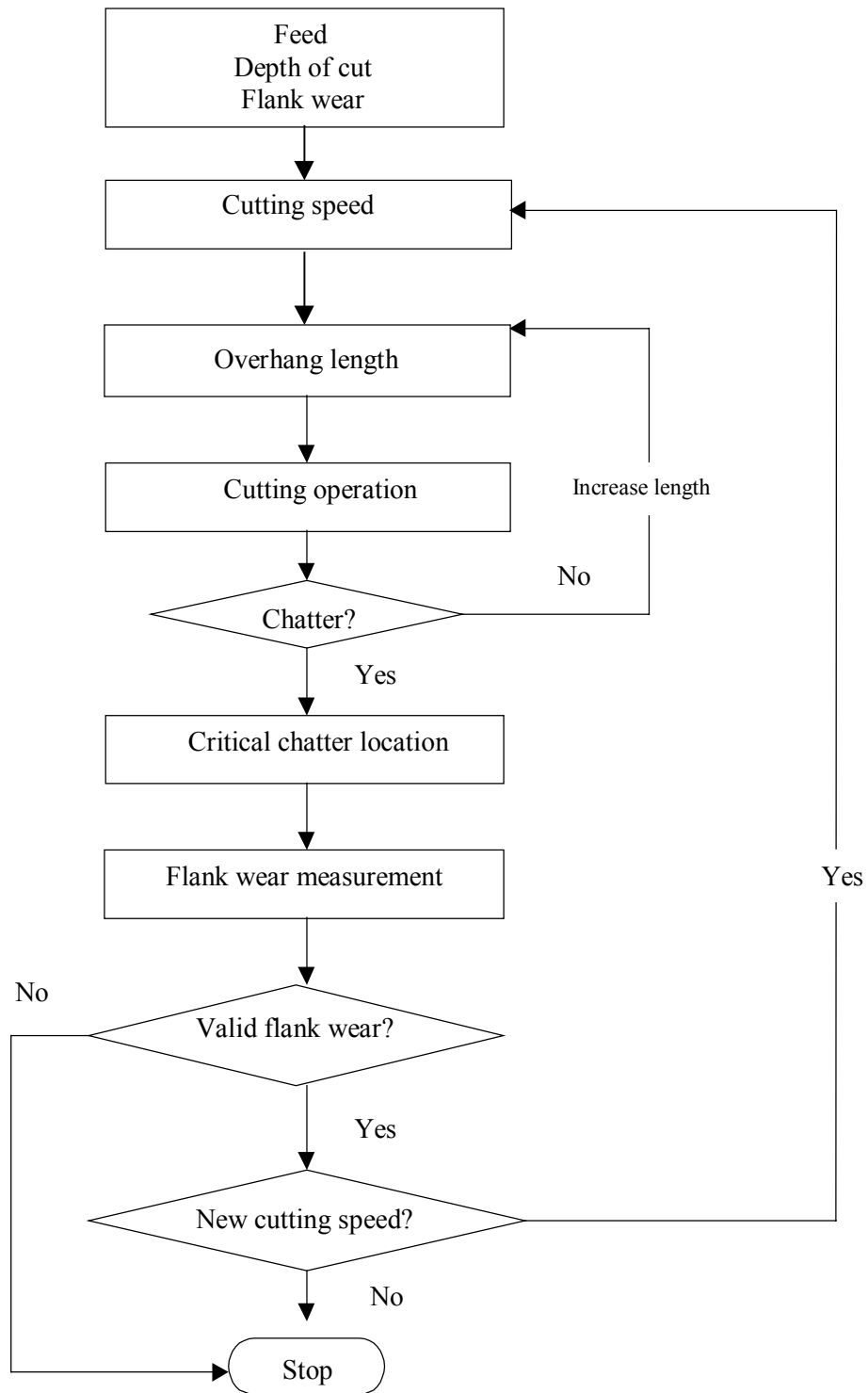
Figure 7-8. Flow chart of experimental procedures to measure stability limits in outward turning

7.2.3.2. Determination of Stability Limits in Inward Turning

Another series of cutting experiments is performed to find chatter stability in inward turning with the feed direction toward the collar, which is more commonly used in practice. The experimental set up is shown in Figure 7-9. A series of cutting tests is carried out from the end of the workpiece for the range of 12.7 mm. The feed rate is fixed to 0.0762 mm/rev. The cutting operation is limited to such a short range since the structural stiffness increases rapidly as the tool advances inward. Slightly worn tools and very worn tools, which have flank wear in the range of [40, 60] μm and [140 160] μm respectively, are used for inward cutting tests. The experimental procedures to determine the stability limits in inward turning are summarized in a flow chart as shown in Figure 7-10.

Figure 7-9. Schematic diagram of the experimental setup for measuring stability limits in inward turning
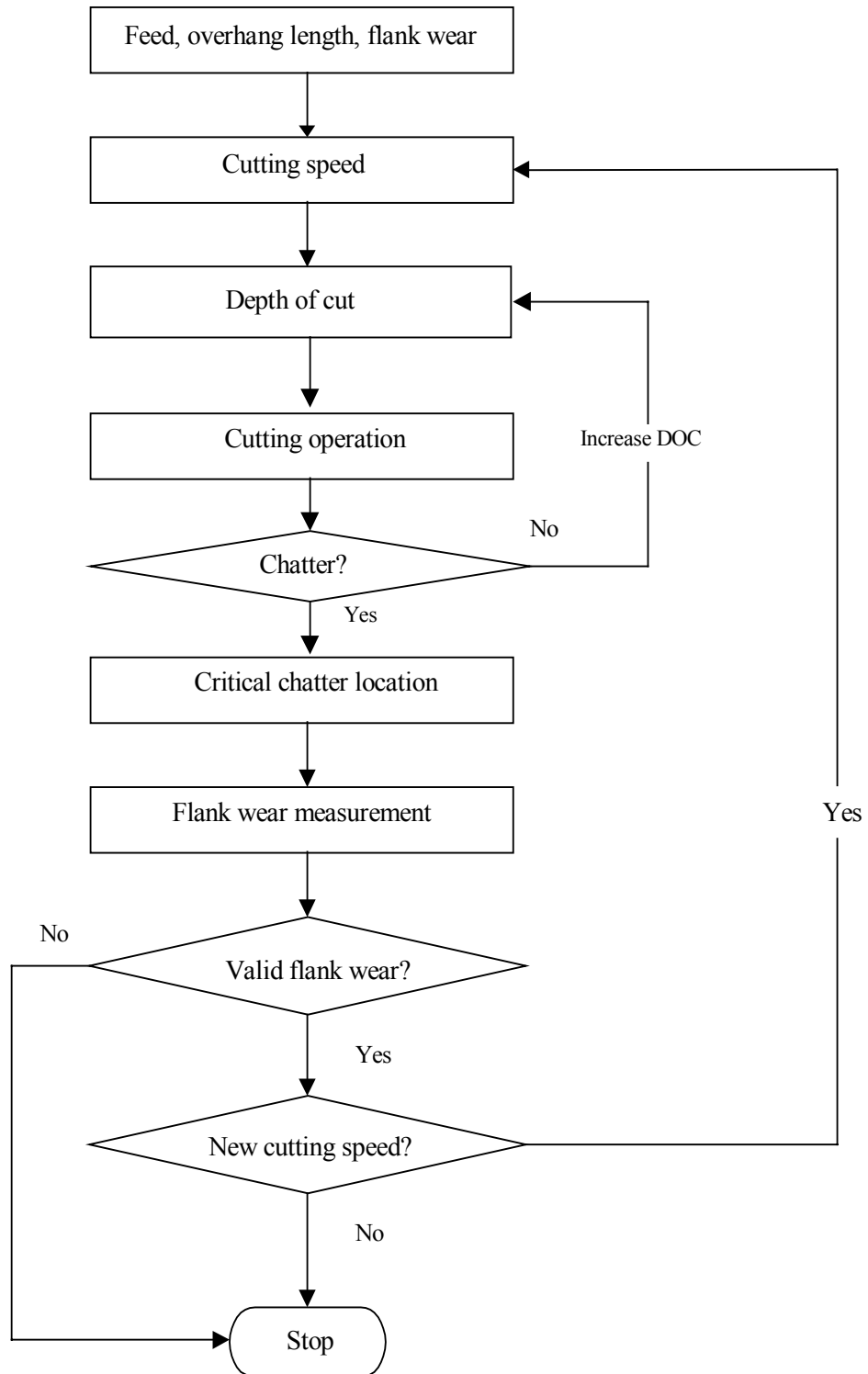
Figure 7-10. Flow chart of experimental procedures to measure stability limits in inward turning
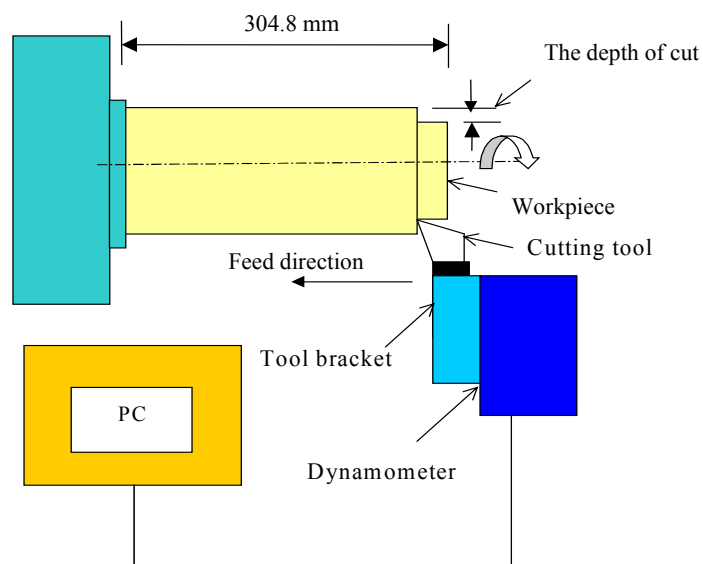
In order to determine "the critical depth of cut" where chatter incurs, a value of the depth of cut is increased by a certain amount each time until vibration is observed satisfying chatter identification criteria. For slightly worn tools, the depth of cut is increases by 0.0635 mm from the initial value of 0.0635 mm. For very worn tools, the same amount is increased from the initial value of 0.127 mm. The same procedures are repeated over the range of cutting speed between 6 and 17 rps.

7.2.4. Experimental Results in Straight Turning

7.2.4.1. Chatter Stability Limits in Outward Turning

The experimental results of critical chatter locations in outward turning with fresh tools are shown in Figure 7-11. Each circle corresponds to the location where chatter starts for a given cutting speed. The dash line connecting data points is added to show the tendency with cutting speed more clearly. In experiments, chatter occurs as the tool advances over a certain location on the bar. In other words, chatter is observed when the structural stiffness of the bar decreases below a certain critical value. It is consistent with the result of the stability analysis that instability is induced as the stiffness ratio is larger than a critical value. The experimental results for slightly worn tools and very worn tools are also shown in Figure 7-12 and Figure 7-13, respectively. The precision of experiments is examined by repeating the cutting test for selected cutting speeds. For example, the standard deviation of chatter locations for slightly worn tools is 2 mm at the speed of 13 rps.

Figure 7-11 Critical chatter locations for fresh tools in outward turning

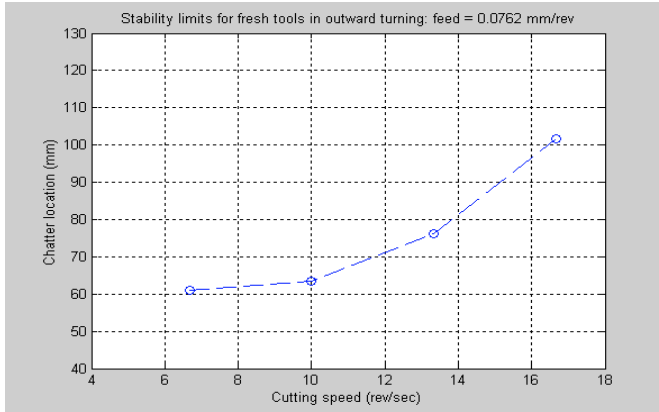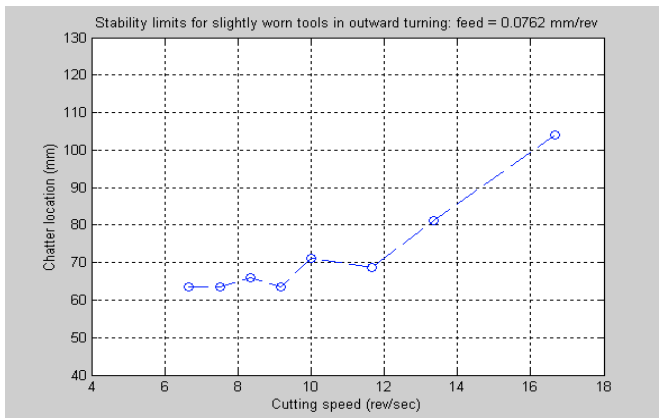Figure 7-12 Critical chatter locations for slightly worn tools in outward turning
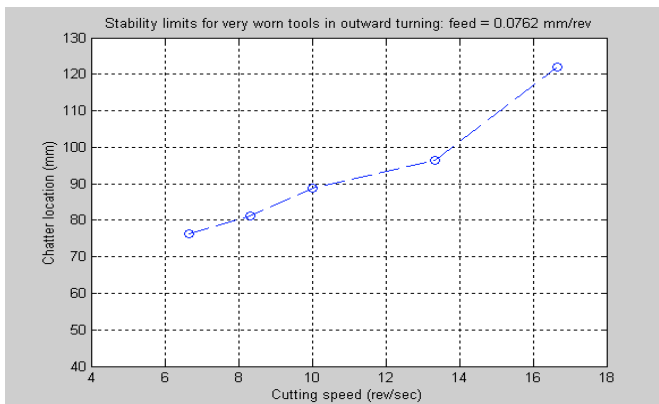
Figure 7-13 Critical chatter locations for very worn tools in outward turning

The features of chatter in outward turning are found from experimental results. Outward turning of 52100 steels with slightly worn tools has the tendency that the critical chatter location slowly increases when speed increases from 6 to 12 rps. However, it is clearly seen that the critical chatter location is increased rapidly in the high-speed region (>12rps). Similar tendency is commonly found in stability limits measurements for other tool groups. The feature of chatter found in outward turning of 52100 bars is contrast with that of chatter in mild turning. Chiou (1995) found that the chatter location in mild turning is inversely proportional to speed in the low-speed range (<12 rps).

In Figure 7-14, critical chatter locations from three tool groups are overlapped together in order to see the flank wear effect on chatter stability. The lowest line and the middle line correspond to fresh tools and slightly worn tools, respectively. Slightly worn tools have 7% larger critical chatter locations in average than fresh tools. The highest stability line corresponds to very worn tools, which have 28 % larger critical chatter locations than fresh tools in average. In conclusion, the stabilizing effect of flank wear is clearly shown in chatter of hard turning.

7.2.4.2. Chatter Stability Limits in Inward Turning

The experimental stability limits are obtained for slightly worn tools in inward turning, and the results are shown in Figure 7-15. The circle and the triangle correspond to the existence of chatter and no chatter, respectively. In experiments, chatter occurs as the depth of cut increases over a certain value for given cutting conditions. Since the cutting stiffness is proportional to the depth of cut, the results are consistent with the
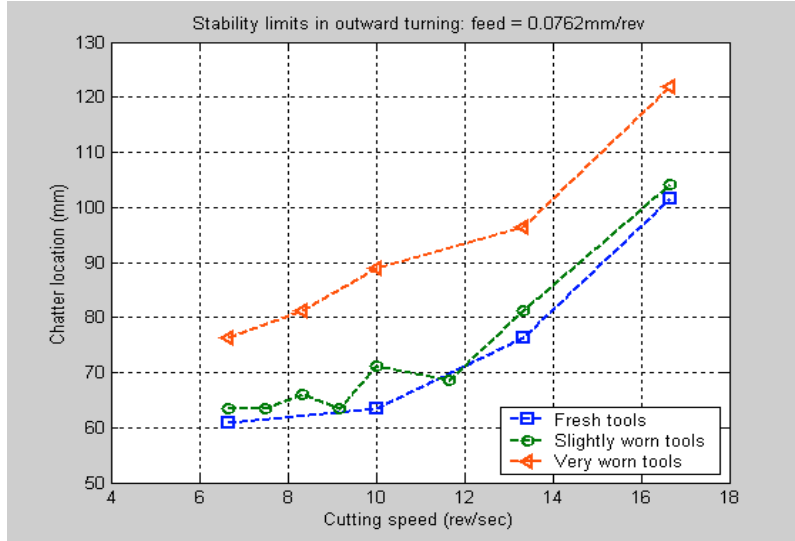
Figure 7-14. Comparison of critical chatter locations for different flank wear in outward turning

stability analysis of the present study that chatter is predicted when the stiffness ratio is larger than a critical value. Because the cutting range is so short, the structural stiffness can be assumed to be constant.

The characteristics of chatter for slightly worn tools in inward turning are found from experimental results. As shown in Figure 7-15, the critical depth of cut varies between 0.0625 and 0.127 mm for the cutting speed range from 8 to 12 rps. At cutting speeds higher than 12 rps, it is found that the critical depth of cut increases with cutting speed. In Figure 7-15, the dash line connecting the critical depth cut is added to show the tendency with cutting speed. It should be noticed that the critical depth of cut is slightly overestimated since discrete values of the depth of cut are applied during experiments.

The variation of the critical depth of cut for very worn tools is shown in Figure 7-16. The critical depth of cut decreases in the range of cutting speed between 8 and 12 rps. At speeds higher than 12 rps, the abrupt increase of the stable region is observed. At the

speed range of between 13 and 16 rps, chatter is detected at the range of the depth of cut

between 0.32 and 0.38 mm. When the speed is larger than 16 rps, no chatter is observed

even at 0.38 mm of the depth of cut. Since the tool failures happen for the depth of cut

larger than 0.38 mm when the cutting speed is larger than 16 rps, no data is collected for

the depth of cut larger than 0.38 mm. Even in the case that the critical depth of cut at 16.7

rps is assumed as 0.44 mm, which is the smallest possible value, it is clearly seen that the

critical depth of cut rapidly increases in the high-speed range (> 12 rps). A very similar

tendency is observed in the measurement of the critical width of cut in Chapter 4.

The critical depth of cut for both tool wear conditions are compared each other in

Figure 7-17. Very worn tools have 3 times larger critical depth of cut in average than

slightly worn tools. Both groups of tools show the same tendency in the high cutting

speed region (> 12 rps). However, the decrease of the critical depth of cut is not observed

in slightly worn tools.
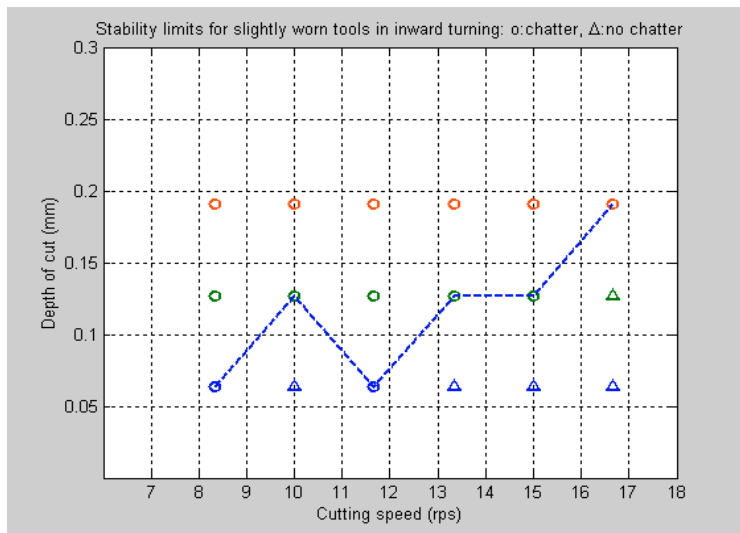
Figure 7-15. Chatter stability for slightly worn tools in inward turning
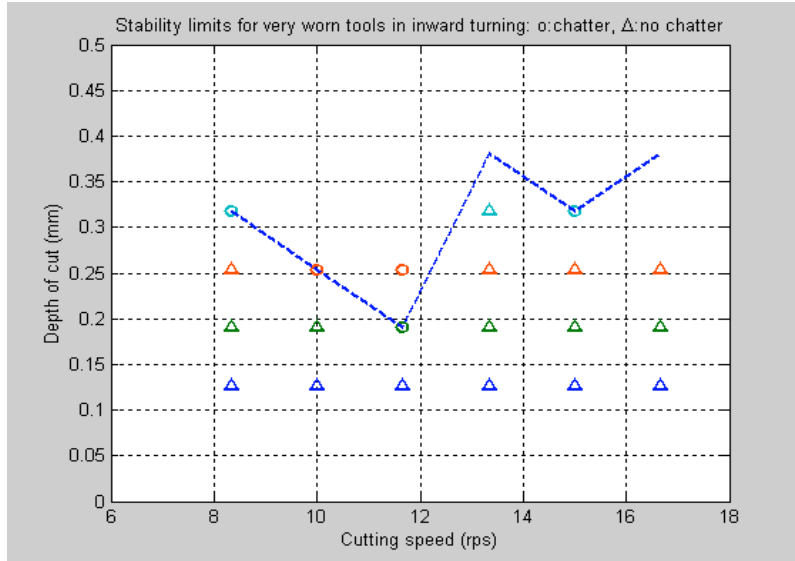
Figure 7-16. Chatter stability for very worn tools in inward turning
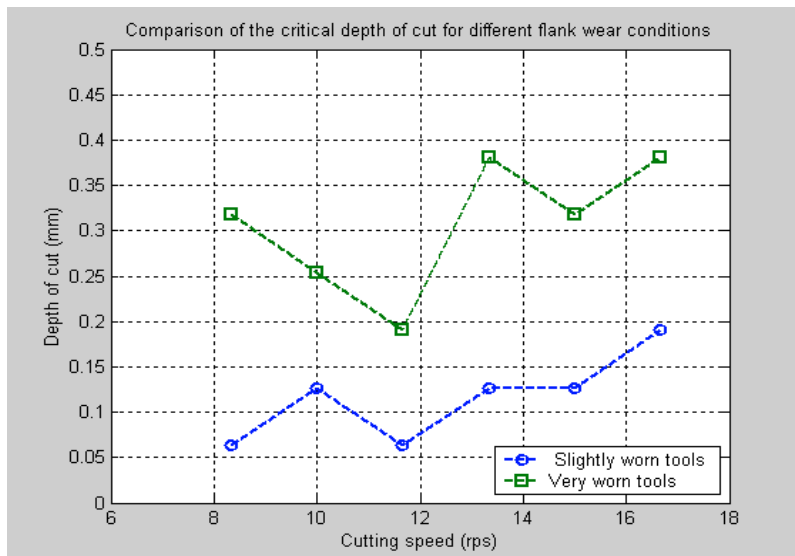
Figure 7-17. Comparison of the critical depth of cut for different flank wear

7.3. Model Validation

7.3.1. Predictions from the Linear Model versus Experimental Data

The validity of the proposed linear chatter model is examined by comparing experimental data in outward turning with stability prediction as shown in Figure 7-18. Solid lines correspond to stability predictions from the linear model for different flank wear length. The region above the solid line is unstable, in which chatter is predicted. The comparison of predictions with experimental data are summarized as followings: First of all, the proposed linear model predicts 25% smaller chatter locations in average than experimental data for fresh tools and the difference from the experimental results increases as cutting speed increases. Second, there is good agreement between the prediction for slightly worn tools and experimental results, especially when the cutting speed is lower than 12 rps. However, underestimated stability limits are predicted the other portion of the cutting speed range. Last, the prediction for very worn tools agrees with experimental data very well for the full range of cutting speed. The prediction shows the same tendency of experimental data for very worn tools, which is the rapid increase of the stable region at the high-speed range.

Theoretical predictions from the linear model for inward turning with slightly worn tools are compared with corresponding experimental data in Figure 7-19. There is good agreement between the prediction and experimental data except for a slight deviation near 12 rps and the very high-speed range (> 16 rps). The stability predictions for very worn tools overlap with experimental data in Figure 7-20, and some disagreement is found at the low-speed range (< 12 rps).
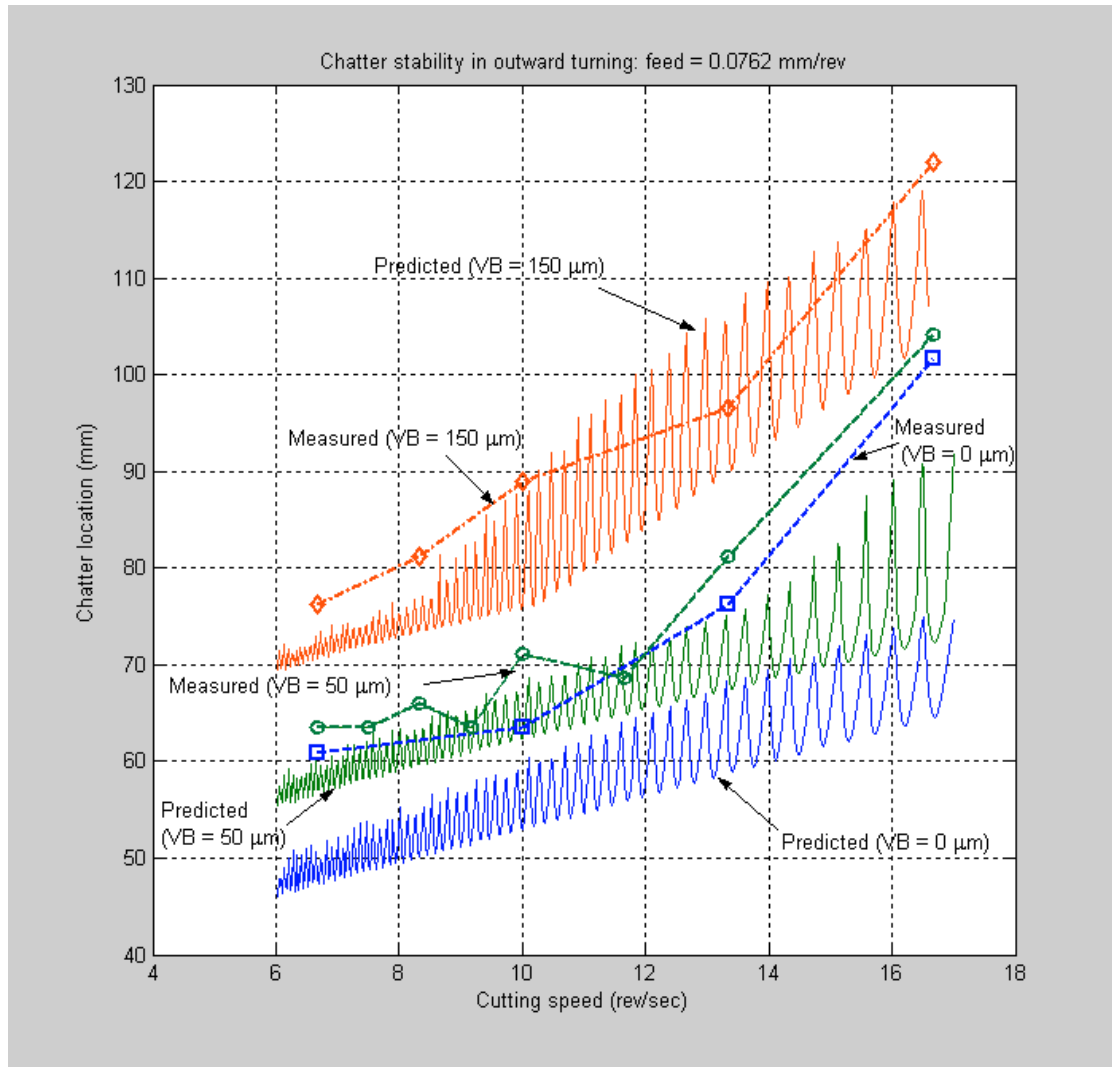
Figure 7-18. Validation of the proposed linear model by experimental data in outward turning

Figure 7-19. Prediction from the linear model versus experimental data for slightly worn tools in inward turning

Figure 7-20. Prediction from the linear model versus experimental data for very worn tools in inward turning

7.3.2. Predictions from the Nonlinear Model versus Experimental Data

The prediction from the nonlinear model is verified by experimental data. The nonlinear stability line is obtained when the value of A_1 is 0.012 mm. Compared to the linear model, the nonlinear model predicts a larger stable area over the full range of cutting speed. When nonlinearity is considered in the chatter modeling for fresh tools case in outward turning, the agreement between predictions and experimental data is improved especially in the speed range higher than 12rps as shown in Figure 7-21. This result is consistent with that the nonlinear terms of the structural stiffness can not be ignored in the range of measured chatter locations in outward turning.

The critical depth of cut for slightly worn tools in inward turning is obtained based on the nonlinear model and compared with experimental data as shown in Figure 7-22. The nonlinear stability line is obtained when the value of A_1 is 0.01mm. The agreement between the predicted stability line and the measured critical depth of cut is improved in the speed range large higher than 13 rps. However, the disagreement further increases at the other range of cutting speed. Since the effect of nonlinear terms of the structure is diminished in inward turning since the cutting is carried out at the end of the 304.5 mm long bar. In addition, the nonlinear terms of cutting force is assumed the same regardless of the variation of the depth of cut. Thus, the nonlinear model doesn't provide improved agreement for inward turning.

The existence of the nonlinear effect on chatter stability is verified by the improved agreement between the stability line from the nonlinear model and experimental data. However, the applicability of the nonlinear model in the machining operations is limited since there is no prior information on A_1 unless an extra sensor is implemented to

measure it. The results of experimental stability limit measurements in outward turning as well as model validations are summarized in Table 7-1.
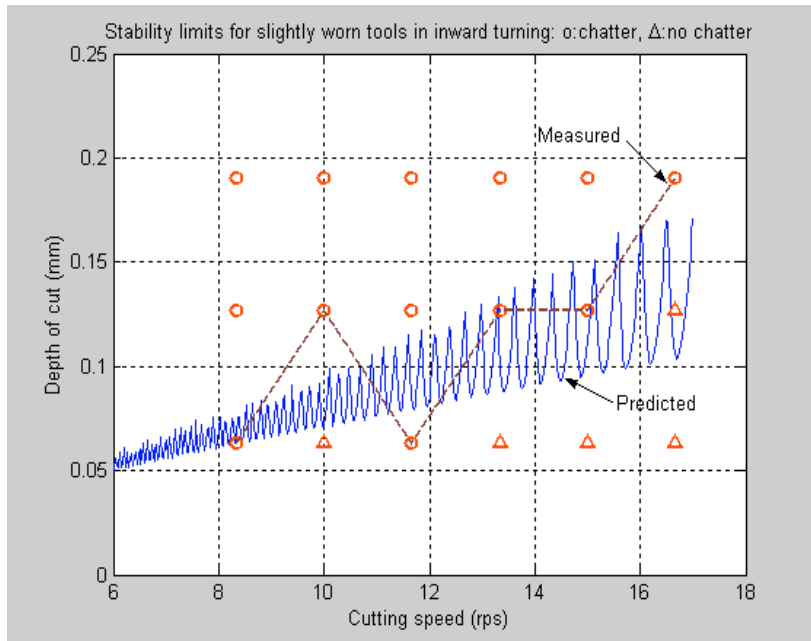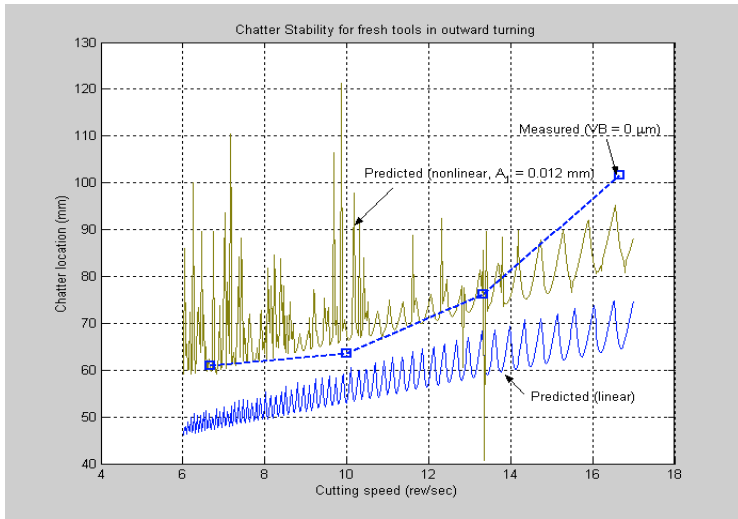

Figure 7-21. Prediction from the nonlinear model versus experimental data for fresh tools in outward turning

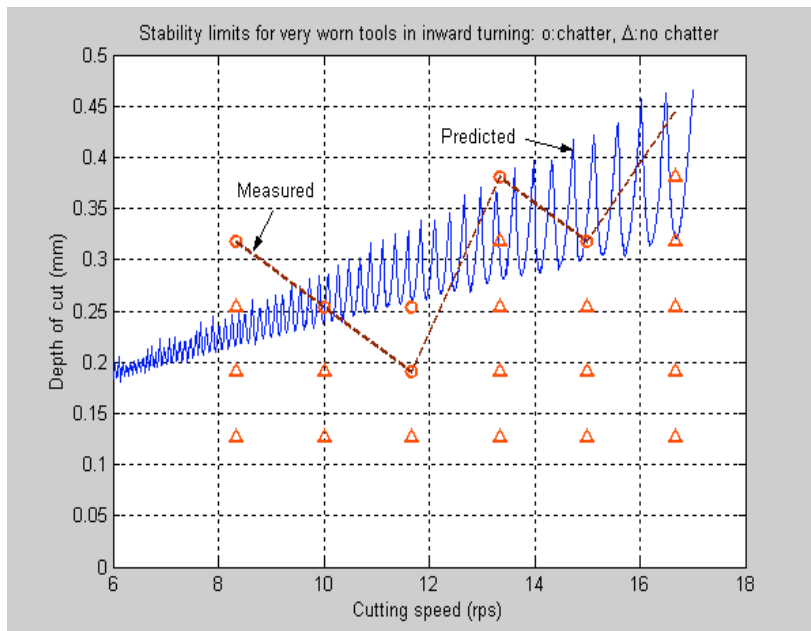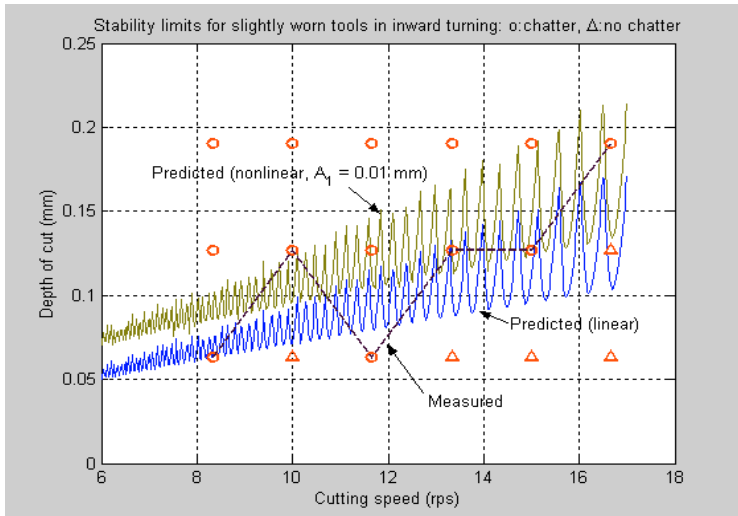Figure 7-22. Prediction from the nonlinear model versus experimental data for slightly worn tools in inward turning

Table 7-1. Summary of experimental results and model validations in straight turning of 52100 bars

	Tools	Stable area variation with speed	Experimental data vs. Prediction	Mild turning
Outward turning	Fresh	• Slow increase in 6<Ω<13 rps; • Fast increase 13<Ω<17 rps.	• Predicted stability limits are smaller than experimental data for the full speed range; • Disagreement increases as speed increases; • More accurate stability lines from the nonlinear model in the high-speed range.	Critical chatter location is inversely proportional to speed at the low-speed range and proportional at the high-speed range (Chiou, 1996).
	Slightly worn	• Slow increase in 6<Ω<12 rps; • Fast increase in 12<Ω<17 rps; • 7% larger chatter location than fresh tools.	• Good agreement in 6<Ω<12 rps; • Minor disagreement in 12<Ω<17 rps.	
	Very worn	• Slow increase in 6<Ω<13 rps; • Fast increase in 13<Ω<17 rps; • 28% larger chatter location than fresh tools.	• Very good agreement in the full speed range.	
Inward turning	Slightly worn	• Slow decrease in 8<Ω<12 rps; • Slow increase in 12<Ω<17 rps.	• Good agreement in 8<Ω<16 rps; • Predicted stability limits are smaller than experimental data at Ω>16rps; • Nonlinear model reduces the disagreement at Ω>16rps.	Critical depth of cut decreases with speed in the low-speed range. After reaching a minimum, it slightly increases with speed in the high-speed range. (Minis *et al.*, 1990)
	Very worn	• Fast decrease in 8<Ω<12 rps; • Fast increase in 12<Ω<17 rps; • 3 times larger depth of cut than slightly worn tools.	• Very good agreement in 12<Ω<17 rps; • Opposite tendency in 8<Ω<12 rps.	

7.3.3. Empirical Model

Even though the nonlinear model provides improved predictions relative to those of the linear model, the disagreement between the predicted stability line and experimental stability limits still remains, especially when very worn tools are applied in inward turning at very low (<8 rps) and very high (>16 rps) cutting speeds. Furthermore, the lack of information on certain parameters such as A_1 restricts the usage of the nonlinear model. As an alternative approach, an empirical model is proposed to fit experimental stability limits for the full range of cutting speed. The new stability line is obtained by following relations:

$$doc_{new} = [0.85\cos(36/\Omega) + 1.7]doc$$

where *doc* is the critical depth of cut, which is predicted in the linear model. Since the empirical model provides larger stable region in the very low and the very high speed range, the accuracy of the prediction is certainly improved for the full range of the speed as shown in Figure 7-23.
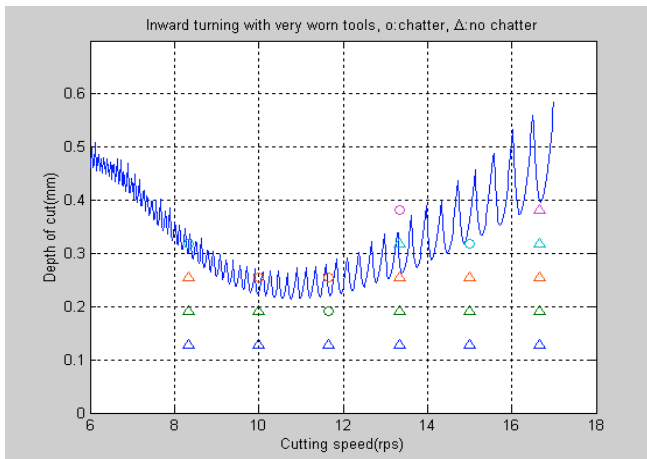
Figure 7-23. Verification of the empirical model by experimental data

7.4. Conclusion

The characteristics of chatter stability in straight turning of 52100 bars are found through a series of cutting experiments. The slow increase of the stable region with the increase of cutting speed at the low cutting speed range (< 12 rps) and the rapid increase of the stable region at the high-speed region (> 12 rps) are commonly found for all flank wear conditions in outward turning. The stabilizing effect of flank wear is also confirmed by experiments suggesting that very worn tools have about 28% larger values of the critical chatter location than fresh tools. It is found that the experimental stability limits in inward turning are proportional to cutting speed when cutting speed is larger than 12 rps. In addition, it is found that the experimental stability limits abruptly decreases with speed at the low cutting speed range (< 12 rps).

The proposed model is validated by experimental data. There is very good agreement between the prediction and the experimental stability limits, especially for very worn tools in outward turning. However, the proposed linear model predicts a smaller stable region in the high-speed range (> 12 rps) of outward turning for the other tool conditions. The predictions for inward turning also show good agreement with experimental results except for a minor disagreement at very high cutting speed (> 16 rps). The empirical model is proposed as an alternative way to fit the experimental data for the full speed range.

CHAPTER 8

CONCLUSIONS AND RECOMMENDATIONS

8.1. Contributions

This research is motivated by the need for a effective chatter model in order to predict chatter-free cutting conditions, which are crucial for achieving higher productivity in hard turning. In order to satisfy the objective, the contributions of this research include the following:

8.1.1. Modeling

- A linear chatter model for worn tools in facing operations with non-uniform load distribution (Chapter 2);

- A nonlinear model of chatter for worn tools in straight turning considering the effects of cutting speed and tool geometry (Chapter 5);

- Stability analysis for worn tools to decide the critical stability parameter (Chapter 2 and 5).

Chatter of a flexible tool in facing operations is modeled by considering the regenerative effect and the flank wear effect. A non-uniform load distribution has the ability to reflect the change of flank wear length as well as the degree of the plastic deformation on flank wear. Furthermore, the modeling for sharp tools can be derived as a

special case of the modeling for worn tools by specializing non-uniform load distribution to be the Dirac delta function.

A one-degree-of-freedom nonlinear model is developed to describe the radial chatter of a flexible workpiece in straight turning. The assumption of radial chatter is verified by the equivalent side cutting edge angle, considering the tool geometry effect caused by the large tool nose radius and the shallow depth of cut. The proposed model can be applied to mild turning as well as hard turning by considering the material property through the cutting stiffness. In addition, the linear model can be derived as a special case of the nonlinear model with the chatter amplitude of zero.

The stability analysis for worn tools is provided based on the root locus method. The behavior of root loci indicates that the minimum stiffness ratio is the critical stability parameter. In addition, the sufficient condition to have a larger chatter-free region with the increase of cutting speed is derived. The describing function method is employed to incorporate a third-order polynomial nonlinearity in both the structure and cutting force. It is found that the minimum stiffness ratio is the critical stability parameter, which needs to satisfy harmonic balance equations simultaneously.

8.1.2. Characteristic Parameter Measurements

- Experimental measurements of the natural frequency and the damping ratio for the tool system (Chapter 3) and the workpiece (Chapter 6);

- Experimental measurements of the linear cutting stiffness for various values of the width of cut (Chapter 3) and the depth of cut (Chapter 6) considering the effect of cutting speed;

- Experimental measurements of the nonlinear cutting stiffness for a fixed depth of cut considering the effect of flank wear and cutting speed (Chapter 6);

- Experimental measurements of the linear (Chapter 3) and nonlinear (Chapter 6) structural stiffness of the workpiece;

- Derivation of converting relationships between the stiffness ratio and a cutting parameter (Chapters 3 and 6).

Characteristic parameters including the natural frequency, the damping ratio, the structural stiffness and the cutting stiffness of the tool system are measured experimentally for the purpose of predicting chatter stability.

After extensive cutting force measurements, the nonlinear cutting stiffness is obtained as a third-order polynomial for a fixed depth of cut. Since cutting force is measured for various flank wear and cutting speed, the proposed model implicitly includes the nonlinearity caused by friction, which depends on speed and tool wear. The tendencies of force data are consistent with those of existing experimental investigations and the confidence intervals of force data confirm the reliability of the experiments. The cutting stiffness increases as flank wear increases or cutting speed decreases. The linear cutting stiffness for various depths of cut is measured in order to derive the converting relationship between the stiffness ratio and the depth of cut. The structural stiffness of the workpiece decreases as the overhang length increases. Furthermore, the converting relationships between the stiffness ratio and a practical cutting stiffness are obtained as a function of cutting speed for given tool wear conditions.

8.1.3. Predictions of Stability Limits

- Determination of the minimum stiffness ratio as a critical stability parameter over the range of cutting speed based on the proposed linear model (Chapter 3) and the nonlinear model (Chapter 6);

- Demonstration of the effects of flank wear and nonlinearity on stability charts (Chapters 3 and 6);

- Explanation of nonlinear phenomena of chatter based on theoretical predictions (Chapter 6).

Based on characteristic parameters and converting relations, 2-D and 3-D stability charts are plotted from the linear and the nonlinear model, respectively. The stabilizing effect of flank wear is shown in theoretical predictions when the area under the stability line is calculated for divided speed regions. The effect of flank wear is the most significant in the high-speed range (> 12 rps). The nonlinear phenomena of chatter can be explained by the stability chart on the A_1 and k_c/k_m plane. The evolution of chatter with the variation of the stiffness ratio causes the finite amplitude and jump phenomena in chatter. The effect of nonlinearity results in either smaller or larger stable region depending on the value of A_1 and cutting speed. Therefore, the prior information on A_1 is required to utilize the nonlinear model for chatter predictions.

Even though linear models have certain limits in their application, the development of the linear model are still valid since the lack of information of A_1 for most machining cases in practice. In addition, linear models are much easier to solve than nonlinear models. Furthermore, when the converting relation is obtained as a function of speed and

tool wear, the effect of friction is considered implicitly even in linear models, which certainly improves agreement with experimental data.

8.1.4. Chatter Stability Limit Measurements

- Measurements of the critical width of cut in facing of 52100 bars (Chapter 4);

- Measurements of the critical chatter location in outward straight turning of 52100 bars for three different ranges of flank wear (Chapter 7);

- Measurements of the critical depth of cut in inward straight turning of 52100 bars for two different ranges of flank wear (Chapter 7);

- Validation of the proposed linear chatter model (Chapter 4) and the nonlinear chatter model (Chapter 7) with experimental data;

- Derivation of an empirical model (Chapters 4 and 7).

The critical width of cut is measured in facing of 52100 bars and the characteristics of chatter in hard turning are discovered. A large stable region at very low speed (6 rps) and a rapid increase in the size of the stable region at high speed (>12.5 rps) are found. In contrast to mild turning, the abrupt increase in the size of the stable region at the high cutting speed is the distinct feature in hard turning. The proposed model is verified by experimental results and very good agreement is confirmed for the cutting speed range between 6 and 10 rps. However, the proposed model predicts somewhat smaller stable region in both low (< 6 rps) and high cutting speeds (> 10 rps). The accuracy of predictions is clearly improved when the flank wear effect is included in the model. The

new stability boundary of the empirical model is obtained in order to provide predictions matched with experimental data over the full cutting speed range.

The critical chatter location is measured in outward straight turning of 52100 hardened steel bars for three groups of tools with different flank wear. Experimental data confirm the flank wear effect on chatter stability in turning. The critical chatter location slowly increases proportional to cutting speed when the speed is less than 12 rps (slightly worn tools) or 13 rps (fresh/very worn tools) while it abruptly increases otherwise. The feature of chatter found in outward turning of 52100 bars is contrast with that of chatter in mild turning, which is inversely proportional to speed in the low-speed range. There is very good agreement between the prediction by the proposed linear model and experimental data for cases involving very worn tools. The minor inconsistency between the prediction and measured data is observed especially in the high-speed range (> 12 rps) for fresh tools. The nonlinear model provides an improved prediction by indicating an increase in the area of the stable region in the high-speed range.

The critical depth of cut is measured in inward straight turning of 52100 bars and the characteristics of chatter depend on flank wear conditions. For slightly worn tools, the critical depth of cut is remained between 0.0625 and 0.127 mm for the range of cutting speed $6 < \Omega < 14$ rps. It is found that the critical depth of cut rapidly increases at very high cutting speeds (> 14 rps). For very worn tools, the critical depth of cut is decreased as cutting speed increases when the cutting speed is between 8 and 12 rps. However, it is increased rapidly in the high cutting speed range (> 12 rps). The stability predictions are verified by experimental data and the result shows good agreement except in low and

very high-speed ranges for cases involving very worn tools. In order to fit with experimental data over the full range of speed, an empirical model is proposed.

The flank wear effect on the chatter stability limit is observed for all feed directions. The dependency of the flank wear effect on cutting speed is found in experimental data of inward turning.

8.2. Critical Evaluations and Recommendations for Future Works

In this section, a critical evaluation on the material presented in this thesis is offered. Some recommendations are offered for further advancement of the state of the art.

8.2.1. Modeling

Friction is one of the major sources of nonlinearity and is closely related to flank wear. Even though its effect is considered in the prediction implicitly through measuring cutting force for different flank wear and cutting force, a model can be further developed to address the effect of friction explicitly.

In the present study, a 1-DOF modeling is proposed to describe a radial direction chatter. However, the dominant direction of chatter can be changed in straight turning as the cutting conditions change (Pratt and Nayfeh, 1999). Therefore, a 3-DOF chatter model may be considered to obtain more accurate predictions for an even wider range of cutting conditions combined with a 3-D force model for oblique cutting.

8.2.2. Characteristic Parameter Measurements

In the present study, the nonlinear cutting stiffness is obtained only for one value of the depth of cut. For more accurate predictions from the nonlinear model, additional measurement of the nonlinear cutting stiffness should be conducted for various values of the depth of cut. Eventually, a 3-D force model for hard turning can be combined with the chatter model, in order to provide the cutting stiffness for chatter predictions as long as reliable force predictions are available for the wide range of cutting parameters and tool wear conditions.

8.2.3. Predictions of Stability Limits

In the present study, critical stability parameters are obtained from the converting relations, which depend on cutting speed and flank wear conditions. However, the converting relations for facing and inward turning are considered only for cases involving slightly worn tools. For more accurate predictions, the converting relations for very worn tools should be obtained for facing and inward turning.

The evolution of chatter shown in the stability charts can be verified either by analytic methods such as Floquet theory or direct numerical methods. Since the harmonic balance method only approximates nonlinear elements, some additional independent methods may need to be introduced to confirm the predictions.

8.2.4. Chatter Stability Limit Measurements

In practice, the feed rate is another important factor affecting the stability in machining process. The proposed model reflects the effect of the feed rate variations by

allowing the different values of the nonlinear cutting stiffness. However, experimental chatter stability limits of the present study are obtained only for a nominal feed rate. In other words, the validity of the current model has not been examined for other feed rates.

Even though chatter evolution is available for continuous variation of the stiffness ratio, no experiments are carried out to verify predictions for a specific value of chatter amplitude. For the validation of nonlinear chatter behaviors, chatter amplitude measurements with continuous variation of the critical stability limit should be conducted.

The abrupt decrease of the stable area at very low speed is a characteristic of inward turning with very worn tools and facing. However, the prediction provides a smaller stable region for corresponding cutting conditions. Since the contact force model (Chiou and Liang, 1998) predicts a large stable region in the low-speed region, it can be considered as a viable alternative for the future modeling as long as reliable measurement of the contact volume is available.

8.3. Concluding Remarks

The chatter model in this study will contribute to identifying less conservative chatter-free cutting conditions during machining operations. In addition, these chatter-free cutting conditions can be used as a guideline for designing tools and machines. Experimental data on chatter stability limits in hard turning are obtained for the first time. Newly found characteristics of chatter in hard turning can contribute to broaden our physical understanding on the interactions between the tool and the workpiece in hard

turning. Experimental results on stability limits for different flank wear may serve to help to develop more sensible approaches to consider the flank wear effect in chatter models for hard turning. As a result of these contributions, the proposed chatter model will help to improve productivity in manufacturing process. The chatter experimental data will be useful to develop other theoretical chatter models in hard turning.

APPENDIX A

STABILITY ANALYSIS FOR WORN TOOLS WITH ROOT LOCUS METHOD

A.1. Analytical Determination of Locations of Poles and Zeros

The closed loop characteristic equation with non-uniform load distribution is

$$s^2 + 2\zeta\omega_n s + \omega_n^2 + \frac{k_c}{k_m}\omega_n^2 \int_{-h}^{0} \sigma(\theta)e^{s\theta}d\theta(1 - e^{-sT_p}) = 0 \tag{A-1}$$

The closed loop characteristic equation (A-1) can be represented for k_c/k_m as

$$\frac{k_c}{k_m} = \frac{s^2 + 2\zeta\omega_n s + \omega_n^2}{\omega_n^2 \int_{-h}^{0} \sigma(\theta)e^{s\theta}d\theta(e^{-sT_p} - 1)} \tag{A-2}$$

where $\left| \dfrac{s^2 + 2\zeta\omega_n s + \omega_n^2}{\omega_n^2 \int_{-h}^{0} \sigma(\theta)e^{s\theta}d\theta(e^{-sT_p} - 1)} \right| = \left| \dfrac{k_c}{k_m} \right|$ and $\angle\left(\dfrac{s^2 + 2\zeta\omega_n s + \omega_n^2}{\omega_n^2 \int_{-h}^{0} \sigma(\theta)e^{s\theta}d\theta(e^{-sT_p} - 1)} \right) = 0$

Poles of the closed loop system correspond to roots of equation (A-1) for $k_c/k_m = 0$. When the numerator of equation (A-2) is 0 with a non-zero value of the denominator, there are two finite poles given by

$$s = -\zeta\omega_n \pm \sqrt{\zeta^2\omega_n^2 - \omega_n^2} \tag{A-3}$$

The value of k_c/k_m can also go to 0 as the denominator of equation (A-2) becomes infinite while the numerator remains finite. Let the value of s be $-\infty \pm j\,2n\pi/T_p$. Then, the magnitude of the denominator of equation (A-2) becomes

$$\left| \omega_n^2 \int_{-h}^{0} \sigma(\theta)e^{s\theta}d\theta(e^{-sT_p} - 1) \right| = \left| \omega_n^2 \int_{-h}^{0} \sigma(\theta)e^{(-\infty \pm j\frac{2n\pi}{T_p})\theta}(e^{\infty T_p}e^{\mp j2n\pi} - 1)d\theta \right|$$

$$= \left| \omega_n^2 \int_{-h}^{0} \sigma(\theta)e^{(-\infty \pm j\frac{2n\pi}{T_p})\theta}(e^{\infty T_p} - 1)d\theta \right| = \infty \tag{A-4}$$

Therefore there are an infinite number of poles with a negative infinite real part, which are apart from each other by $2n\pi/T_p$, in addition to two finite poles in the left-hand side of the *s*-plane.

Zeros of the closed loop system correspond to roots of equation (A-1) as k_c/k_m tends to infinity. The value of k_c/k_m becomes infinite as the denominator tends to 0 while the numerator is finite. Let the value of *s* be $\pm j2n\pi/T_p$, then the magnitude of the denominator of equation (A2) becomes

$$\left| \omega_n^2 \int_{-h}^{0} \sigma(\theta) e^{s\theta} d\theta (e^{-sT_p} - 1) \right| = \left| \omega_n^2 \int_{-h}^{0} \sigma(\theta) e^{s\theta} e^{-sT_p} d\theta - \omega_n^2 \int_{-h}^{0} \sigma\theta) e^{s\theta} d\theta \right|$$

$$= \left| \omega_n^2 \int_{-h}^{0} \sigma(\theta) e^{(\pm j\frac{2n\pi}{T_p})\theta} e^{-(\pm j\frac{2n\pi}{T_p})T_p} d\theta - \omega_n^2 \int_{-h}^{0} \sigma\theta) e^{(\pm j\frac{2n\pi}{T_p})\theta} d\theta \right| = 0 \qquad \text{(A-5)}$$

Therefore, there are an infinite number of zeros on the imaginary axis, which are apart from each other by $2n\pi/T_p$.

A.2. Analytical Sign Determination

Substituting $a+jb$ into *s* in equation (A-1) yields

$$(a + jb)^2 + 2\zeta\omega_n(a + jb) + \omega_n^2 + \frac{k_c}{k_m}\omega_n^2 \int_{-h}^{0} \sigma(\theta) e^{(a+jb)\theta} d\theta (1 - e^{-(a+jb)T_p}) = 0 \qquad \text{(A-6)}$$

The real part of equation (A-6) is

$$a^2 - b^2 + 2\zeta\omega_n a + \omega_n^2 + \frac{k_c}{k_m}\omega_n^2 \left\{ \begin{array}{l} [1 - e^{-aT_p}\cos(bT_p)]\int_{-h}^{0}\sigma(\theta)e^{a\theta}\cos(b\theta)d\theta \\ -[e^{-aT_p}\sin(bT_p)]\int_{-h}^{0}\sigma(\theta)e^{a\theta}\sin(b\theta)d\theta \end{array} \right\} = 0 \qquad \text{(A-7)}$$

Equation (A-7) can be solved for k_c/k_m giving

133

$$\frac{k_c}{k_m} = \frac{a^2 - b^2 + 2\zeta\omega_n a + \omega_n^2}{\omega_n^2 \left\{ \begin{array}{l} [e^{-aT_p}\cos(bT_p) - 1]\int_{-h}^0 \sigma(\theta)e^{a\theta}\cos(b\theta)d\theta \\ + [e^{-aT_p}\sin(bT_p)]\int_{-h}^0 \sigma(\theta)e^{a\theta}\sin(b\theta)d\theta \end{array} \right\}}$$ (A-8)

Since we are interested in the sign of the real apart of the roots near zeros, substitute $\pm 2n\pi/T_p$ into b in equation (A-8)

$$\lim_{|a|\to 0, b\to\pm\frac{2n\pi}{T_p}} \frac{k_c}{k_m} = \frac{-\left(\frac{2n\pi}{T_p}\right)^2 + \omega_n^2}{\omega_n^2 \int_{-h}^0 \sigma(\theta)\cos\left(\frac{2n\pi}{T_p}\theta\right)d\theta} \Gamma = \infty$$ (A-9)

where Γ is $1/(e^{-aTp} - 1)$ as the absolute value of a approaches zero. The absolute value of Γ is infinite and the sign is opposite that of a.

When $-(2n\pi/T_p)^2 + \omega_n^2 > 0$, the condition to have a positive k_c/k_m requires that

$\omega_n^2[-\text{sgn}(a)]\int_{-h}^0 \sigma(\theta)\cos(2n\pi\theta/T_p) > 0$. Thus,

If $\int_{-h}^0 \sigma(\theta)\cos(2n\pi\theta/T_p)d\theta > 0$, then $-\text{sgn}(a)>0$ i.e. $a<0$ (A-10a)

If $\int_{-h}^0 \sigma(\theta)\cos(2n\pi\theta/T_p)d\theta < 0$, then $-\text{sgn}(a)<0$ i.e. $a>0$ (A-10b)

When $-(2n\pi/T_p)^2 + \omega_n^2 < 0$, the condition to have a positive k_c/k_m requires that

$\omega_n^2[-\text{sgn}(a)]\int_{-h}^0 \sigma(\theta)\cos(2n\pi\theta/T_p)d\theta < 0$. Thus,

If $\int_{-h}^0 \sigma(\theta)\cos(2n\pi\theta/T_p)d\theta > 0$, then $-\text{sgn}(a)<0$ i.e. $a>0$ (A-11a)

If $\int_{-h}^0 \sigma(\theta)\cos(2n\pi\theta/T_p)d\theta < 0$, then $-\text{sgn}(a)>0$ i.e. $a<0$ (A-11b)

A.3. Numerical Procedures to Find Root Loci

Substituting $a+jb$ into s in equation (A-1) yields

$$(a+jb)^2 + 2\zeta\omega_n(a+jb) + \omega_n^2 + \frac{k_c}{k_m}\omega_n^2[1-e^{-(a+jb)T_p}]\int_{-h}^{0}\sigma(\theta)e^{-(a+jb)\theta}d\theta = 0 \qquad \text{(A-12)}$$

The real part of equation (A-12) is given as

$$f(a,b) = a^2 - b^2 + 2\zeta\omega_n a + \omega_n^2 + \frac{k_c}{k_m}\omega_n^2[1-e^{-aT_p}\cos(bT_p)]\int_{-h}^{0}\sigma(\theta)e^{-a\theta}\cos(b\theta)d\theta$$

$$+\frac{k_c}{k_m}\omega_n^2[e^{-aT_p}\sin(bT_p)]\int_{-h}^{0}\sigma(\theta)e^{-a\theta}\sin(b\theta)d\theta \qquad \text{(A-13)}$$

The imaginary part of equation (A-12) is

$$g(a,b) = 2ab + 2\zeta\omega_n b + \frac{k_c}{k_m}\omega_n^2[e^{-aT_p}\cos(bT_p)-1]\int_{-h}^{0}\sigma(\theta)e^{-a\theta}\sin(b\theta)d\theta$$

$$+\frac{k_c}{k_m}\omega_n^2[e^{-aT_p}\sin(bT_p)]\int_{-h}^{0}\sigma(\theta)e^{-a\theta}\cos(b\theta)d\theta \qquad \text{(A-14)}$$

The partial derivatives of $f(a, b)$ and $g(a, b)$ with respect to a and b are derived as followings:

$$\frac{\partial f}{\partial a} = 2a + 2\zeta\omega_n + \frac{k_c}{k_m}\omega_n^2 \left\{ \begin{array}{l} J_{tc}[e^{-aT_p}\cos(bT_p)-1] + J_c[T_p e^{-aT_p}\cos(bT_p)] \\ -J_{ts}[e^{-aT_p}\sin(bT_p)] - J_s[T_p e^{-aT_p}\sin(bT_p)] \end{array} \right\}$$

$$\frac{\partial f}{\partial b} = -2b + \frac{k_c}{k_m}\omega_n^2 \left\{ \begin{array}{l} J_{ts}[e^{-aT_p}\cos(bT_p)-1] + J_c[T_p e^{-aT_p}\sin(bT_p)] \\ +J_{tc}[e^{-aT_p}\sin(bT_p)] + J_s[T_p e^{-aT_p}\cos(bT_p)] \end{array} \right\}$$

$$\frac{\partial g}{\partial a} = 2b - \frac{k_c}{k_m}\omega_n^2 \left\{ \begin{array}{l} J_{tc}[e^{-aT_p}\sin(bT_p)] + J_c[T_p e^{-aT_p}\sin(bT_p)] \\ +J_{ts}[^{-aT_p}\cos(bT_p)-1] + J_s[T_p e^{-aT_p}\cos(bT_p)] \end{array} \right\}$$

$$\frac{\partial g}{\partial a} = 2a + 2\zeta\omega_n + \frac{k_c}{k_m}\omega_n^2 \left\{ \begin{array}{l} -J_{ts}[e^{-aT_p}\sin(bT_p)] + J_c[T_p e^{-aT_p}\cos(bT_p)] \\ +J_{tc}[e^{-aT_p}\cos(bT_p)] - J_s[T_p e^{-aT_p}\sin(bT_p)] \end{array} \right\} \quad \text{(A-15a-d)}$$

where

$$J_c = \int_{-h}^{0} \sigma(\theta)e^{-a\theta}\cos(b\theta)d\theta \quad J_{tc} = \int_{-h}^{0} \sigma(\theta)e^{-a\theta}\theta\cos(b\theta)d\theta$$

$$J_s = \int_{-h}^{0} \sigma(\theta)e^{-a\theta}\sin(b\theta)d\theta \quad J_{ts} = \int_{-h}^{0} \sigma(\theta)e^{-a\theta}\theta\cos(b\theta)d\theta \tag{A-15e-h}$$

Suppose $a = q$, $b = r$ is a root, and expand both functions $f(a, b)$ and $g(a, b)$ as a Taylor series about the point (a_i, b_i) in terms of $(q-a_i)$, $(r-b_i)$, where (a_i, b_i) is a point near the root at the i-th step. Then $f(a, b)$ and $g(a, b)$ are represented as the following:

$$f(q,r) = 0 = f(a_i,b_i) + \frac{\partial f}{\partial a}(q - a_i) + \frac{\partial f}{\partial b}(r - b_i) + \dots \tag{A-16}$$

$$g(q,r) = 0 = g(a_i,b_i) + \frac{\partial g}{\partial a}(q - a_i) + \frac{\partial g}{\partial b}(r - b_i) + \dots \tag{A-17}$$

Truncating the series and rearranging them yields

$$\begin{bmatrix} 0 \\ 0 \end{bmatrix} = \begin{bmatrix} f(a_i,b_i) \\ g(a_i,b_i) \end{bmatrix} + \begin{bmatrix} \frac{\partial f}{\partial a}(a_i,b_i) & \frac{\partial f}{\partial b}(a_i,b_i) \\ \frac{\partial g}{\partial a}(a_i,b_i) & \frac{\partial g}{\partial b}(a_i,b_i) \end{bmatrix} \begin{bmatrix} q - a_i \\ r - b_i \end{bmatrix} \tag{A-18}$$

The value of $\Delta a_i = q - a_i$ and $\Delta b_i = r - b_i$ can be obtained by multiplying the inverse of the Jacobian matrix to each term of equation (A-18) as the following:

$$\begin{bmatrix} \Delta a_i \\ \Delta b_i \end{bmatrix} = -\begin{bmatrix} \frac{\partial f}{\partial a}(a_i,b_i) & \frac{\partial f}{\partial b}(a_i,b_i) \\ \frac{\partial g}{\partial a}(a_i,b_i) & \frac{\partial g}{\partial a}(a_i,b_i) \end{bmatrix}^{-1} \begin{bmatrix} f(a_i,b_i) \\ g(a_i,b_i) \end{bmatrix} \tag{A-19}$$

Based on the results of equation (A-19), an improved estimate of the root, (q, r) is obtained by the following manner:

$$\begin{bmatrix} a_{i+1} \\ b_{i+1} \end{bmatrix} = \begin{bmatrix} a_i \\ b_i \end{bmatrix} + \begin{bmatrix} \Delta a_i \\ \Delta b_i \end{bmatrix} \tag{A-20}$$

Those above processes are repeated until $f(a, b)$ and $g(a, b)$ are close enough to zero within tolerance.

A.4. The Effect of Time Delay on Stability

The characteristic closed loop equation (A-1) can be separated into the time delay term and the non-time delay term by writing

$$A(s) + C(s)e^{-sT_p} = 0 \tag{A-21}$$

where $A(s) = s^2 + 2\zeta\omega_n s + \omega_n^2(1 + k_c/k_m) + \dfrac{\omega_n^2 k_c}{k_m}\displaystyle\int_{-h}^{0}\sigma(\theta)e^{s\theta}d\theta$ \hfill (A-22)

and

$$C(s) = -k_c\omega_n^2/k_m\int_{-h}^{0}\sigma(\theta)e^{s\theta}d\theta . \tag{A-23}$$

Differentiating equation (A-21) with respect to T_p results in

$$A'(s)\frac{ds}{dT_p} + C'(s)\frac{ds}{dT_p}e^{-sT_p} + C(s)(-T_p)e^{-sT_p}\frac{ds}{dT_p} + C(s)(-s)e^{-sT_p} = 0 \tag{A-24}$$

where $A'(s) = dA/ds$ and $B'(s) = dB/ds$.

Then equation (A-24) can be rearranged such that

$$\frac{ds}{dT_p} = \frac{sC(s)e^{-sT_p}}{A'(s) + C'(s)e^{-sT_p} - C(s)T_p e^{-sT_p}} = -s\left[\frac{A'(s)}{A(s)} - \frac{C'(s)}{C(s)} + T_p\right]^{-1} \tag{A-25}$$

If the real part of equation (A-25) is larger than zero, the root crosses the imaginary axis from left to right parallel to the real axis. This movement indicates the transition to the unstable region. Substituting the real part of equation (A-25) into a sign function at $s = j\omega$ yields

$$\text{sgn}\left[\text{Re}\left(\frac{ds}{dT_p}\right)\right] = -\text{sgn}\left\{\text{Re}\frac{1}{j\omega}\left[\frac{A'(j\omega)}{A(j\omega)} - \frac{C'(j\omega)}{C(j\omega)} + T_p\right]\right\} \tag{A-26}$$

Because the sgn function is independent of T_p, equation (A-26) can be rearranged as

$$\text{sgn}\left[\text{Re}\left(\frac{ds}{dT_p}\right)\right] = \text{sgn}\left\{\text{Im}\frac{1}{\omega}\left[\frac{C'(s)}{C(s)} - \frac{A'(s)}{A(s)}\right]\right\} \tag{A-27}$$

where $A(j\omega) = -\omega^2 + \omega_n^2 + \dfrac{k_c}{k_m}\omega_n^2 I_c + j(2\zeta\omega_n\omega + \dfrac{k_c}{k_m}\omega_n^2 I_s)$ (A-28a)

$$A'(j\omega) = 2\zeta\omega + \frac{k_c}{k_m}\omega_n^2 I_{tc} + j(2\zeta\omega + \frac{k_c}{k_m}\omega_n^2 I_{ts}) \tag{A-28b}$$

$$C(j\omega) = -\frac{k_c}{k_m}\omega_n^2(I_c + jI_s) \tag{A-28c}$$

$$C'(j\omega) = -\frac{k_c}{k_m}\omega_n^2(I_{tc} + jI_{ts}) \tag{A-28d}$$

$$I_c = \int_{-h}^{0}\sigma(\theta)\cos(\theta)d\theta \qquad I_{tc} = \int_{-h}^{0}\sigma(\theta)\theta\cos(\theta)d\theta$$

$$I_s = \int_{-h}^{0}\sigma(\theta)\sin(\theta)d\theta \qquad I_{ts} = \int_{-h}^{0}\sigma(\theta)\theta\sin(\theta)d\theta \tag{A-28 e-h}$$

Substituting equation (A-28a)-(A-28h) into equation (A-27) yields

$$\text{sgn}\left[\text{Re}\left(\frac{ds}{dT_p}\right)\right] = \text{sgn}\left\{\frac{1}{\omega}\begin{bmatrix}\left[\left(\frac{k_c}{k_m}\omega_n^2\right)^2(I_{tc}I_s - I_c I_{ts}) + \left(2\zeta\omega_n + \frac{k_c}{k_m}\omega_n^2 I_{tc}\right)\left(2\zeta\omega_n\omega + \frac{k_c}{k_m}\omega_n^2 I_s\right)\right] \\ -\left(2\omega + \frac{k_c}{k_m}\omega_n^2 I_{ts}\right)\left(-\omega^2 + \omega_n^2 + \frac{k_c}{k_m}\omega_n^2 I_c\right)\end{bmatrix}\right\}$$

$$\tag{A-29}$$

A.5. Stability Analysis for Sharp Tools

The characteristic equation of the closed loop system for $\sigma(\theta) = \delta(\theta)$ is

$$s^2 + 2\zeta\omega_n s + \omega_n^2 + \frac{k_c}{k_m}\omega_n^2(1 - e^{-sT_p}) = 0 \tag{A-30}$$

Equation (A-30) can be solved for k_c/k_m to yield

$$\frac{k_c}{k_m} = \frac{s^2 + 2\zeta\omega_n s + \omega_n^2}{\omega_n^2(e^{-sT_p} - 1)} \tag{A-31}$$

where $\left|\dfrac{s^2 + 2\zeta\omega_n s + \omega_n^2}{\omega_n^2(e^{-sT_p} - 1)}\right| = \dfrac{k_c}{k_m}$ and $\angle\left(\dfrac{s^2 + 2\zeta\omega_n s + \omega_n^2}{\omega_n^2(e^{-sT_p} - 1)}\right) = 0$

Poles of the closed loop system correspond to roots of equation (A-30) for $k_c/k_m = 0$.

When the numerator of equation (A-31) is 0, there are two finite poles.

$$s = -\zeta\omega_n \pm \sqrt{\zeta^2\omega_n^2 - \omega_n^2} \tag{A-32}$$

The value of k_c/k_m is also 0 as the denominator becomes infinite while that of the

numerator remains finite. Let the value of s be $-\infty \pm j\, 2n\pi/T_p$; then the denominator of

equation (A-31) becomes

$$\left|\omega_n^2(e^{-sT_p} - 1)\right| = \left|\omega_n^2(e^{\infty T_p}e^{\mp j2n\pi} - 1)\right| = \left|\omega_n^2(e^{\infty T_p} - 1)\right| = \infty \tag{A-33}$$

Therefore there are an infinite number of poles with a negative infinite real part, which

are separated from each other by $2n\pi/T_p$ in addition to two finite poles in the left-hand

side of the s-plane.

Zeros of the closed loop system correspond to roots of equation (A-30) when the

value of k_c/k_m tends to infinity. The value of k_c/k_m becomes infinite as the denominator

tends to zero while the numerator is finite. Let the value of s be $\pm j\,2n\pi/T_p$, then the

magnitude of the denominator of equation (A-31) becomes

$$\left|\omega_n^2(e^{-sT_p}-1)\right| = \left|\omega_n^2\left[e^{-(\pm j\frac{2n\pi}{T_p})T_p}-1\right]\right| = 0 \tag{A-34}$$

Therefore, there are an infinite number of zeros on the imaginary axis, which are

separated from each other by $2n\pi/T_p$. As a result, the root locus for a sharp tool has the

same locations of poles and zeros as the worn tool in this study.

The sign of the real part in roots of equation (A-30) can be determined analytically.

Since values of integral in equation (A-10) and (A-11) are unity for a sharp tool, the sign

of the real part of the root is determined as follows:

If $-(2n\pi/T_p)^2 + \omega_n^2 > 0$, then $\omega_n^2[-\operatorname{sgn}(a)] > 0$, i.e. $a<0$. \hfill (A-35a)

If $-(2n\pi/T_p)^2 + \omega_n^2 < 0$, then $\omega_n^2[-\operatorname{sgn}(a)] < 0$, i.e. $a>0$. \hfill (A-35b)

The integrals in equation (A-19a-d) evaluate to zero except for I_c which becomes

unity. Equation (A-20) simplifies for $\sigma(\theta) = \delta(\theta)$ to

$$\operatorname{sgn}\left[\operatorname{Re}\left(\frac{ds}{dT_p}\right)\right] = \omega^2 - \omega_n^2\left(1 + \frac{k_c}{k_m}\right) + 2\zeta^2\omega_n^2 \tag{A-36}$$

The effect of a time delay T_p on stability is expressed in analytical form in equation

(A-36). When $\omega^2 - \omega_n(1 + k_c/k_m) + 2\zeta^2\omega_n^2 > 0$, the system becomes unstable as the time

delay T_p increases.

REFERENCES

Berger, B.S., Rokni, M., and Minis, I., 1992, "The Nonlinear Dynamics of Metal Cutting," *International Journal of Engineering Science*, Vol. 30, pp. 1433-1440.

Black, A.J., Kopalinsky, E.M., and Oxley, P.L.B., 1993, "Asperity Deformation Models for Explaining the Mechanisms Involved in Metallic Sliding Friction and Wear –A Review," *Journal of Mechanical Engineering Science*, Vol. 207, pp. 335-353.

Challen, J.M., and Oxley, P.L.B., 1979, "An Explanation of the Different Regimes of Friction and Wear using Asperity Deformation Models," *Wear*, Vol. 53, pp. 229-243.

Chiou, R.Y., 1995, *Acoustic Emission Dynamics in Turning with Tool Wear and Chatter*, Ph.D. Dissertation, Georgia Institute of Technology.

Chiou, R.Y., and Liang, S.Y., 1998, "Chatter Stability of a Slender Cutting Tool in Turning with Tool Wear effect," *International Journal of Machine Tools and Manufacture*, Vol. 38, pp. 315-327.

Chou, Y.K., and Evans, C.J., 1999, "White Layers and Thermal Modeling of Hard Turned Surfaces," *International Journal of Machine Tools and Manufacture*, Vol. 39, pp. 1863-1881.

Clancy, B.E., and Shin, Y.C., 2002, "A Comprehensive Chatter Prediction Model for Face Turning Operation Including Tool Wear Effect," *International Journal of Machine Tools and Manufacture*, Vol. 42, pp. 1035-1044.

Daswon, T., 2002, *Machining Hardened Steel with Polycrystalline Cubic Boron Nitride Cutting Tools*, Ph. D. Dissertation, Georgia Institute of Technology.

Davies, M.A., 1998, "Dynamic Problems in Hard-Turning, Milling, and Grinding," *Dynamics and Chaos in Manufacturing Processes*, John Wiley & Sons, New York, pp. 57-91.

Deshpande, N., and Fofana, M.S., 2001, "Nonlinear Rgenerative Chatter in Turning," *Robotics and Computer Integrated Manufacturing*, Vol. 17, pp. 107-112.

Elbestawi, M.A., Ismali, F., Du, R.X., and Ullagaddi, B.C., 1991, "Modeling Machining Dynamics Including Damping in the Tool-Workpiece Interface," *Tribological Aspects in Manufacturing*, Vol. 54, pp. 253-258.

Gradisek, J., Govekar, E., and Grabec, I., 2001, "Chatter Onset in Non-Regenerative Cutting: A Numerical Study," *Journal of Sound and Vibration*, Vol. 242(5), pp. 829-838.

Hanna, N.H., and Tobias, S.A., 1969, "The Nonlinear Dynamic Behaviour of a Machine Tool Structure," *International Journal of Mach. Tool. Des. Res.*, Vol. 9, pp. 293-307.

Hanna, N.H., and Tobias, S.A., 1974, "A Theory of Nonlinear Regenerative Chatter," *Trans. ASME Journal of Engineering for Industry*, Vol. 96, pp. 247-255.

Kalmar-Nagy, T., Stepan, G., and Moon, F.C., 2001, "Subcritical Hopf Bifurcation in the Delay Equation Model for Machine Tool Vobrations," *Nonlinear Dynamics*, Vol. 26, pp. 121-142.

Kishawy, H.A. and Elbestawi, M.A., 1999, "Effects of Process Parameters on Material Side Flow during Hard Turning*", International Journal of Machine Tools and Manufacture,* Vol. 39, pp. 1017-1030.

Kobayashi, S., and Thomsen, E.G., 1960, "The Role of Friction in Metal Cutting," *Trans. ASME Journal of Engineering for Industry*, Vol. 82, pp. 324-332.

Kondo, E., Ota, H., and Kawai, T., 1997, "New Method to Detect Regenerative Chatter using Spectral Analysis, Part 1: Basic Study of Criteria for Detection of Chatter," *Trans. ASME Journal of Manufacturing Science and Engineering*, Vol. 119, pp. 461-466.

Konig, W., Komanduri, R., Tonshoff, H.K., and Ackershott, G., 1990, "Machining of Hard Materials," *Annals of the CIRP*, Vol. 39, pp. 417-427.

Lin, J.S. and Weng, C.I., 1991, "Nonlinear Dynamics of The Cutting Process," *International Journal of Mechanical Sciences*, Vol. 33, pp. 645-657.

Litak, G., 2002, "Chaotic Vibrations in a Regenerative Cutting Process," *Chaos, Solitons and Fractals*, Vol. 13, pp. 1531-1535.

Merritt, H.E., 1965, "Theory of Self-Excited Machine-Tool Chatter," *Trans. ASME Journal of Engineering for Industry*, Vol. 87, pp. 447-454.

Minis, I.E., Magrab, E.B., and Pandelidis, I. O., 1990, "Improved Methods for the Prediction of Chatter in Turning, Part3: A Generalized Linear Theory," *Trans. ASME Journal of Engineering for Industry*, Vol. 112, pp. 28-35.

Nakayama, K., Arao, M., and Kanda, T., 1988, "Machining Characteristics of Hard Materials," *Annals of the CIRP*, Vol. 37, pp. 89-92.

Neyfeh, A.H., Chin, C.-M., and Pratt, J., 1998, "Applications of Perturbation Methods to Tool Chatter Dynamics," *Dynamics and Chaos in Manufacturing Process*, John Wiley & Sons, New York, pp. 193-213.

Nosyreva, E.P., and Molinari, A., 1997, "Analysis of Nonlinear Vibrations in Metal Cutting," *International Journal of Mechanical Sciences*, Vol. 40, pp. 735-748.

Olgac, N., and Hosek, M., 1998, "A New Perspective and Analysis for Regenerative Machine Tool Chatter," *International Journal of Machine Tools and Manufacture*, Vol. 38, pp. 783-398.

Pratt, J.R., and Nayfeh, A.H., 1999, "Design and Modeling for Chatter Control," *Nonlinear Dynamics*, Vol. 19, pp. 49-69.

Pratt, J.R., Davies, M.A., Evans, C.J., and Kennedy, M.D., 1999, "Dynamic Interrogation of a Basic Cutting Process," *CIRP Annals*, Vol. 48, pp. 39-42.

Rao, B.C. and Shin, Y.C., 1999, "A Comprehensive Dynamic Cutting Force Model for Chatter Prediction in Turning," *International Journal of Machine Tools and Manufacture*, Vol. 39, pp. 1631-1654.

Rekasius, Z.V., 1980, "A Stability Test for Systems with Delays," in *Proc. Joint Automatic Control Conference*, Paper No. TP9-A.

Saravanja-Fabris, N. and D'Souza, A.F., 1974, "Nonlinear Stability Analysis of Chatter in Metal Cutting," *Trans. ASME Journal of Engineering for Industry*, Vol. 96, pp. 670-675.

Shi, H.M., and Tobias, S.A., 1984, "Theory of Finite Amplitude Machine Tool Instability," *International Journal of Machine Tool Des. Res.*, Vol. 23, pp. 45-69.

Smithey, D.W., Kapoor, S.G., and DeVor, R.E., 2001, "A New Mechanistic Model for Predicting Worn Tool Cutting Forces," *Machining Science and Technology*, Vol. 5, pp. 23-42.

Stepan, G., 1998, "Delay-Differential Equation Models for Machine Tool Chatter," *Dynamics and Chaos in Manufacturing Processes*, John Wiley & Sons, New York, pp. 165-191.

Tewani, S.G., Rouch, K.E., and Walcott, B.L., 1993, "A Study of Cutting Process Stability of a Boring Bar with Active Dynamic Absorber," *International Journal of Machine Tools and Manufacture*, Vol. 35, pp. 91-108.

Thomsen, E.G., MacDonald, A.G., and Kobayashi, S., 1962, "Flank Friction Studies with Carbide Tools Reveal Sublayer Plastic Flow," *Trans. ASME Journal of Engineering for Industry*, Vol. 84, pp. 53-62.

Tlusty, J., 1978, "Analysis of the State of Research in Cutting Dynamics," *Annals of the CIRP*, Vol. 27, pp. 583-589.

Tlusty, J., and Polacek, M., 1963, "The Stability of the Machine Tool Against Self-Excited Vibration in Machining," in *ASME Production Engineering Research Conference, Pittsburgh*.

Tobias, S.A., 1965, *Machine Tool Vibration*, Blackie and Son, London.

Waldorf, D.J., 1996, *Shearing, Ploughing, and Wear in Orthogonal Machining*, Ph.D. Dissertation, ME Department, University of Illinois at Urbana-Champaign.

Waldorf, D.J., DeVor, R.E., and Kappor, S.G., 1997, "A Slip-Line Field for Ploughing during Orthogonal Cutting," *Manufacturing Science and Technology*, Vol. 2, pp. 37-44.

Wang, J.Y., and Liu, C.R., 1999, "The Effect of Tool Flank Wear on the Hear Transfer, Thermal Damage and Cutting Mechanics in Finish Hard Turning," *Annals of the CIRP*, Vol. 48, pp. 53-58.

Wu, D.W., 1988, "Application of a Comprehensive Dynamic Cutting Force Model to Orthogonal Wave Generating Processes," *International Journal of Mechanical Science*s, Vol. 30, pp. 581-660.

Wu, D.W., and Liu, C.R., 1985, "An Analytical Model of Cutting Dynamics. Part 1: Model Building," *Trans. ASME Journal of Engineering for Industry*, Vol. 107, pp. 107-111.